TECHNISCHE UNIVERSITÄT WIEN
Vienna University of Technology

D I P L O M A R B E I T

Studies on the synergetic effect between Pd and Co_3O_4 or γFe_2O_3 in CO oxidation

Ausgeführt am Institut für

Materialchemie

der Technischen Universität Wien

unter der Anleitung von

Univ.Prof. Mag.rer.nat. Dr.rer.nat Günther Rupprechter,
Ass.Prof. Dipl.-Ing. Dr.techn. Karin Föttinger,
und MSc Liliana Lukashuk

durch

Elisabeth Kolar

Tiefer Graben 12/14

1010 Wien

Wien, 09.12.2014

Danksagung

An dieser Stelle möchte ich all den Personen danken, die einen großen Teil zum Erstellen dieser Arbeit beigetragen haben.

Zuerst ein Dankeschön an Prof. Rupprechter, der mir ermöglicht hat meine Arbeit in seiner Arbeitsgruppe durchzuführen.

Ein besonderes Dankeschön an Ass. Prof. Karin Föttinger, für die exzellente Betreuung in jeglicher Hinsicht. Hiermit meine ich ihre fachlich kompetente Beantwortung von einer Vielzahl von mir gestellten Fragen, ihre zeitintensiven Diskussionen über die Durchführung von Experimenten bis hin zu Interpretation von Ergebnissen, ihre außerordentlich gewissenhafte und rasche Korrektur meiner Arbeit und natürlich ihre liebenswürdige und respektvolle Art.

Lieben Dank auch an MSc Liliana Lukashuk, für ihre von Anfang an tatkräftige Unterstützung im Labor, ihre Hilfestellung beim Lösen von auftretenden Problemen, Verfassen von Abstracts und Zusammenstellen von Präsentationen, für die Ermöglichung der XPS Messungen am Synchrotron aber natürlich auch für ihre motivierenden und liebevollen Worte.

Prof. Michael Stöger-Pollach und Dr. Stefan Löffler für die Durchführung der TEM Aufnahmen an der TU Wien und Dipl. Hartfelder für die TEM Aufnahmen an der ETH Zürich (EMEZ).

Werner Artner für die Durchführung der XRD Messungen.

Ing. Rainald Rosner für seine Hilfestellung in vielen technischen Bereichen.

Dr. Christoph Rameshan für die tatkräftige Unterstützung bei den APXPS Messungen in Berlin.

Danke an den FWF (Fonds zur Förderung wissenschaftlicher Forschung) für die finanzielle Unterstützung.

Außerdem geht ein riesen Dankeschön an meine Arbeitsgruppe und allen anderen lieben Kollegen, welche für nette Gespräche und ein wohltuendes Institutsklima gesorgt haben.

Zuletzt möchte ich noch meinen Eltern und Freunden herzlichst danken, die mich in allen Lebenslagen motiviert und mir den nötigen Rückhalt gegeben haben.

Zusammenfassung

Es hat sich gezeigt, dass Edelmetalle (Pd, Pt) geträgert auf leicht reduzierbaren Übergangsmetalloxiden (Co_3O_4, NiO, Fe_2O_3) eine erhöhte katalytische Aktivität in der CO Oxidation aufweisen, welches auf starke Metall-Träger Wechselwirkungen zurückzuführen ist. Die Natur (elektronisch oder chemisch) dieser Wechselwirkung ist allerdings noch nicht geklärt. Eine Erhöhung der katalytischen Aktivität in der CO Oxidation ist vor allem bei niedrigen Temperaturen in der Autoabgasreinigung erstrebenswert, bei welcher bis heute die CO Vergiftung des Katalysators während des sogenannten „Kaltstartens“ ein großes Problem darstellt.

Ziel der Arbeit war die Synthese von zwei geträgerten Pd Katalysatoren, nämlich einem PdO/Co_3O_4 und einem PdO/Fe_2O_3 Katalysator, deren Charakterisierung in Bezug auf Struktur und Zusammensetzung und die Ermittlung des Einflusses der Pd Beladung auf die katalytische Aktivität in der CO Oxidation. Außerdem wurden mittels *in situ* Methoden dynamische Wechselwirkungen der Reaktanden mit der Katalysatoroberfläche unter Reaktionsbedingungen untersucht. Zur Charakterisierung der Struktur wurden Methoden wie z.B. die Transmissionselektronenmikroskopie (TEM) eingesetzt. Als *in situ* Methoden wurde die Fourier Transform Infrarot Spektroskopie (FTIR) und die Photoelektronenspektroskopie unter Umgebungsdruck (APXPS) zur Anwendung gebracht. Die Katalysatoren wurden mittels Nassimprägnierung synthetisiert, welche folglich Pd Partikeln in einer Größenordnung von sub-2 nm auf dem Co_3O_4 und von 5-10 nm auf dem γFe_2O_3 aufwiesen. Eine Erhöhung der katalytischen Aktivität in der CO Oxidation wurde nach der Pd Beladung für beide Katalysatoren erzielt. Interessanterweise zeigten die Katalysatoren unter Reaktionsbedingungen ein von Grund auf verschiedenes Adsorptionsverhalten von CO. Anhand von *in situ* FTIR Aufnahmen wurden auf dem PdO/Co_3O_4 keine CO-Pd^o Banden und nur Karbonat-Banden verzeichnet. Im Gegensatz dazu wurden auf dem PdO/Fe_2O_3 starke CO-Pd^o Banden bereits bei RT zum Vorschein gebracht, welches auf eine Reduktion des PdO durch CO zurückzuführen ist. Mittels *in situ* APXPS Messungen wurde schlussendlich auch bestätigt, dass kein metallisches Pd auf dem Co_3O_4 vorlag, sondern PdO und PdO_2 die stabilen Phasen unter Reaktionsbedingungen waren. Zusammenfassend kann aufgezeigt werden, dass im Falle des PdO/Co_3O_4, die CO Oxidation auf dem Co_3O_4 Träger und unter der Bildung von Karbonaten abläuft, wobei PdO und PdO_2 als Promotoren agieren. Im Gegensatz dazu liegt das Pd auf dem Fe_2O_3 Träger in metallischer Form unter Reaktionsbedingungen vor und stellt Adsorptionsplätze für CO zu Verfügung.

Abstract

It is well known that the loading of a noble metal (e.g. Pt, Pd) on an easily reducible transition metal oxide (e.g. Co_3O_4, γFe_2O_3, TiO_2 or MnO_2) results in an enhancement in the catalytic activity in CO oxidation at low temperatures due to interactions at the metal-support interface. However, the underlying nature of the interactions ("electronical" or "geometrical") is still under debate. Enhancing the CO oxidation activity in the low temperature range is of special interest for controlling automotive emissions during the cold start of a car (T< 250 °C), where the strong CO adsorption on the noble metal remained an unsolved issue.

The aim of the thesis was the synthesis of two different supported Pd catalysts, namely PdO/Co_3O_4 and $PdO/\gamma Fe_2O_3$, their characterization in terms of structure and composition and the investigation of the influence of the Pd loading on the catalytic activity in CO oxidation. Furthermore, *in situ* studies were utilized to investigate dynamical interactions between the reactants and products and the catalyst surface under reaction conditions. The structural characterization of the catalysts was performed by transmission electron microscopy (TEM). As *in situ* methods, the Fourier Transform Infrared (FTIR) and the ambient-pressure X-ray photoelectron spectroscopy (APXPS) were applied. The catalysts were prepared by wet impregnation method yielding highly dispersed Pd particles with a mean size of sub-nm to 2 nm on the Co_3O_4 and of 5 to 10 nm on the γFe_2O_3 support according to TEM images. The kinetic CO oxidation studies revealed that after Pd loading an enhancement of the activity was achieved for both catalysts. Interestingly, significant differences in the adsorption behavior of CO under reaction conditions could be observed. The *in situ* FTIR studies showed that on the PdO/Co_3O_4, no CO-Pd^o absorption bands were evident and only surface carbonate formation was detected, while on the PdO/Fe_2O_3 catalyst strong CO-Pd^o bands appeared already at RT indicating a reduction of PdO to metallic Pd by the CO. The CO-Pd^o bands on PdO/Fe_2O_3 were also present at higher temperatures (~150 °C), where a full CO conversion was observed. Thus, it was concluded that on both catalysts the CO oxidation rate was not affected by the well-known CO poisoning of Pd. *In situ* APXPS measurements confirmed the absence of metallic Pd on Co_3O_4 and the presence of stable PdO and PdO_2 phases under reaction conditions. Overall, the nature of CO adsorption sites and thus the CO oxidation pathways are apparently very different on the two catalysts. On PdO/Co_3O_4 the CO oxidation proceeds most likely via surface carbonates on the Co_3O_4 with PdO and PdO_2 acting as promoters, while on PdO/Fe_2O_3 metallic Pd provides adsorption sites for CO during the reaction.

Contents

Chapter 1

1 Introduction

1.1 Catalysis in general

About 90 % of industrial reaction processes are performed in the presence of heterogeneous catalysts which are found in a wide range of different fields e.g. chemical, food, automobile and petrochemical industries [1].

Nowadays, the performance and the costs of a heterogeneous catalyst in a specific application have to be optimized to fulfill the increasing environmental and energy demands and needs of the society.

For the optimization of the catalyst performance, catalytic studies have to be conducted where the performance of the catalyst, meaning the catalytic properties including activity, selectivity and stability, is determined under a variety of reaction conditions (T, p, space velocity of the reactants' feed). In addition, an in-depth study of the reaction kinetics (e.g. reaction rates and orders, activation energies) is required.

Another relevant issue for achieving a further improvement of the catalyst performance is the fundamental understanding of the catalytic properties in terms of structure and chemistry of the catalyst, the reaction mechanism including kinetically relevant reaction steps and highly active intermediates, and the nature ("chemical" and "geometrical") of active sites [1]. Moreover, deactivation mechanisms (e.g. sintering, carbon deposition, phase change) occurring on the catalyst surface have to be identified with the aim to eliminate them.

In recent years, the development of a variety of surface analysis methods has given the possibility to advance towards the fundamental understanding of the catalytic properties by revealing the surface structure and chemistry of the catalyst on a molecular level. Especially, *in situ* studies where the catalyst is studied under reaction conditions provide an insight into dynamic processes on the catalyst surface and structural and chemical changes of the catalyst itself induced by the present reactants and products which could not be revealed by ex situ methods.

Lately, also theoretical methods e.g. DFT calculations helped to get an insight into the nature of highly reactive intermediates and active sites.

To enable these catalytic and fundamental studies, the catalyst has first to be synthesized with a defined structure and composition in a well-controlled way. Frequently applied instrumental techniques and procedures for the characterization of structural, chemical and catalytic properties of heterogeneous catalysts are illustrated in figure 1.1.

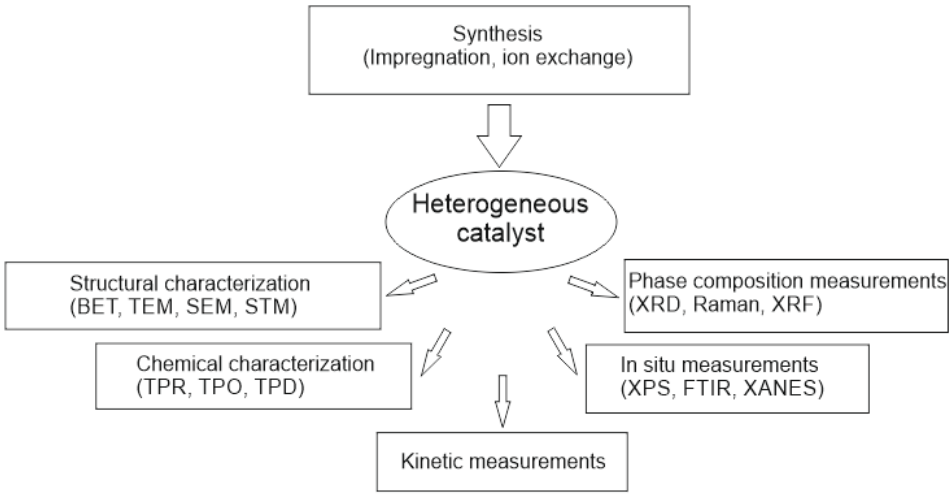

Figure 1.1.: Instrumental techniques and procedures applied to investigate the structural, the chemical and the catalytic properties of a heterogeneous catalyst after its synthesis.

1.2 The three-way catalyst (TWC)

Today around 30 % of all industrially applied heterogeneous catalysts are used in the environmental sector including the controlling of automotive exhaust emissions, stack gas emissions from power stations and gaseous effluents in the refining and chemical industry [1].

One of the greatest achievements in this sector is the introduction of the three-way catalyst (TWC) in the 80s, which is responsible for the automotive emission control.

Today the usage of a TWC in automotive exhausts, shown in figure 1.2, is the most effective and safe technology for achieving a reduction of harmful pollutants including hydrocarbons (HC), carbon monoxide (CO) and nitrogen oxide (NO_x) during the normal operating mode of the

combustion engine [2]. The active material of the TWC consists of the noble metal Pd or Pt supported on Al_2O_3 and CeO_2 (oxygen storage) for the oxidation reactions and Rh supported on ZrO_2 for the NO_x reduction [3]. However, during the start of the engine, when the catalyst temperature is still low (T< 250 °C), the catalyst is in its inactive state and cannot convert the toxic pollutants to the more harmless products including nitrogen, CO_2 and water, which is also referred to the "cold start problem" [3]. Thus, high amount of pollutants (50-80 %) [2] are released into the environment till the ignition temperature of the catalytic reaction is reached (around 250-300 °C) meaning where the catalyst gets in its active state [3].

Due to environmental concerns and stricter legislations concerning automotive exhaust, there is a motivation to reduce these toxic emissions during the cold start by improving the low-temperature catalytic activity of the TWC.

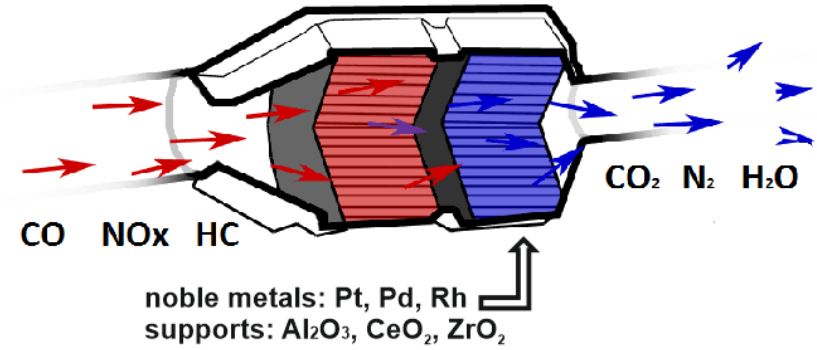

Figure 1.2.: Schematic drawing of a three-way catalyst, its main components and the involved chemical reactants [4].

The underlying reason for the suppression of CO oxidation $2CO + O_2 \xrightarrow{Cat} 2CO_2$ at low temperatures is the rapid self-poisoning of Pd or Pt by high levels of CO meaning that CO exclusively adsorbs on the active surface sites of Pd preventing the adsorption and activation of O_2 shown in Scheme 1.1.

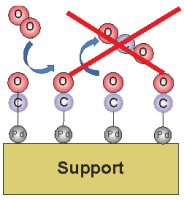

Scheme 1.1: Schematic drawing of a self-poisoning of Pd by CO.

To facilitate the catalytic CO oxidation at low temperatures, one approach is to combine easily reducible transition metal oxides e.g. Co_3O_4, Fe_2O_3, TiO_2 or MnO_2 with the noble metals e.g. Pd, Pt or Au. The high catalytic activity at low temperatures is mainly attributed to synergetic interaction between the oxide support and the noble metal at the metal-support interface defined as a "strong metal-support interaction" (SMSI) state [5,6,7]. Most authors propose that the reaction proceeds at or nearby the metal-support interface where the noble metal provides adsorption sites for CO and the support supplies oxygen species to react with adsorbed CO [8,9]. However, the underlying nature ("electronical" or "geometrical") of the SMSI state, the active sites, respectively states and the reaction mechanism are still controversially discussed.

1.3 State of the art

In recent time, there is an increased demand to understand the fundamental surface processes and the structure and chemistry of the active states/sites on the catalyst surface, which guide the catalytic activity, selectivity and stability of the catalyst.

In the particular field of noble metals supported on transition metal oxides most of the research is interested in the nature of the SMSI state at the metal-support interface which is assumed to have an effect on active sites and the reaction mechanism and thus, the catalytic activity in a variety of different reactions e.g. the CO oxidation, methane steam reforming [10], methane oxidation [10], water-gas shift reaction [11] and methanol decomposition [12].

Herein, we especially focus on the noble metal Pd supported on various transition metal oxides in the CO oxidation reaction. The CO oxidation is one of the most intensively studied reactions as it is often used as a prototype reaction for many other reactions. Furthermore, Pd has got intensively under investigation as it is known for its higher activity and lower costs for CO oxidation compared to Pt or Au [3]. As a suitable transition metal oxide, Co_3O_4 has attracted a lot of attention due to its excellent intrinsic CO oxidation activity already at room temperature (RT) and its even greater activity in combination with a noble metal [13,14].

In the following, a summary is given of the already released studies of transition metal oxides supported noble metals in CO oxidation in the model and the real catalysis field which include

the study of (1) the nature of the SMSI state and its influence on the catalytic activity, (2) the influence of the pretreatment (oxidative or reductive) on the SMSI state i.e. on the catalytic activity, (3) proposed reaction mechanisms including intermediates and involved active states (e.g. oxidation states) of the metal and the support and finally (4) proposed deactivation mechanisms.

In addition, already published results and postulations about the properties of the transition metal oxides Co_3O_4 and γFe_2O_3 and their behavior in CO oxidation are represented. It will be made clear that the results are contradictory and open questions still remain. On the one hand this is due to a lack of insight on the surface chemistry at a molecular level as only a limited number of experimental techniques can be utilized under reaction conditions such as high-pressure scanning

tunneling microscopy (STM), Fourier transform infrared spectroscopy (FTIR), synchrotron based near-edge X-ray absorption fine structure (NEXAFS), ambient-pressure X-ray photoelectron spectroscopy (APXPS), whereas most of them are not suitable for the investigation of oxide surfaces due to charging effects. On the other hand it is due to the enormous complexity of the catalyst surface structure (e.g. different crystallographic facets and sizes, lattice distortions, defects) and chemistry especially at the metal-support interface which is getting influenced by a variety of factors involving the composition of the reaction mixture, the temperature and the pressure, the pretreatment conditions, the geometrical and chemical nature of the noble metal and the support (e.g. particle size and distribution, crystallite size) and many others.

1.3.1 Strong-metal-support interactions (SMSI)

In the late seventies Tauster et al. [15] first introduced the concept of “strong metal-support interactions” (SMSI) based on the observation of a decreased CO and H_2 chemisorption on different noble metals supported on TiO_2 after a reduction pretreatment at high temperatures.

Nowadays, the SMSI state is used as a description for any kind of interaction between a noble metal and a metal oxide support which modifies, either in a positive or negative way, the catalytic activity or selectivity of the catalyst.

Until today, the SMSI state has been reported to occur between noble metals including Pd, Pt, Rh and a variety of different reducible oxides like Co_3O_4, Fe_2O_3, Ta_2O_5, CeO_2, V_2O_3, MnO_2 or TiO_2 [7].

However, the nature of the SMSI state ("electronical" or "geometrical") and its influence on the catalytic activity in particular in CO oxidation is widely discussed mainly due to limitations of insight of the metal-oxide interface under reaction conditions. Interactions of "electronical" nature imply a charge transfer between the metal and the oxide modifying the valence-band electronic density of states which could result in the formation of metal-metal bonds, whereas the interactions of "geometrical" nature involving a mass transport described by an encapsulation of the metal by the oxide support or/and interdiffusion of metal ions at the metal-support interface [6]. Also a combination of "electronical" and "geometrical" interactions are reported to exist [6].

An and co-workers [13] for example, observed for a variety of transition metal oxides (Co_3O_4, NiO, CeO_2, αFe_2O_3 and MnO_2) an enhancement in CO oxidation rates after loading them with Pt whereas the greatest enhancement was observed for the Pt/Co_3O_4 catalyst. They were implying that charges at the metal-support interface provided from the redox chemistry of the support e.g $Co_3O_4 \leftrightarrow CoO$ are responsible for an enhancement in CO oxidation activity. This postulation was based on NEXAFS and APXPS studies.

A variety of other studies of noble metals deposited on oxide single crystals by surface sensitive techniques revealed that the SMSI effect is often related to an encapsulation of the noble metal by a reduced thin layer of the oxide support which was reported to be either from advantage or disadvantage with respect to the catalytic CO oxidation activity. Naumann d'Alnoncourt et al. [7] stated for a Pd/FeO_x catalyst that an encapsulation of Pd particles by an FeO_x layer was evident after a reduction pretreatment at 250 °C resulting in an enhanced CO oxidation activity which they derived from a combination of CO chemisorption, electron microscopy and APXPS experiments. Furthermore, Qin and co-workers [17] postulated for Pt deposited on a Fe_2O_3 (111) film that after a mild reduction pretreatment at 230 °C or an annealing process above 570 °C, Pt particles got encapsulated (derived from STM) leading to an increase in CO oxidation activity. To mention one example where the encapsulation of the noble metal had a negative effect on the catalytic CO oxidation activity, the work of Bonanni and co-workers [18] can be pointed out in

which they observed a decreased CO oxidation activity over encapsulated Pt clusters supported on a rutile TiO_2 (110) surface after the annealing up to ~ 830 °C.

According to Knözinger [19], the driving force for the encapsulation seems to be the minimization of the surface energy. He stated that noble metals on oxides with relatively low surface energies like TiO_2, CeO_x and V_2O_5 reveal the encapsulation effect, while Al_2O_3 and SiO_2 do not. However, this statement would be in disagreement with the study by Ivanova et al. [20], who reported about the SMSI state between Pd and the support Al_2O_3 which they related to the formation of "core-shell" structures consisting of Pd particles covered by an aluminate phase which was observed via morphological changes with high-resolution TEM (HRTEM).

Besides the encapsulation effect, the SMSI effect was also associated with an interdiffusion of the noble metal into the oxide support lattice according to the studies by Sun [12] and Hinokuma et al. [21]. They reported about cationic Pd^+ species which diffused into the CeO_2 lattice forming a chemical bond like Pd-O-Ce stabilizing the Pd^+ species which they derived from electron microscopy, extended X-ray absorption fine structure (EXAFS) and X-ray photoelectron spectroscopy (XPS) studies.

A variety of other studies reported about an enhancement in activity after loading a transition metal oxide with a noble metal without discussing the potential present SMSI state in detail. These studies include the work of Jin et al. [22], who observed an improvement in CO oxidation catalytic activity after loading with Pd on highly ordered mesoporous metal oxides (meso-MO_x) including CeO_2, Co_3O_4, Mn_2O_3, SnO_2 and TiO_2 compared to the pure meso-MO_x which they attributed to some metal-support interactions. The highest activity was obtained for Pd/Co_3O_4, although the greatest enhancement compared to the pure meso-MO_x was achieved for Pd/CeO_2. Moreover, the studies by Luo et al. [16,23] revealed that the light-off temperatures for Pd loaded MnO_x-CeO_2, FeO_x-CeO_2 and Co_3O_4-CeO_2 catalysts decreased by 70 °C, 100 °C and 36 °C compared to the unloaded oxides which they ascribed to some synergetic effect between the Pd and the support. The Pd/Co_3O_4-CeO_2 catalyst showed activity already at RT.

1.3.2 Influence of the pretreatment on the SMSI

Different pretreatments of the catalyst, whether in oxidizing or reducing atmosphere, are often reported to induce or have an impact on the SMSI state between the noble metal and the transition metal oxide i.e. on the catalytic activity.

Skoglundh et al. [24] concluded that a prereduction (4 % H_2; 600 °C) of Co_3O_4 supported Pt and Pd catalysts significantly lowered the light-off temperatures for CO conversion by up to 100 °C compared to the catalyst after peroxidation. This would be in agreement with the observations by Mergler et al. [25], who showed that a reduction pretreatment (H_2; 400 °C) increased the light-off temperature by 75 °C for a $Pt/CoO_x/SiO_2$ catalyst in CO oxidation compared to an oxidation pretreatment. In contrast, the work of Jin and co-workers [22] pointed out that already a calcination in air (300 °C) was sufficient to induce a SMSI state between the metal Pd and different mesoporous metal oxides (CeO_2, Co_3O_4, Mn_2O_3, SnO_2, and TiO_2) resulting in an enhanced CO oxidation rate. However, a subsequent reduction pretreatment (5% H_2; 150 °C) even further improved the catalytic CO oxidation activities of the catalysts. In contrast, Luo et al. [26] reported that a reduction pretreatment (H_2; 200 °C) of a Pd/CeO_2 catalyst did not significantly alter the catalytic activity in CO oxidation compared to an oxidation pretreatment.

Until lately, in the particular case of the encapsulation effect, it was well established that the reduction in H_2 atmosphere at different temperatures (230-500 °C) [7,27] or the annealing in vacuum above 430 °C [17,28] are required to induce the encapsulation. However, recently Ivanova et al. [20] reported that a calcination of a Pd/Al_2O_3 catalyst in air (550 °C) was sufficient to induce an encapsulation of Pd by the Al_2O_3 support exhibiting a high activity in CO oxidation at ambient temperatures.

1.3.3 Postulated CO oxidation mechanism, intermediates and active states

In general it is known that the CO oxidation reaction cannot proceed in the gas phase at low temperatures because the reaction is spin forbidden [29]. O_2 first has to dissociate to atomic adsorbed O to enable the reaction.

It is further known that in the presence of noble metals e.g. Pt, Pd, Rh supported on non-reducible oxides e.g. SiO_2, CO oxidation follows the competitive Langmuir-Hinshelwood mechanism [29], described by the equations (1.2-.1.4) where CO chemisorbs associatively and O_2 dissociatively on the noble metal resulting in the formation of CO_2 .

$$CO_{gas} \leftrightarrow CO^* \qquad (1.2)$$

$$O_{2gas} \leftrightarrow 2O^* \qquad (1.3)$$

$$CO^* + O^* \leftrightarrow CO_2^* \qquad (1.4)$$

$$CO_2^* \leftrightarrow CO_{2gas} \qquad (1.5)$$

*Illustrates the chemisorbed molecule on the noble metal.

However, the CO oxidation mechanism on noble metals supported on reducible transition metal oxides is still not well understood as it is believed that the reaction mechanism is very complicated including the involvement of different kinds of active oxygen species at or close the metal-support interface [30], carbonates and hydroxyl groups [31].

Mergler et al. [25] for example proposed a reaction mechanism where CO molecularly adsorbs on the Pt and O_2 dissociates on the CoO_x promoted by the presence of oxygen vacancies followed by a reaction to CO_2 either at the metal-support interface or due to oxygen spillover to the Pt. This is in agreement with Haruta's study [32], who postulated the same CO oxidation mechanism for an Au/Co_3O_4 catalyst where he proposed in addition some bidentate carbonate species as reaction intermediates. Schubert et al. [33] postulated a CO oxidation mechanism for an Au/Fe_2O_3 catalyst where CO adsorbs on the Au particles and O_2 in a molecular form (O_2^-) on the support Fe_2O_3 followed by a dissociation at the metal-support interface and a possible spillover onto the Au particles to react with the adsorbed CO. In contrast to Haruta, Schubert excluded carbonates as intermediates based on their isotope studies.

A completely different reaction mechanism was postulated by Luo et al. [23] shown in figure 1.4, where CO molecules adsorb as bidentate carbonates on a Co_3O_4-CeO_2 support followed by a reaction with adsorbed oxygen species from the metallic Pd via an oxygen spillover process. This would be in agreement with the work by Zou et al. [34] in which he proposed the same CO oxidation mechanism on a Pd/CeO_2-MnO_2 catalyst. Furthermore, Zou included in his model some active interface O_2^- species adsorbed on oxygen vacancies which are needed for the formation of the bidentate carbonates.

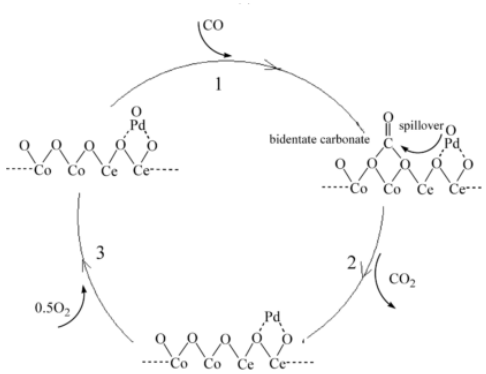

Figure 1.4: CO oxidation reaction pathway over an Pd/Co_3O_4-CeO_2 catalyst proposed by Luo et al. [23].

In terms of active states of noble metals (e.g. oxidation state) supported on transition metal oxides, the studies of supported Pd catalysts are most notable, in which the oxidation state of Pd providing the active sites for CO oxidation at low temperatures is controversially discussed.

Schalow et al. [35] found out that the CO oxidation activity at low reaction temperatures (T< 170 °C) was significantly higher in the presence of metallic Pd compared to partially oxidized Pd particles both deposited on a well ordered Fe_3O_4 film. The work was based on a combination of multi-molecular beam (MB) experiments and *in situ* time-resolved infrared reflection absorption spectroscopy (TR-IRAS). The lower activity of the supported partially oxidized Pd was attributed to the weak CO adsorption on the Pd oxide surface resulting in a lower reaction probability. This is consistent with the work of Satsuma et al. [36] in which it was pointed out that the formation of metallic Pd on the metal oxide supports CeO_2 and TiO_2 is essential for the high CO oxidation activity at low temperatures. Furthermore, according to the work by Hinokuma et al. [21], an increase of CO oxidation at ambient temperatures by more than 20 times was reached after the thermal decomposition of PdO to Pd nanoparticles on CeO_2 support which was demonstrated by EXAFS and XPS studies.

In contrast, Luo et al. [37] related the high activity of a $PdO/Ce_{0.5}Zr_{0.5}O_2$ catalyst in CO oxidation to the presence of PdO or/and Pd hydroxide species. Moreover, Meng et al. [9] suggested that the high CO oxidation catalytic activity of a $PdO/Ce_{1-x}Pd_xO_{2-\delta}$ catalyst synthesized by a solid-solution combustion method could be explained by the free PdO species providing CO adsorption sites in combination with the Pd^{2+} species incorporated in the matrix creating oxygen vacancies for activating the O_2. Priolkar et al. [38] concluded that only Pd^{2+} ions in the CeO_2 matrix (1wt% Pd) provide the active sites for CO oxidation.

1.3.4 Deactivation mechanisms

The deactivation of transition metal oxide based catalysts at low temperatures under CO oxidation conditions was extensively investigated by researchers and therefore approaches were applied to prevent the catalysts from deactivation. A variety of deactivation mechanisms occurring on the catalyst surface were postulated.

In the case of Co_3O_4 based catalysts, it is proposed that the deactivation can occur due to an irreversible reduction of the catalyst's surface in addition to a blocking of active sites by carbonyl, carbonate, coke or/and water [39,40]. Especially, the presence of moisture was reported to strongly deactivate the catalyst at low temperatures [41]. For example, Skoglundh et al. [42] stated that the presence of moisture strongly poisoned a Pt loaded CoO_x/AL_2O_3 catalyst at low temperatures in CO oxidation. In contrast, Jansson et al. [39] suggested that the reconstruction of the pure Co_3O_4 surface is the main reason for the deactivation.

To prevent the Co_3O_4 catalysts form deactivation, researches succeeded with different approaches. Jansson et al. [40] suppressed the deactivation by increasing either the O_2/CO ratio or the temperature from 30 to 80 °C Moreover, Haruta et al. [43] reported that the addition of Au on Co_3O_4 prevented the catalyst from deactivation due to moisture at temperatures of -54 °C.

Based on XPS and STEM measurements of a Pd/FeO_x catalyst, Naumann d'Alnoncourt et al. [7] revealed that the deactivation occurred in two ways including changes in the oxidation state of the iron species and a sintering of the Pd particles

However, moisture was not only reported to act as an inhibiting factor but was also mentioned in the context of having a promoting role in CO oxidation in the presence of other transition metal oxides like Fe_2O_3 and TiO_2.

For example Schubert et al. [33] suggested that the presence of OH groups on an Au/Fe_2O_3 catalyst surface even prevents the catalyst from deactivation due to the transformation of carbonates to less stable bicarbonates.

1.3.5 Catalytic and structural properties of the two different oxides Co_3O_4 and γFe_2O_3

Co_3O_4 has been proposed as a promising catalyst in various reactions (e.g. CO, hydrocarbon and ammonia oxidation, Fischer-Tropsch synthesis). An outstanding high catalytic activity was achieved in CO oxidation at low temperatures. The high activity was related to its favorable redox properties arising from its unique structure. Co_3O_4 has a spinel structure based on a cubic close-packing array of oxide ions where one half of the octahedral sites are occupied by Co^{3+} and one-eighth of the tetrahedral sites by Co^{2+} cations (see figure Figure 1.3).

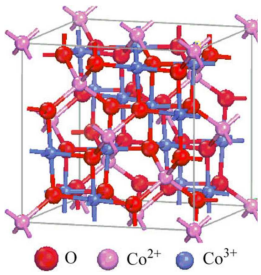

Figure 1.3: Crystal structure of the spinel oxide Co_3O_4.

Haruta et al. [32] for example reported about a light-off temperature, also defined as T_{50} (temperature where 50 % CO conversion is reached), of ~ 80 °C over Co_3O_4 in CO oxidation, while Thormählen et al. [42] even found a T_{50} of -63 °C. In the study by Xiaowei et al. [43] Co_3O_4 nanorods showed 100 % CO conversion even at -77 °C. These differences are apparently due to different feed composition, different morphology, texture and particle and crystallite size of Co_3O_4.

Subjecting the Co_3O_4 to a reduction pretreatment, the high catalytic activity at low temperatures was drastically reduced (increase of T_{50} by 70 °C) [40]. This is in contrast to studies by Skoglundh, Mergler and Jin (described in chapter 1.3.2) which revealed for noble metals loaded Co_3O_4 catalysts that the reduction pretreatment improved the catalytic activity in CO oxidation.

Concerning the CO oxidation mechanism over Co_3O_4 it is assumed that it occurs via a redox cycle [42,44]. However, the involved active states and oxygen species are still under discussion.

On the one hand Pollard et al. [44] postulated a mechanism where CO adsorbs on the Co^{2+} sites followed by the reaction with an oxygen bonded to a Co^{3+} ion to form CO_2 which desorbs from the surface. A partially reduced site (oxygen vacancy) is formed which can be reoxidized by oxygen from the gas phase. This is in agreement with the study by An et al. [13] where they identified the Co^{2+} states at the metal-oxide interface of a Pt/Co_3O_4 catalyst as active in CO oxidation.

On the other hand Jansson et al. [40] proposed a mechanism for a Co_3O_4/Al_2O_3 catalyst, where CO presumably adsorbs on a Co^{3+} site and reacts with a neighboring oxygen bonded to the Co^{3+} forming CO_2 which desorbs from the catalyst surface. Herein, oxygen from the gas phase can also refill the formed oxygen vacancy to reactivate the site again. This would be consistent with the study by Xiaowei et al. [43], who found out that Co_3O_4 nanorods which predominantly expose (110) facets that are rich in Co^{3+} exhibit higher catalytic activity in CO oxidation than conventional nanoparticles revealing (111) and (001) facets and thus have no enrichment in Co^{3+} on the surface. Therefore, he concluded that the activity depends on the amount of Co^{3+} sites. Possible deactivation mechanisms are discussed in chapter 1.3.4.

Besides the intensively studied Co_3O_4, lately also different iron oxides like αFe_2O_3, γFe_2O_3 and Fe_3O_4 became attractive candidates to study in their structure-activity behavior in low temperature CO oxidation. Maghemite (γFe_2O_3) for example also exhibits a spinel structure similar to the Co_3O_4 where Fe^{3+} ions are located in tetrahedral and octahedral sites, while the charge neutrality is fulfilled by the presence of cation vacancies [45]. If the vacancies are filled with Fe^{2+}, magnetite Fe_3O_4 is formed. However, the activity of these iron oxides was reported to be significantly lower compared to Co_3O_4. El-Sheikh et al. [46] revealed that over a pure iron oxide consisting of Fe_3O_4 and γFe_2O_3 full CO conversion was reached at temperatures of 200 °C.

However, the very high catalytic activity of different iron oxides in CO oxidation was mainly reported in combination with noble metals [7,19,17,33].

1.4 Aim of the work

Based on the debates and open questions, the aim of this work was to (1) synthesis a Co_3O_4 and a γFe_2O_3 supported Pd catalyst[1], (2) characterize the structure and the composition of the two catalysts, (3) determine and study the influence of the Pd loading and (4) the influence of the pretreatment (oxidative and reductive) on the catalytic activity in CO oxidation. Furthermore an insight should be gained into the nature of active states (e.g. SMSI state, oxidation states of the noble metal and the support), reaction intermediates and inhibiting surface species under relevant catalytic reaction conditions by means of *in situ* spectroscopic methods to approach towards an understanding of the CO oxidation and deactivation mechanisms together with an identification of active sites. For the characterization of the structure and the composition of the catalysts ex situ methods like N_2 sorption, X-Ray powder diffraction (XRD) and transmission electron microscopy (TEM) combined with energy-dispersive X-Ray spectroscopy (EDX) measurements were performed. The influence of the Pd loading on the catalytic activity of the catalysts in CO oxidation was determined via kinetic measurements and studied via CO/CO_2 adsorption followed by Fourier transform infrared spectroscopy (FTIR) and CO- and O_2 temperature-programmed desorption (CO-TPD/O_2-TPD) experiments. Furthermore, the influence of the pretreatment on the catalytic activity was estimated by subjecting the catalysts either to an oxidation or a reduction prior to the kinetic measurements and correlated with H_2 temperature-programmed reduction/oxidation (H_2-TPR/TPO) measurements. The applied *in situ* spectroscopy studies included *in situ* Fourier transform infrared (*in situ* FTIR) and *in situ* ambient-pressure X-ray photoelectron spectroscopy (APXPS).

[1] The Co_3O_4 was chosen because it is extensively used in its pure state due to its very high activity in CO oxidation at low temperatures and its even enhanced activity in combination with a noble metal. γFe_2O_3 was chosen as a support because it has a similar crystal structure to the Co_3O_4 and because it was also reported to be highly active in combination with noble metals [7].

Chapter 2

2 Experimental

2.1 Catalyst Preparation

Table 2.1.: Overview of the used chemicals.

Chemicals	Purity / %	Producer
$Pd(OAc)_2$	>99.9	Sigma Aldrich
Co_3O_4	>71 %	Fluka
γFe_2O_3		Sigma Aldrich
SiO_2		Alfa Aesar
Toluene	>99.5	Carl Roth

The oxide supported Pd catalysts were prepared by wetness impregnation of 2 g of the oxide supports Co_3O_4, γFe_2O_3 or SiO_2 with 84 mg of $Pd(OAc)_2$ dissolved in toluene[2], to obtain a 2 wt% Pd loading[3]. After impregnation, the catalysts were dried at 100 °C for 1h followed by a calcination step in static air at 400 °C for 4 h. The catalysts were denoted as oxidized PdO/Co_3O_4, PdO/Fe_2O_3 and PdO/SiO_2. The PdO/SiO_2 was only used as a reference catalyst in catalytic studies. In addition, the pure oxides Co_3O_4 and γFe_2O_3 were prepared as references by calcination at 400 °C for 4h as well. The oxide γFe_2O_3 was in the following denoted as Fe_2O_3.

[2] $Pd(OAc)_2$ could not be dissolved in methanol or ethanol wherefore toluene was taken as a solvent.

[3] 5 wt% Pd catalyst were also prepared but didn't show any significant difference in activity (shown in appendix).

2.2 Textural, structural and chemical characterization

2.2.1 Nitrogen sorption

The N_2 sorption experiments recording full adsorption-desorption isotherms were carried out at 77 K using Micrometrics ASAP 2020 for the pure oxide supports Co_3O_4, Fe_2O_3 and SiO_2.

The specific surface area (SSA_{BET}) was determined according to the Brunauer-Emmet-Teller (BET) method. The average pore diameter (D_p) and pore volume (V_p) were derived from the desorption branch of the isotherm based on Barrett–Joyner–Halenda (BJH) model. Before the measurements, the oxide supports were heated at 80 °C under vacuum for 3 hours for degassing.

2.2.2 X-Ray powder diffraction (XRD)

The XRD patterns were collected on a Philips X'Pert Pro XRD-diffractometer using a Bragg-Brentano focusing geometry with a Cu Kα radiation source (λ=0.1542 nm) and recorded in a 2θ scan from 5 to 90 ° with a step size of 0.02° and a time per step of 280 s. The calcined catalysts were directly taken for the analysis or were subjected to a reduction pretreatment externally. The reduction was performed ex situ in a flow of 5 % H_2 in He at 100°C for the Co_3O_4 supported Pd and at 300 °C for the Fe_2O_3 supported Pd catalysts. The reduced catalysts were denoted as Pd/CoO_x and Pd/FeO_x. Crystallite phases were identified by comparison the diffraction peaks with standard compounds from the diffraction data base. Crystallite sizes were calculated from Scherrer equation using the software package TOPAS. Based on the Rietveld refinement, a quantification of the different components was obtained for the prereduced catalysts.

2.2.3 Transmission electron microscopy (TEM)

The TEM images were obtained using a FEI TECNAI F20 S-TWIN at the University Service Center for Transmission Electron Microscopy, Vienna University of Technology. It was equipped with a field emission source and an energy-dispersive X-Ray (EDX) Si detector.

The TEM micrographs including bright field images, high resolution TEM (HRTEM) and high angle annular dark field (HAADF) image were recorded for the oxidized PdO/Co_3O_4 and PdO/Fe_2O_3 and the reduced Pd/CoO_x (red. 100 °C) and Pd/FeO_x (red. 300 °C) catalysts. The reduction was performed under the same conditions as the reduction of the samples prepared for the XRD measurements.

In addition, the scanning transmission electron microscope (STEM) Hitachi HD-2700 at the Electron Microscopy ETH Zurich (EMEZ) was utilized for the analysis of the samples including the oxidized PdO/Co_3O_4 and the pure Co_3O_4 where high angle annular dark field (HAADF) images were obtained.

The samples were prepared on a carbon film mounted on a copper grid.

2.2.4 CO and O_2 temperature-programmed desorption (CO-TPD/O_2-TPD)

The CO- and the O_2-TPD experiments were performed in a continuous flow fixed bed quartz tube reactor equipped with a quadrupole mass spectrometer (OmniStar). The experiments were conducted for all synthesized and calcined Co_3O_4 and Fe_2O_3 based catalysts.

In the case of the CO-TPD measurement, 20 mg of the catalyst was pretreated in synthetic air at 400 °C for 30 min to remove surface contaminants. After cooling down to RT in synthetic air, 5 % CO in He (50 ml min^{-1}) was purged through the catalyst for 30 min. Following this, pure He was flown and the catalyst was heated up to 600 °C with 10 °C min^{-1}, while the mass signal of CO and CO_2 was recorded.

For the O_2-TPD measurement, 80 mg of the catalyst was heated up in synthetic air to 400 °C and held for 30 min in pure O_2 flow (10 ml min^{-1}). After cooling down to RT, pure He was switched

on and the catalyst was heated up to 800 °C, while a mass spectrometer recorded the amount of desorbed O_2.

2.2.5 H_2 temperature-programmed reduction (H_2-TPR) and temperature programmed oxidation (TPO)

The H_2-TPR and the TPO experiments were performed in a continuous flow fixed bed quartz tube reactor coupled with a quadrupole mass spectrometer (QMS). Prior to the TPO experiment, the H_2-TPR was performed. The experiments were conducted for all synthesized Co_3O_4 and Fe_2O_3 based catalysts.

In the H_2-TPR experiment, 20 mg of the catalyst was pretreated in synthetic air at 400 °C and held for 30 min. After cooling down to RT, a flow of 10 % H_2 in He (50 ml min^{-1}) was passed through the sample and heated up to 500 °C with a rate of 5 °C min^{-1}, while the QMS was recording the mass signal of H_2.

After completing the H_2-TPR test, the sample was again cooled down to RT in He and the TPO was conducted. Therefore, the reduced catalyst was heated in a 10 % O_2 in He flow (50 ml min^{-1}) from RT to 600 °C with a rate of 10 ° min^{-1}, while the QMS was recorded the mass signal of O_2.

2.3 Kinetic measurements

Kinetic measurements were carried out in a continuous flow fixed bed quartz reactor under atmospheric pressure which was connected to the feed gas supply.

The flow rates of the reactants were controlled by calibrated mass flow controllers (MKS) for CO, O_2 and H_2 and rotameters for N_2 and synthetic air.

The reactant CO and the product CO_2 were recorded on-line with a HP 6890 gas chromatograph (GC) equipped with a 6 way-valve for injection, a HP-Plot Q column, a Flame Ionization Detector (FID) and a Thermal Conductivity Detector (TCD). The FID was used for quantification which detected CO and CO_2 as CH_4 after a mechanizing unit with the same sensitivity and CO conversion was calculated directly from the ratio of the peak areas of CO and CO_2.

The temperature was regulated via an Eurotherm temperature controller and was measured with a type K thermocouple placed in the reactor directly above the sample.

A scheme of the experimental set up is shown in figure 2.1.

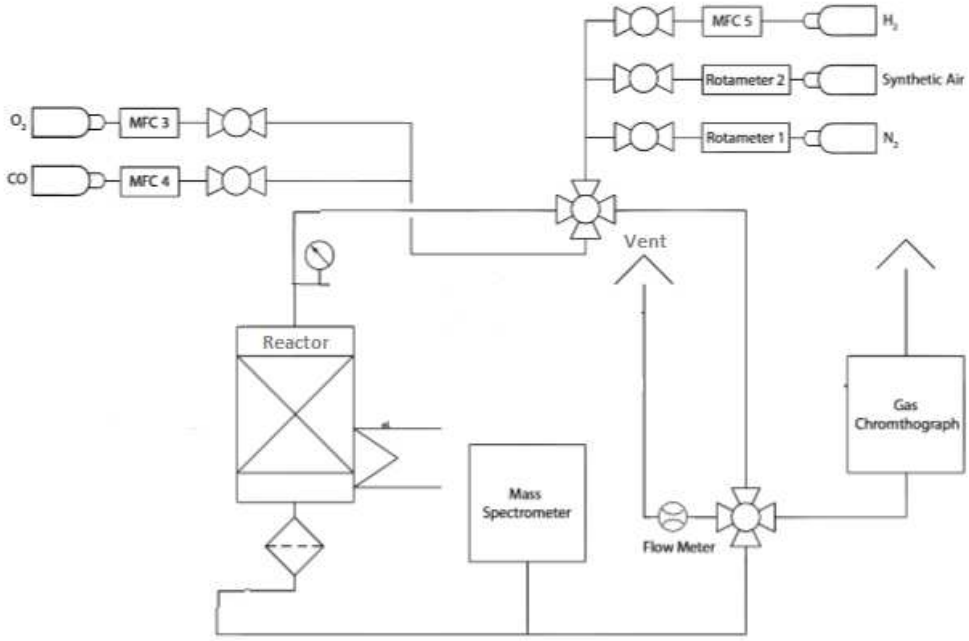

Figure 2.1: Scheme of the experimental set up for the catalytic measurements in the fixed bed flow reactor [47].

20 mg of the catalyst diluted with 100 mg of quartz sand was used for all experiments. The activity of the catalyst was measured after applying an oxidative, respectively a reductive pretreatment.

The reaction gas mixture consisted of 5 % CO and 10 % O_2 in He ($CO:O_2$ = 1:2), while the conditions during pretreatment for each of the investigated catalysts are listed in table 2.2. A total flow of 50 ml min^{-1} was chosen for all pretreatment and reaction gas mixtures. In the case of the PdO/Co_3O_4 catalyst, the kinetic measurements were also conducted in the absence of traces of moisture (3-10 ppm in the normal feed [43]) by using a cold trap filled with a mixture of ethanol and liquid N_2 (T= -80°C).

The time on stream experiment (TOS) was performed at RT where changes of activity were followed by a GC injections series till no CO conversion was observed anymore, followed by a stepwise temperature programmed experiment, consisting of 3 GC injections every 10 °C (15 min holding time at each temperature) and a heating ramp of 5 °C min^{-1}. The reactant CO and product CO_2 were analyzed in temperature intervals of 10 °C.

Table 2.2: Pretreatment conditions for the investigated catalysts used for kinetic measurments.

Pretreatment conditions	Oxidation at 400 °C; ½ h; 10 °C min^{-1} (syn. air)	Reduction; ½ h; 5 °C min^{-1} (5 % H_2 in N_2)	
T	at 400 °C	at 100 °C	at 300 °C
Sample	PdO/Co_3O_4 PdO/Fe_2O_3 Co_3O_4 Fe_2O_3 PdO/SiO_2	Pd/CoO_x* Pd/FeO_x	Pd/FeO_x

*The reduction pretreatment for the Pd/CoO_x was only conducted at 100 °C because it is known that at 300 °C the Co_3O_4 already transforms to the inactive metallic Co.

2.4 Fourier transform infrared spectroscopy (FTIR)

FTIR spectra were taken in transmission mode on a Bruker Vertex 70 spectrometer equipped with a mercury cadmium telluride (MCT) detector and with a resolution of 4 cm^{-1}. All FTIR measurements were recorded in the flow transmission cell, equipped with CaF_2 windows and containing the sample holder which was connected to a type K thermocouple, measuring the temperature, and a ring-shaped heating wire regulated via an Eurotherm controller. Each spectrum consisted of 256 scans (recording time: 2 min) to obtain a good signal to noise ratio. A background spectrum was recorded of the empty cell during He flow at RT, which was subtracted

from all other sample spectra. The spectra were evaluated with the OPUS software. For each FTIR experiment a fresh sample was prepared.

The sample (~ 4 mg) was pressed together with KBr, as a support, into a pellet, and placed into the sample holder. Prior to the IR experiment, the catalyst was subjected to an oxidation, respectively a reduction pretreatment. The procedure during the pretreatment, the IR adsorption and *in situ* experiments are listed in table 2.3. The gas flows were purged through the flow cell controlled by MKS mass flow controllers. The total flow rate of the pretreatment gas mixtures was kept at 50 ml min^{-1}, while a total flow rate of 25 ml min^{-1} was used for all IR experiments. In the case of the *in situ* experiments, an online GC and a mass spectrometer were coupled to the exit of the flow cell and recorded simultaneously the reactants and the product (defined as *operando* FTIR) [48].

Table 2.3: The overview of the procedures for the pretreatment, the IR adsorption and the *in situ* experiments.

Procedures		
Pretreatment	IR adsorption experiments	*in situ* IR experiments
Oxidation at 400 °C; ½ h; 10 °C min^{-1} (synthetic air)	1. 5 % CO/CO_2 in He flow at RT; ½ h	1. 5 % CO + 10 % O_2 in He flow at RT; 1 h
	2. He flow at RT; 1h	2. He flow at RT; 1h
Reduction at 100 °C; ½ h; 5 °C min^{-1} (5 % H_2 in N_2)	3. 5 % CO/CO_2 in He flow from RT to 200 °C; 2 °C min^{-1}	3. 5 % CO + 10 % O_2 in He flow from RT to 200 °C; 2 °C min^{-1}
	4. He flow at 200 °C; ½ h	4. He flow at 200 °C; ½ h

2.5 Ambient pressure photoelectron spectroscopy (APXPS)

The APXPS measurements were performed at the ISISS beam line at BESSY II, Berlin, Germany. Details of the set-up have been described previously [49]. Measurements were only conducted over the PdO/Co_3O_4 catalyst.

The catalyst was pressed into a self-supporting wafer and mounted on a sapphire sample holder. It was subjected to an oxidation pretreatment (0.5 mbar O_2 at 400 °C for ½ h at flow rates of 3.5 ml min^{-1}) in the reaction cell to remove contaminates e.g. carbon.

After cooling down to RT in oxygen atmosphere, the reaction mixture (0.5 mbar $CO+O_2$) was introduced at flow rates of 3 ml min^{-1} for CO and 1.5 ml min^{-1} for O_2 ($CO:O_2$ = 1:2), while a differential quadrupole mass spectrometer (QMS) and a GC were simultaneously recording the reactants and the products. The Pd 3d, Co 2p, O 1s and C 1s core level spectra were recorded with appropriated selected excitation photon energies hv = 1015, 540, 730 and 465 eV resulting in the same electron kinetic energies (E_{kin} = 200 eV).

In addition, a depth profile analysis was applied for the Pd 3d (hv= 540, 740, 940 and 1040 eV) and the Co 2p (hv = 1015 and 1215 eV) to obtain information about the atomic composition at different sample depths. The spectra obtained at different excitation energies were normalized by the storage ring current and the energy-dependent incident photon flux, which was obtained from the previous measurements using a gold foil.

The corresponding inelastic mean free path was calculated for pure Pd using calibration curves from the literature [50]. For calculating the atomic ratio of the fitted areas of the Pd 3d and the Co 2p core levels, the areas were first normalized by the atomic subshell photo ionization cross section, listed in table A1.

The XPS O 1s spectra were calibrated in respect to the 2^{nd} order peak of the O 1s, while all other XPS spectra were calibrated with respect to the Fermi level of the O 1s. The fitting of the Pd 3d doublet was performed with mixed Gaussian/Lorentzian functions, while the relative ratio and the distance between the $3d_{3/2}$ and $3d_{5/2}$ core level peaks were kept constant. The subtraction of the background was done by the Shirley method. The elemental atomic ratios were obtained by dividing the calculated areas of the fitted peaks.

Chapter 3

3 Results and Discussion

3.1 Textural and structural characterization

3.1.1 N_2 sorption

The N_2 sorption measurements were carried out for the three different oxide supports Co_3O_4, Fe_2O_3 and SiO_2.

The obtained N_2 adsorption-desorption isotherms for the three oxides are shown in figure A1 (A→appendix).

From the N_2 adsorption-desorption isotherms the texture parameters including specific surface areas SSA_{BET}, average pore sizes D_p and pore volume V_p, which are known to be closely related to the catalytic properties [51], were calculated and are summarized in Table 3.1. For the oxides Co_3O_4 and Fe_2O_3 the texture parameters were very similar with e.g. a SSA_{BET} of 38.3 and 37.3 m^2 g^{-1}, respectively. The SiO_2 exhibited a significantly higher SSA_{BET} of 88.5 m^2 g^{-1}. We assume that the SSA_{BET} for the different oxides did not change after impregnation of Pd, based on previous results [10,52]. Thus, it is reasonable to directly compare the catalytic properties of the Co_3O_4 and Fe_2O_3 based catalysts excluding strong SSA_{BET}, D_p and V_p influences. For the SiO_2 based catalysts, we have to consider the higher SSA_{BET} when comparing catalytic properties in the CO oxidation experiments.

Table 3.1: Textural properties of the pure oxides Co_3O_4, Fe_2O_3 and SiO_2.

Sample	SSA_{BET} / m^2 g^{-1}	D_p / nm	V_p / cm^3 g^{-1}
Co_3O_4	38.3	16	0.16
Fe_2O_3	37.3	15.8	0.09
SiO_2	88.5	21.7	0.3

3.1.2 XRD

X-Ray diffractograms were recorded *ex situ* for the oxidized (400 °C) and the reduced (100, respectively 300 °C) supported Pd catalysts and the pure supports to determine characteristic parameters including crystalline phases, the crystallite sizes and the catalyst phase composition. These structural parameters are known to be closely related to e.g. the metal dispersion and size, the active sites and overall to catalytic properties [51]. Panagiotopoulou et al. [53] for example showed for a Pt/TiO_2 catalyst that the conversion of CO was strongly enhanced with decreasing crystallite size of the metal oxide support.

The XRD pattern of the Co_3O_4 based catalysts including PdO/Co_3O_4, Pd/CoO_x (red. 100°C) and the pure Co_3O_4 are shown in figure 3.1(a) whereas the Fe_2O_3 based catalysts including PdO/Fe_2O_3, Pd/FeO_x (red. 300°C) and Fe_2O_3 are represented in figure 3.1(b).

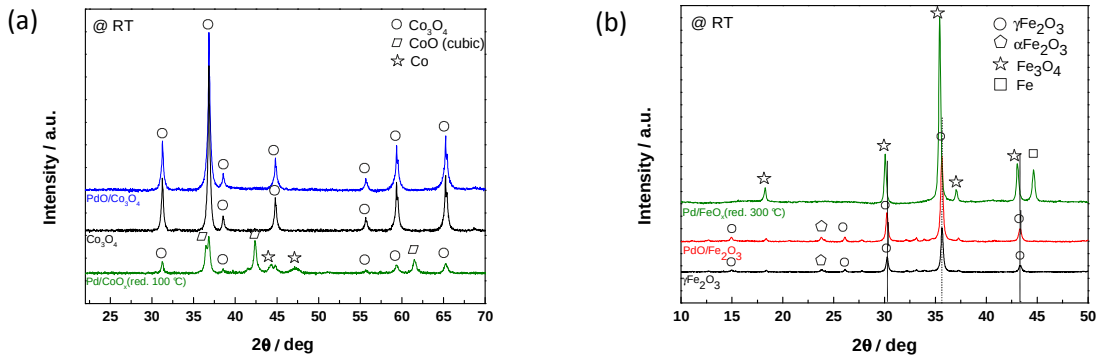

Figure 3.1: X-ray diffractograms of (a) PdO/Co_3O_4 (blue), Pd/CoO_x (red. 100 °C) (green) and pure Co_3O_4 (black) and (b) of PdO/Fe_2O_3 (red), Pd/FeO_x (red. 300 °C) (green) and pure Fe_2O_3 (black) recorded at RT.

The diffraction patterns for the oxidized PdO/Co_3O_4 and pure Co_3O_4 samples, shown in figure 3.1(a), were identical and included diffraction peaks which can be ascribed to a spinel Co_3O_4 phase. This indicates that no phase transformation had occurred during the impregnation. The diffraction pattern for Pd/CoO_x (red. 100 °C) clearly revealed a partial phase transformation of Co_3O_4 to cubic CoO and metallic Co (Composition: 44 % Co_3O_4; 42 % CoO; 14 % Co). Neither the oxidized PdO/Co_3O_4 nor the Pd/CoO_x (red. 100 °C) catalyst, revealed diffraction peaks corresponding to a Pd phase suggesting that the Pd particles were highly dispersed on the catalyst

surface [54]. Another reason for the absence of the Pd diffraction peaks could be the low loading of only 2 wt%.

In the case of the oxidized PdO/Fe_2O_3 and the pure Fe_2O_3 sample, the diffraction patterns were almost identical exhibiting both the presence of mainly maghemite Fe_2O_3 and a minor amount of hematite Fe_2O_3 (see figure 3.1(b)). In contrast, the Pd/FeO_x revealed diffraction peaks mainly related to magnetite Fe_3O_4 and a minor amount of metallic Fe indicating that Fe_2O_3 had exclusively transformed to Fe_3O_4 and Fe (Composition: 90 % Fe_3O_4; 10 % Fe). Neither the oxidized PdO/Fe_2O_3 nor the Pd/FeO_x (red. 300 °C) catalyst revealed diffraction peaks of a Pd phase suggesting the same as for Co_3O_4 supported Pd catalysts, that the Pd particles were highly dispersed on the catalyst surface. Based on the Scherrer-Equation, crystallite sizes were calculated for all Co_3O_4 and Fe_2O_3 based catalysts and listed in table 3.2.

Table 3.2: Calculated crystallite sizes for the Co_3O_4 and Fe_2O_3 based catalysts.

Sample	Crystallite sizes / nm		
	Co_3O_4	CoO	Co
PdO/Co_3O_4	26.8	/	/
Pd/CoO_x (red. 100 °C)	29.1	25.7	10.8
Co_3O_4	31.6	/	/

Sample	Crystallite sizes / nm		
	Fe_2O_3	Fe_3O_4	Fe
PdO/Fe_2O_3	39.7	/	/
Pd/FeO_x (red. 300 °C)	/	53.8	33.2
Fe_2O_3	38.7	/	/

Oxidized PdO/Co_3O_4 exhibited a crystallite size of 26.8 nm for the Co_3O_4 phase, which was slightly smaller compared to the crystallite size of pure Co_3O_4 with 31.6 nm presumably resulting from the impregnation process of Pd (see table 3.2). After the reduction at 100 °C of the catalyst, a crystallite size of 29.1 nm for the Co_3O_4 phase was obtained indicating that no significant growth of the crystallite size had occurred. For the CoO and metallic Co phases, crystallite sizes of 25.7 and 10.8 nm were calculated.

In the case of the oxidized PdO/Fe_2O_3 and the pure Fe_2O_3 catalysts, similar crystallite sizes of 39.7 and 38.7 nm for the Fe_2O_3 phase were obtained (shown in table 3.2). For the reduced Pd/FeO_x (red. 300 °C) catalyst, the transformation of the Fe_2O_3 phase to the Fe_3O_4 and metallic Fe phases resulted in changes of the crystallite sizes. The magnetite Fe_3O_4 phase had a significantly larger crystallite size of 53.8 nm, while the crystallite size of the metallic Fe exhibited a smaller value of 33.2 nm compared to that of the Fe_2O_3 phase in the oxidized sample.

To sum up the XRD results, we can state that the crystallite sizes of the Co_3O_4 based catalyst were slightly smaller compared to the crystallite sizes of the Fe_2O_3 based catalysts.

Loading Pd on Co_3O_4 and Fe_2O_3 had neither changed the present crystalline phase nor the crystallite sizes of the catalysts enabling the comparison of catalytic properties between the supported Pd catalysts and the pure supports, while excluding strong crystallite phase and size effects.

In contrast, the change of the phase composition for both, the Co_3O_4 and Fe_2O_3 based catalysts after the reduction process, is important to consider when comparing catalytic properties of the catalysts. Horv et al. [19] for example, stated for an Au/Fe_2O_3 catalyst that the support composition whether it consists of γFe_2O_3 or a mixture of Fe_3O_4 and FeO influenced the catalytic activity in CO oxidation. Moreover, we can state that highly dispersed Pd particles are presumably present on the catalyst surface for both, the Co_3O_4 and the Fe_2O_3 based catalyst, which is from importance in obtaining a high catalytic activity [22,55].

3.1.3 TEM

To obtain information about the morphology and explicit details of particles sizes and shapes of the metal and the support, bright field TEM, HRTEM and HAADF micrographs in combination with EDX spectra were recorded. The supported Pd catalysts after oxidation and reduction pretreatment were examined with TEM.

Bright field TEM, HRTEM and HAADF images of the PdO/Co_3O_4 are shown in figure 3.2.

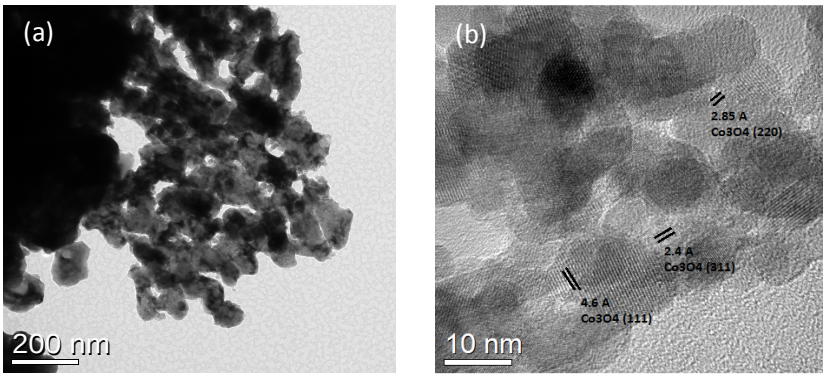

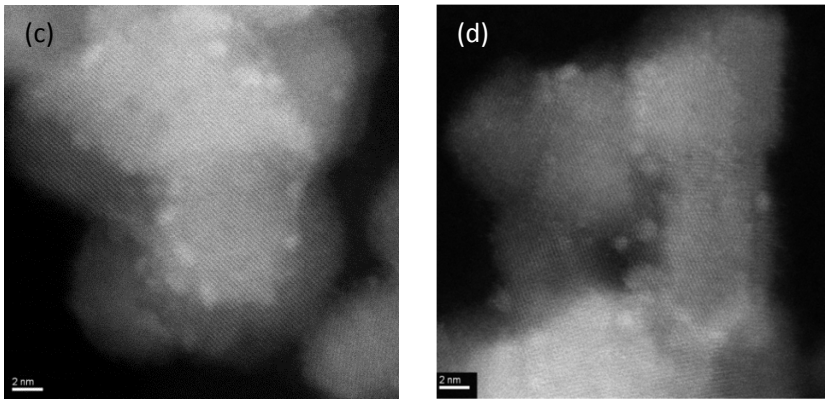

Figure 3.2: (a) Bright field TEM and (b) HRTEM image of the oxidized PdO/Co_3O_4 catalyst and (c,d) HAADF images of the oxidized PdO/Co_3O_4 catalyst. The HAADF images were obtained on the STEM Hitachi at ETH Zurich.

No details about the morphology of the PdO/Co_3O_4 catalyst could be gained from the bright field TEM image, shown in figure 3.2(a).

However, HRTEM images of the PdO/Co_3O_4 catalyst, displayed in figure 3.2(b), indicated spherical Co_3O_4 particles with a homogeneous size distribution and particle diameters between 10 and 15 nm. Moreover, different crystal planes including (111), (311) and (220) corresponding to Co_3O_4, were identified. Nevertheless, characteristic crystal planes for PdO or Pd were not found. Also the HAADF images, shown in figure A2 (a,b) , did not reveal detectable single Pd particles, and therefore we assumed that the PdO particles were highly dispersed and in the sub-nanometer range, which is in good agreement with the XRD results shown in Figure 3.1(a).

This assumption was proved by the HAADF images obtained from the STEM Hitachi HD-2700, shown in figure 3.2(c,d), where bright spots from the sub-nm range up to 2 nm could be identified which were assigned to the Pd particles. Furthermore, it seems likely that the Pd particles were epitaxially grown on the support which was also reported in literature [20]. However, it is not reasonable to calculate a particle size distribution of the Pd particles as the number of measured particles was too small.

In the case of the Pd/CoO_x (red. 100 °C) catalyst, the HRTEM images revealed a change in the morphology of the support from spherical particles to more angular shaped ones, shown in figure A3 (c,d), apparently resulting from the phase transformation to CoO and metallic Co according to XRD and EDX analysis. In addition, the HAADF images of Pd/CoO_x, shown in figure A3 (a,b), revealed highly dispersed bright spots with diameters of 1-3 nm. We assume that the bright spots

correspond to Pd according to the EDX analysis. We suggest that the Pd particles had aggregated during the reduction pretreatment as they appeared to be larger in size.

Micrographs of the PdO/Fe_2O_3, recorded in bright field TEM, HRTEM and HAADF mode are shown in figure 3.3.

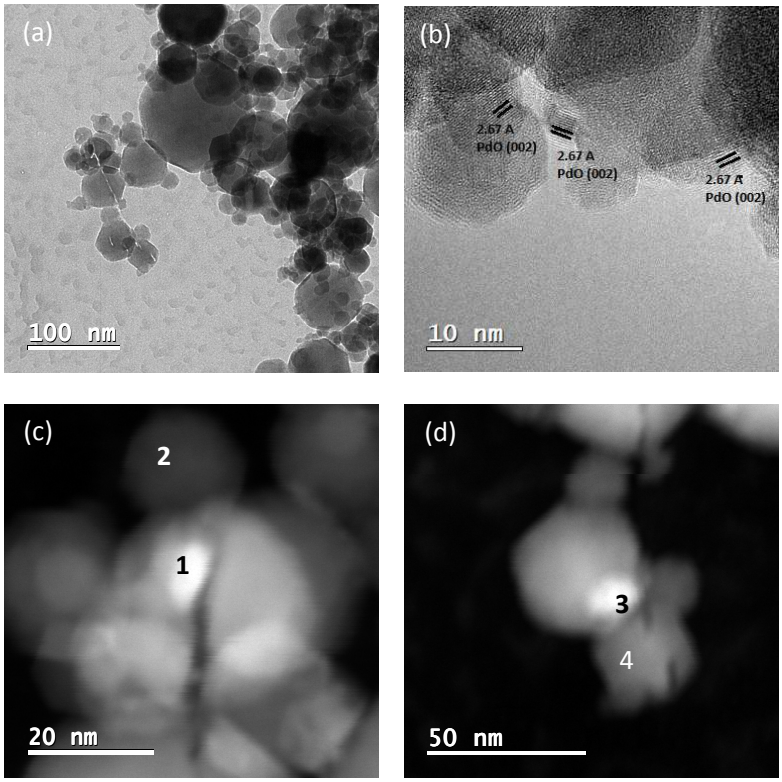

Figure 3.3: (a) Bright field TEM, (b) HRTEM and (c,d) HAADF images of the PdO/Fe_2O_3 catalyst.

The bright field TEM micrograph of PdO/Fe_2O_3, shown in figure 3.3(a), revealed that the particles of the support Fe_2O_3 are almost spherical but irregular in size and between 10 and 100 nm. The HRTEM images, as for example, seen in figure 3.3(b), revealed (002) crystallographic planes, corresponding to the PdO phase.

In the HAADF images, shown in figure 3.3(c,d) , bright spots with sizes between 5-10 nm could be observed which were identified as Pd particles according to EDX (EDX spectra are shown in figure A6).

For reduced Pd/Fe_2O_3 (300 °C), HAADF images (shown in figure A4 (e)) revealed neither changes in particle sizes nor in the morphology of the Fe_2O_3 support.

To summarize the results from the TEM measurements, we can state that the Pd particles on Co_3O_4 are very small with mean sizes from the sub-nm range up to 2 nm, whereas the Pd particles on the Fe_2O_3 are in the size range of 5-10 nm. The reason for the differences in the Pd particle sizes on the Co_3O_4 and the Fe_2O_3 supports can arise from the difference in the chemical nature of the supports and thus, the interaction of the surface with the Pd precursor species during the impregnation process. Furthermore, the supports Co_3O_4 and Fe_2O_3 revealed different size distributions, with a homogeneous particle size distribution for Co_3O_4 (~ 10 nm) and an inhomogeneous one for the Fe_2O_3 support (10-100 nm). These differences in particle size of Pd and the supports could influence the catalytic properties in CO Oxidation and thus, have to be considered when comparing catalytic properties of the catalysts, even though the SSA_{BET} was very similar.

3.2 Influence of the Pd loading

3.2.1 Kinetic studies in CO oxidation reaction

For the kinetic measurements of PdO/Co_3O_4 and PdO/Fe_2O_3 in comparison to the pure Co_3O_4 and Fe_2O_3 supports in the CO oxidation reaction ($CO:O_2$ = 1:2), the catalysts were first subjected to time-on stream experiments (TOS) at RT, discussed in chapter 3.5., till a complete deactivation of the catalysts was reached, followed by temperature-programmed experiments. In order to compare the catalytic activities, different kinetic parameters were evaluated from the light-off curves obtained from the temperature-programmed experiments. These kinetic parameters included on the one hand the so called light-off temperature for 50 % CO conversion T_{50} (°C) and on the other hand reaction rates r (mol s^{-1} g^{-1}) at two different temperatures (50 and 70 °C) at where the rates were not limited by the pore or film diffusion (CO conversion < 15 %). Moreover, activation energies E_a (kJ mol^{-1}) were calculated for differentiating between potentially different reaction mechanisms and rate determining steps [56,57]. To estimate the contribution of

only Pd nanoparticles in the catalytic activity, Pd supported on an inert oxide e.g. SiO_2 [13], was studied in the CO oxidation experiments as well.

Figure 3.4 shows the light-off curves for PdO/Co_3O_4, PdO/Fe_2O_3, PdO/SiO_2 and the pure oxides Co_3O_4 and Fe_2O_3.

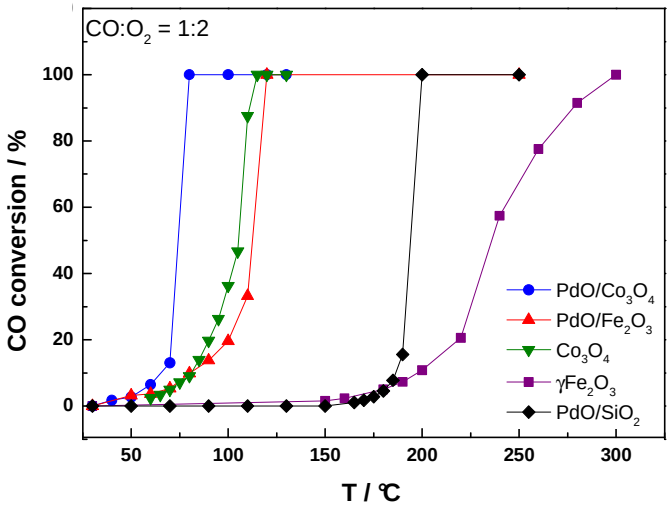

Figure 3.4: CO conversion over the PdO/Co_3O_4, PdO/Fe_2O_3 and PdO/SiO_2 and the pure Co_3O_4 and Fe_2O_3 catalysts as a function of temperature. The catalysts were previously treated in synthetic air (400 °C; ½ h) and subjected to time-on stream experiments at RT.

According to the T_{50} values and the reaction rates given in table 3.2, the activity follows the order $PdO/Co_3O_4 < PdO/Fe_2O_3 < Co_3O_4 < PdO/SiO_2 < Fe_2O_3$. Thus, loading Pd on Co_3O_4, respectively on Fe_2O_3 greatly enhanced the catalytic activity, which is in agreement with literature [7,23]. The greatest enhancement in activity was achieved for the PdO/Fe_2O_3 catalyst (decrease of T_{50} by 120 °C) compared to pure Fe_2O_3 with a low intrinsic activity (T_{50}= 230 °C). The activity of PdO/Co_3O_4 was only slightly increased (decrease of T_{50} by 30 °C), though the catalyst revealed a higher activity than PdO/Fe_2O_3 due to a high intrinsic activity of pure Co_3O_4 (T_{50}= 105 °C). The high intrinsic activity of pure Co_3O_4 was expected as its high activity is well established in literature [39].

As stated before, PdO/SiO_2 showed significantly less CO oxidation activity compared to PdO/Co_3O_4 and PdO/Fe_2O_3 implying that the enhancement in activity cannot be simply explained

by summing up the intrinsic activities of the Pd particles (represented by the activity of PdO/SiO_2) and the pure Co_3O_4 or the Fe_2O_3 catalyst, respectively.

These results lead to the following discussions and conclusions.

For PdO/SiO_2 it is well known that the CO oxidation reaction follows the competitive Langmuir-Hinshelwood mechanism where O_2 has to adsorb and dissociate on the same sites on Pd as CO to get activated and to enable the conversion of CO to CO_2. Therefore, a relatively high temperature (in our case 175 °C) is required. In the case of PdO/Co_3O_4 and PdO/Fe_2O_3, the activation of O_2 already occurs at lower temperatures revealed by the significantly lower light-off temperatures (T_{50}) of 75 and 110 °C which lets us conclude that the supports Co_3O_4 and Fe_2O_3 have a major promotional effect in activating oxygen species for CO oxidation and thus, changing the reaction mechanism compared to PdO/SiO_2. However, at this state we cannot prove if the early on oxygen activation arise from a present SMSI state at the metal-support interface or results from a bifunctional mechanism where CO adsorbs on Pd and oxygen on the support followed by a reaction to CO_2 due to an oxygen spillover effect to Pd. Furthermore, we cannot explain why the enhancement is greater for the PdO/Fe_2O_3 compared to the PdO/Co_3O_4 catalyst. A possible reason could be a different reaction mechanism involving different adsorption sites resulting from a different nature of the interaction between the noble metal and the support or/and from different Pd particle sizes (sub-nm to 2 nm for the PdO/Co_3O_4 catalyst, respectively 5-10 nm for the PdO/Fe_2O_3) or/and oxidation states of the metal and the support. Strong effects of the slightly different crystallite and particle sizes of the supports on the differences in catalytic enhancement can be most likely neglected.

Table 3.3: Kinetic parameters including T_{50}, reaction rates and the E_a calculated for the supported Pd catalysts and pure oxides in CO oxidation (50 mbar CO + 100 mbar O_2).

Sample	T_{50} / °C	reaction rate r / mol s^{-1} g^{-1} 10^{-6}		E_a / kJ mol^{-1}
		at 50 °C	at 70 °C	
PdO/Co_3O_4	~75	3.6	10.9	40
PdO/Fe_2O_3	~110	2.5	4.1	38
Co_3O_4	~105	1.2	3.6	66
Fe_2O_3	~235	0	0	65
PdO/SiO_2	~175	0	0	169

Besides the T_{50} and the reaction rates, the E_a are calculated and compared in table 3.3. and resulted from the obtained Arrhenius plots, shown in A7. The Co_3O_4 and Fe_2O_3 supported Pd catalysts exhibited similar E_a values of 40 and 38 kJ mol^{-1} suggesting that the rate determining step might be the same, though the reaction mechanism could differ due to different T_{50} values as it was mentioned before [56]. The pure oxides Co_3O_4 and Fe_2O_3 exhibited higher E_a values of 66 and 65 kJ mol^{-1} compared to the Co_3O_4 and Fe_2O_3 supported Pd catalysts suggesting that the rate determining step of the reaction had changed after loading Pd. For PdO/SiO_2, the E_a was significantly higher with a value of 169 kJ mol^{-1} compared to all other investigated catalysts.

Thus, the calculated activation energies over the different catalysts support the assumption of a different reaction mechanism over PdO/Co_3O_4 and PdO/Fe_2O_3 compared to PdO/SiO_2. Also the reaction orders for the PdO/Co_3O_4 catalyst which were determined by C. Herzig from our group with respect to the CO and the O_2 reactants at a temperature of 60 °C, indicate that the reaction does not follow the competitive Langmuir-Hinshelwood mechanism over PdO/Co_3O_4 as they revealed positive values for both, the CO (0.24) and the O_2 (0.25) reactants.

However, at this state we cannot explain how the reaction proceeds and where and which kind of oxygen species (chemisorbed oxygen, sub-surface oxygen, surface oxides or bulk oxide) reacts with CO. Further studies described in the following will provide more insight into the adsorption sites and surface species on the catalyst surface and thus, the reaction mechanism and a potential present SMSI state.

3.2.2 Study of CO and CO_2 adsorption behavior by FTIR

In order to find the origin of enhancement in catalytic activity after loading the catalysts with Pd, the CO and CO_2 adsorption behavior was studied for PdO/Co_3O_4 and PdO/Fe_2O_3 and compared to the pure Co_3O_4 and Fe_2O_3 catalysts followed by FTIR spectroscopy. Information about changes of the CO/CO_2 adsorption sites, the nature of adsorbed species and the strength of the CO and CO_2 chemical bond to the catalyst surface after loading with Pd were obtained [58,59].

The FTIR spectra of PdO/Co_3O_4 and pure Co_3O_4 as well as of PdO/Fe_2O_3 and pure Fe_2O_3 during 5 % CO (50 mbar) in He flow at RT are displayed in figure 3.5 (a,c). The time resolved FTIR spectra recorded in He flow after the CO exposure are shown in figure 3.5 (b,d).

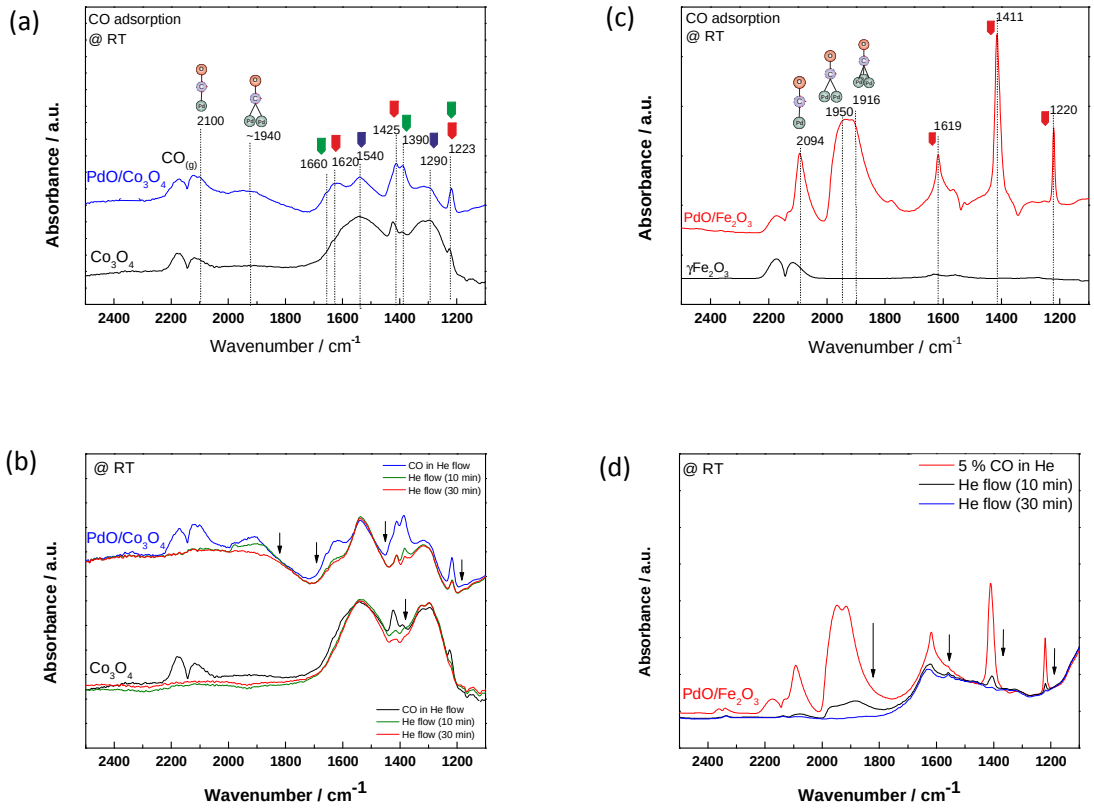

Figure 3.5: FTIR spectra of the PdO/Co_3O_4 (blue curve) and the Co_3O_4 (black curve) catalysts recorded at RT in (a) 5 % CO (50 mbar) in He flow and (b) 5 % CO in He flow followed by flushing in He only (10 and 30 min); FTIR spectra of the PdO/Fe_2O_3 (red curve) and the Fe_2O_3 (black curve) catalysts in (c) 5 % CO (50 mbar) in He flow and (d) 5 % CO in He flow followed by flushing in He flow (10 and 30 min). The catalysts were pretreated in synthetic air (400 °C; ½ h). The structures of the observed carbonates, marked with different colored symbols, are visualized in table 3.4-3.5.

In all FTIR spectra, displayed in figure 3.5, bands in the region of 2200-2050 cm^{-1} were corresponding to gaseous CO. The IR spectra of the PdO/Co_3O_4 and the pure Co_3O_4 catalyst, shown in figure 3.5(a), exhibited similarities but also some differences in the CO absorption behavior. Both exhibited carbonate/bicarbonate species in the region of 1800-1100 cm^{-1} in agreement with previous findings [23,44,60-63]. The vibrational bands at 1540 and 1290 cm^{-1} could be assigned to bidentate carbonates [60,61] whereas bicarbonates gave rise to bands at 1620, 1425 and 1223 cm^{-1} (bidentate) and to bands at 1660, 1390 and 1223 cm^{-1} (mondentate), respectively [61,62]. The amount of bidentate carbonate species relative to the amount of

bicarbonates was significantly higher on pure Co_3O_4 compared to PdO/Co_3O_4. Similar results were observed by Luo et al. [23], where bidentate carbonates were suppressed in intensity on Pd/Co_3O_4-CeO_2 compared to pure Co_3O_4-CeO_2. They argued the suppression in intensity by a decreased surface area due to the Pd loading.

Back to our study, the CO adsorption on the PdO/Co_3O_4 catalyst further resulted in two additional weak bands at 2195 and ~1940 cm^{-1}, where the former could be attributed to linear bonded CO on Pd^o and the latter to two different species including bridged and 3 fold-hollow (3-fh) bonded CO on Pd^o [64,65]. No CO bands on Pd^{1+} (2120-2110 cm^{-1}) neither on Pd^{2+} (2180-2160 cm^{-1}) [64,65] could be detected suggesting the absence of ionic $Pd^{\delta+}$ adsorption sites. Carbonyl bands bonded to Co^{2+} or Co^{3+} were also not found neither in the high frequency range between 2208- 2120 cm^{-1} nor in the low frequency range between 2080-2060 cm^{-1} [61]. This does not surprise as it was reported in literature [61] that they are easily removable, respectively easily transformed to carbonates.

To investigate the strength of chemical bonding of the adsorbed species, time resolved IR spectra of PdO/Co_3O_4 and Co_3O_4 were recorded for 60 min in He flow after the CO exposure shown in figure 2.3(b). It was revealed that in the case of PdO/Co_3O_4, the small amount of CO adsorbed on Pd^o was weakly bonded as the intensity decreased and disappeared after 30 min. The bicarbonate species on both catalysts decreased in intensity too whereas the decrease was more pronounced on PdO/Co_3O_4. In contrast, the intensity of bidentate carbonates remained constant. Thus, the bidentate carbonate species were strongly bonded, whereas the bicarbonate species were more weakly bonded to the catalyst surface.

In addition, CO_2 adsorption experiments were also carried out on PdO/Co_3O_4 and Co_3O_4, shown in A13, to find further causes for the difference in activities of the PdO/Co_3O_4 and the Co_3O_4. However, the CO_2 adsorption experiments revealed almost no adsorption of CO_2 neither on the PdO/Co_3O_4 nor on the Co_3O_4 catalyst.

In the case of PdO/Fe_2O_3 and pure Fe_2O_3, the CO adsorption behaviors were completely different highlighted in figure 3.5(c). On PdO/Fe_2O_3 bicarbonates predominated corresponding to bands at 1619, 1411 and 1220 cm^{-1}. In addition, a sharp and strong vibration band at 2094 cm^{-1} assignable to linear bonded CO on Pd^o and a band at ~ 1930 cm^{-1} characteristic for two species including bridged (1950 cm^{-1}) and hollow (1916 cm^{-1}) bonded CO on Pd^o emerged.

In contrast, on pure Fe_2O_3 no CO adsorption species appeared at all, which is in agreement with Daniells' study [31] of an αFe_2O_3 catalyst however in contradictions to other previous adsorption studies of different iron oxides reporting CO adsorption in the form of carbonates [46,66]. However, at this moment we have no explanation for the absence of CO bands on pure Fe_2O_3.

Moreover, the CO_2 experiments, shown in figure A14, revealed that CO_2 was adsorbed as bicarbonates with bands at 1619, 1411 and 1220 cm^{-1} on both, the PdO/Fe_2O_3 and the Fe_2O_3 catalyst. However, in the case of PdO/Fe_2O_3, bicarbonates were easily removed in He, in contrast to pure Fe_2O_3 where they were strongly bond to the surface at RT.

Table 3.4 summarizes the assignments of the observed IR bands and their corresponding frequencies and compares them with literature. The frequencies of the assigned IR bands stated in literature slightly differ from the observed frequencies in our study as the IR spectra in literature were recorded over a variety of different oxides.

We can conclude that loading Pd on Co_3O_4 resulted in the following differences in the CO adsorption behavior compared to pure Co_3O_4: (1) A higher amount of weakly bonded bicarbonates in relation to the total amount of carbonates and (2) small amounts of easily removable adsorbed CO on metallic Pd. For PdO/Fe_2O_3, the addition of Pd even created CO adsorption sites on the catalyst surface compared to pure Fe_2O_3 with no CO adsorption capacity at all. These findings are in good agreement with the different intrinsic activities of the pure oxides and the enhanced activities after loading Pd.

Comparing the CO adsorption behavior of Co_3O_4 and Fe_2O_3 supported Pd catalysts, it is noticeable that severely less CO adsorbed on Pd for PdO/Co_3O_4 compared to PdO/Fe_2O_3, although the Pd loading is 2 wt% on both catalysts. Possible reasons are discussed in detail in chapter 3.4.1 involving the *in situ* studies.

Table 3.4: Assigned IR bands corresponding to CO adsorbed on Pd species and compared to literature.

	IR band / cm^{-1}			
	This work			Literature*
Species	ν_s(CO)			ν_s(CO)
Sample	PdO/Co_3O_4	PdO/Fe_2O_3	PdO/SiO_2	
CO on Pd^o (linear)	2100	2094	2100	2100-2050
CO on Pd^o (bridged)	1940	~1950	1990	~1985
CO on Pd (111) (bridged)				1939–1948
CO on Pd (100) (bridged)				1990-1970
CO on Pd^o (hollow)		1916	1940	1940-1920
CO on Pd^{1+} (linear)	2140	2140	2120	2120-2110
CO on Pd^{2+} (linear)		2150	2160	2180-2160

Scheme 3.1: Schematic illustration of carbonates.

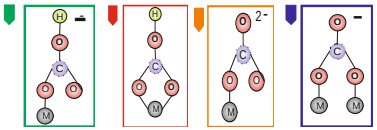

*[64,65] ** [61,63]

Table 3.5: IR bands corresponding to carbonate species adsorbed on the oxides Co_3O_4 and Fe_2O_3 and compared to literature (different oxides).

	IR band / cm^{-1}														
Species	$\nu_{sy}(COO^-)$			$\nu_{as}(COO^-)$			ν(OH)			δ(COH)			ν(CO)		
Sample	Co_3O_4	Fe_2O_3	Literature	Co_3O_4	Fe_2O_3	Literature	Co_3O_4	Fe_2O_3	Literature	Co_3O_4	Fe_2O_3	Literature	Co_3O_4	Fe_2O_3	Literature
Bicarbonates (monodentate)	1390		1420-1390*	1660		1650-1625*			3658*	1223		1250-1180**			
Bicarbonates (bidentate)	1425	1411	1440-1415**	1620	1620	1625-1600*		3600	3625*	1223	1220	1250-1180**			
Monodendate carbonates		1380	1370 1300**		1476	1470-1530**									1080-1040
Bidendate carbonates			1030-980 **	1290	1310	1270-1250**							1540	1540	1670-1530**

3.2.3 Study of CO and O_2 desorption behavior via CO- and O_2-TPD

In order to get further insight into the underlying mechanistic behaviour for the enhanced activity of the Co_3O_4 and Fe_2O_3 supported Pd catalysts, we investigated whether the Pd loading also changes the CO and O_2 desorption behavior by performing CO- and O_2-TPD experiments. Herein, we can point out that the lower the desorption temperature of CO and O_2 is, the weaker is the adsorption of CO and the easier the availability of reactive oxygen species on the catalyst surface. Therefore, low desorption temperatures would suggest a high catalytic activity of the catalyst in CO oxidation at low temperatures.

Figure 3.6(a) displays the TPD profiles of CO_2 after the CO adsorption, while in figure 3.6(b) the TPD profiles of O_2 on the Co_3O_4 supported Pd and the pure Co_3O_4 catalyst are compared.

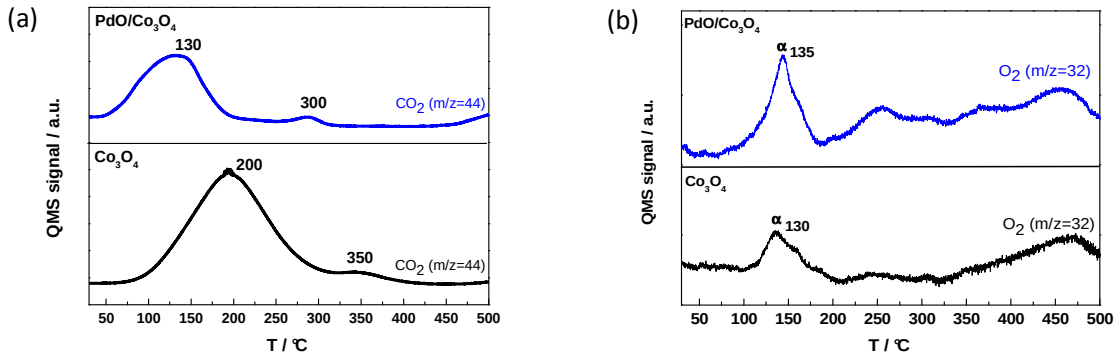

Figure 3.6: (a) CO_2 desorption profiles during the CO-TPD and (b) O_2-TPD profiles of the PdO/Co_3O_4 (blue curve) and pure Co_3O_4 (black curve) catalyst. The catalysts were previously pretreated in synthetic air (400 °C; ½ h).

For both, PdO/Co_3O_4 and Co_3O_4 catalysts, CO exclusively desorbed as CO_2 during the CO-TPD, whereas the desorption temperature for CO_2 was significant lower for PdO/Co_3O_4 compared to Co_3O_4 concerning the intense CO_2 peak with a maximum desorption rate at 130 °C for the PdO/Co_3O_4 and at 200 °C for the Co_3O_4 catalyst.

According to the results from FTIR analysis, shown in figure 3.6(a), it seems that the strong CO_2 signal in the TPD curves resulted from the desorption of mainly surface bonded bidentate carbonates and bicarbonates which was also reported in previous studies for CeO_2-Co_3O_4 catalysts [67,68]. In addition small desorption peaks located at higher temperatures (at 300 °C for PdO/Co_3O_4 and 350 °C for Co_3O_4) were suggested to result from the oxidation and desorption of deposited carbon. Moreover, the TPD results indicated that CO adsorbed in higher amount on Co_3O_4 than on PdO/Co_3O_4 which is consistent with the observations by Jin et al. [22].

The O_2-TPD results exhibited different kinds of oxygen desorption peaks for the PdO/Co_3O_4 and the Co_3O_4 catalyst (see figure 3.6(b)). A very clear oxygen desorption peak, defined as the alpha peak, centered at relatively low temperatures of 135 °C for the PdO/Co_3O_4 and of 130 °C for the Co_3O_4 catalyst while the peak intensity on the PdO/Co_3O_4 was significantly higher. This is in agreement with the previous work by Meng et al. [9], who reported that the introduction of Pd on CeO_2 promoted the adsorption of easily removable oxygen species due to an incorporation of Pd into the CeO_2 lattice and thus, the production of more oxygen vacancies on the catalyst surface.
Trying to attribute the alpha peak in the TPD curve to an specific oxygen species, we can state from literature [69] that adsorbed O_2 can interact with reducible oxides and be incorporated into the bulk involving the following possible elementary steps:
$O_2(ad) \rightarrow O_2^-(ad) \rightarrow O^-(ad) \rightarrow O_2^-(lattice)$.
Li et al. [68] proposed for example that an ionic O_2^- radical is the active oxygen species in CO oxidation. However, at this state it is not possible from our study to tell which oxygen species corresponds to the alpha peak.
For PdO/Fe_2O_3 and Fe_2O_3, the CO-TPD, shown in figure A9 (a), revealed neither a CO nor a CO_2 desorption peak. This is in agreement with the results from the CO adsorption measurements followed by FTIR (5 % CO in He flow), shown in figure 3.5(c,d) which revealed for PdO/Fe_2O_3 weakly bonded bicarbonates and carbonyls on Pd vanishing already at RT and for pure Fe_2O_3 no CO adsorption at all. Weakly bonded bicarbonates and carbonyls on PdO/Fe_2O_3 apparently dissipated during the flushing with He for 30 min at RT.

The O_2-TPD profile of the PdO/Fe_2O_3, shown in figure A9 (b), revealed several oxygen desorption peaks with maximum desorption rates at 50, 100 and 150 °C which were defined as α, β and γ. This indicates that there are several easily removable oxygen species adsorbed on the

PdO/Fe_2O_3 surface which can be involved in CO oxidation at ambient temperatures. For comparison, the O_2-TPD on pure Fe_2O_3 is planned to be carry out in near future.

To summarize the TPD results, we can conclude that for PdO/Co_3O_4, the adsorbed CO was more easily desorbed as CO_2 (lower desorption temperature) and a higher amount of easily removable oxygen was present on the catalyst surface compared to pure Co_3O_4, which is in agreement with the observed enhanced activity in CO oxidation.
The CO-TPD measurements of the Fe_2O_3 based catalysts are in agreement with the FTIR studies but did not provide any new insights.

3.3 Influence of the pretreatment

3.3.1 Kinetic studies in the CO oxidation reaction

With the aim to study the influence of the pretreatment on the CO oxidation activity of the Co_3O_4 and Fe_2O_3 supported Pd catalysts, the catalysts were subjected, in addition to the oxidation pretreatment, to a reduction pretreatment (5 % H_2 in He flow). The reduction was performed at 100 °C for the Co_3O_4 supported Pd and at 100 and 300 °C for the Fe_2O_3 supported Pd catalyst.

The catalytic measurements of the reduced catalysts were carried out in the same way as the measurements of the catalysts subjected to the oxidative pretreatment, as described in chapter 3.2.1.

Moreover, the same kinetic parameters as for the oxidatively pretreated catalysts including T_{50} and reaction rates at 50 and 70 °C were calculated from the light-off curves obtained from the temperature programmed experiments to determine and compare the catalytic activities.

Figure 3.7 shows the CO conversion plotted as a function of temperature for the oxidized PdO/Co_3O_4 and the reduced Pd/CoO_x (red. 100 °C) catalysts, respectively the oxidized PdO/Fe_2O_3 and the reduced Pd/FeO_x (red. 100 and 300 °C) catalysts.

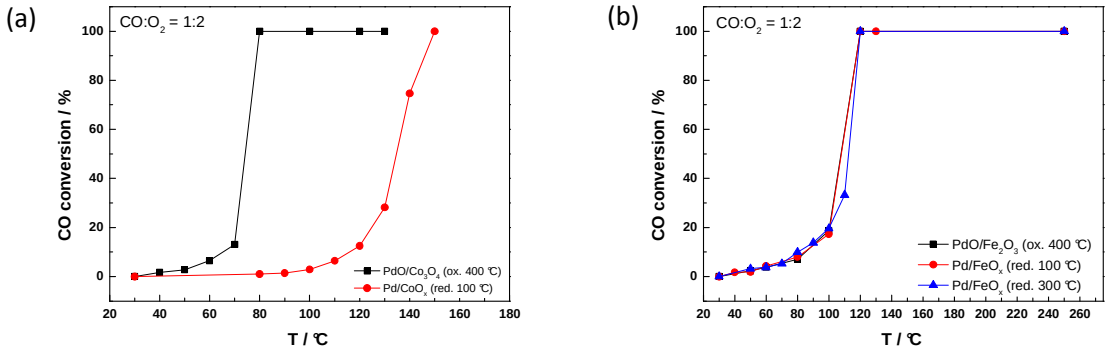

Figure 3.7: CO conversion over the (a) oxidized PdO/Co_3O_4 and the reduced Pd/CoO_x (red. 100 °C) catalysts and (b) oxidized PdO/Fe_2O_3 and reduced Pd/FeO_x (red. 100 or 300 °C) catalysts as a function of temperature. The reduced catalysts were pretreated in synthetic air (400 °C; ½ h) prior to reduction.

The catalytic activity of the Pd/CoO_x catalyst, subjected to a reduction pretreatment at 100 °C, significantly decreased compared to oxidized PdO/Co_3O_4 according to the increase of the T_{50} value by 60 °C and lower reaction rates, listed in table 3.6.

In the case of the reduced (red. 100 or 300 °C) Pd/FeO_x catalysts, no change in activity could be observed compared to the oxidized PdO/Fe_2O_3 catalyst which was indicated by nearly identical T_{50} values (~110 °C) and reaction rates.

Our results are in contradiction with most of previous studies [7,22,42] where a reduction pretreatment of Co_3O_4 and Fe_2O_3 supported noble metal catalysts led to an enhancement of the activity (see chapter 1.3.2). Naumann d'Alnoncourt et al. [7] for example observed a decrease of the T_{50} value by 40 °C after the reduction pretreatment with H_2 at 250 °C for a $PdO/\gamma Fe_2O_3$ catalyst due to an induced encapsulation. However, according to these authors [7], it is also possible that the induced encapsulation decompose in an oxygen rich CO reaction mixture. Therefore, we can assume that even if the reduction pretreatment had induced a potential enhancement due to a SMSI between Pd and the support γFe_2O_3 the potential enhancement is not present anymore under the oxygen rich reaction atmosphere and thus, a similar state of the catalyst is established as after the oxidation pretreatment.

To conclude, we can state that the catalytic activity of the Co_3O_4 supported Pd catalyst is strongly influenced by the different pretreatments, either in oxidizing or reducing atmosphere, in contrast to the catalytic activity of Fe_2O_3 supported Pd which is unaffected.

Table 3.6: Kinetic parameters including T_{50} and reaction rates calculated for the oxidized and the reduced supported Pd catalysts in CO oxidation.

Sample	T_{50} / °C	reaction rate / mol s^{-1} g^{-1} 10^{-6}	
		at 50 °C	at 70 °C
PdO/Co_3O_4	~75	3.6	10.9
Pd/CoO_x (red. 100 °C)	~135	0	0.7
PdO/Fe_2O_3	~110	2.5	4.1
Pd/FeO_x (red. 100 °C)	~110	2.6	4.0
Pd/FeO_x (red. 300 °C)	~110	1.9	4.2

3.3.2 H_2-TPR and TPO

In order to correlate the different influence of the reduction pretreatments on the catalytic activity of the Co_3O_4 and Fe_2O_3 supported Pd catalysts with the redox properties, the catalysts were characterized by performing H_2-TPR and TPO experiments. The H_2-TPR profiles of PdO/Co_3O_4 and PdO/Fe_2O_3 are shown in figure 3.8(a), while the TPO profiles of the reduced Pd catalysts, defined as Pd/Co and Pd/Fe, are highlighted in figure 3.8(b).

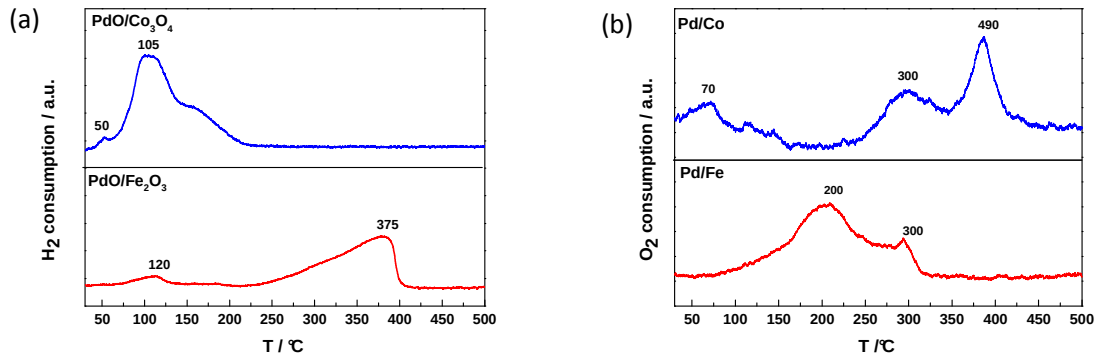

Figure 3.8: Flow reactor (a) H_2-TPR profiles of the PdO/Co_3O_4 (blue curve) and PdO/Fe_2O_3 (red curve) catalysts (10 % H_2 in He flow; heating rate: 5 °C min^{-1}). (b) TPO profiles of the reduced Pd/Co (blue curve) and the Pd/Fe (red curve) catalysts (10 % O_2 in He flow, heating rate: 10 °C min^{-1}).

The H_2-TPR profile of PdO/Co_3O_4, shown in figure 3.8(a), consisted of two overlapping peaks, including a weak one at ~50 °C and a broad and asymmetric one with a maximum at ~106 °C. Based on previous TPR profiles, it is suggested that the former could be attributed to the

reduction of PdO particles and the latter to the two-step reduction of Co_3O_4 to metallic Co via CoO [16]. However, Osakoo et al. [70] also reported that highly interacting PdO particles with the support Co_3O_4 were reduced at significantly higher temperatures of ~200 °C. Thus, we could not exclude that a reduction of PdO also proceeded in parallel to the reduction of Co_3O_4 at higher temperatures.

Furthermore, we want to mention here that the reduction of PdO/Co_3O_4 take place at significantly lower temperatures than the reduction of the pure Co_3O_4 catalyst, shown in figure A10 (a). This can be explained by the dissociation of H_2 to atomic H on the metallic Pd particles present [70] followed by a spillover of H inducing this early-on reduction of Co_3O_4. This would be consistent with our suggestions regarding the assignment of the peak at 50 °C to the reduction of PdO to metallic Pd to accomplish the low temperature reduction of Co_3O_4.

The TPR profile of the PdO/Fe_2O_3 substantially differs from that of PdO/Co_3O_4. PdO/Fe_2O_3 exhibited one small reduction peak at ~120 °C presumably corresponding to the reduction of PdO and one intense at ~375°C attributed to the reduction of Fe_2O_3 to metallic Fe via Fe_3O_4.

To summarize the TPR results, it can be stated that PdO/Co_3O_4 was reduced at significant lower temperatures than PdO/Fe_2O_3.

Additional information regarding the redox properties could be gained from TPO experiments, shown in figure 3.8(b). The profiles of the Pd/Co and Pd/Fe catalysts were considerably different. The Pd/Co exhibited three oxygen consumption peaks located at ~70, 300 and 400 °C. We attributed the peaks at ~300 and ~400 °C to the reoxidation of bulk metallic Co to Co_3O_4 as it was reported in literature [39]. The peak at 70 °C might correspond to the oxidation of metallic Pd together with some Co species as the peak intensity was too high to exclusively assign it to the oxidation of Pd.

In the case of Pd/Fe, the reoxidation profile revealed two overlapping peaks, one intense and broad peak with a maximum at 200 °C and another one at ~300 °C, which were both attributed to the oxidation of Fe to Fe_2O_3 occurring in multiple steps. A peak corresponding to the oxidation of Pd to PdO could not be identified.

According to the TPO profiles, Pd/Fe was retransformed in its oxidized state at lower temperatures compared to Pd/Co.

In conclusion, H_2-TPR and TPO results revealed that PdO/Co_3O_4 and PdO/Fe_2O_3 are substantially different in their redox properties as the support Co_3O_4 is more easily reduced at

lower temperatures than the support Fe_2O_3 but is harder to reoxidize. However, it has to be kept in mind that we mainly record the redox properties of the bulk phases and small changes of the oxidation states on the surface relevant for the catalytic properties might not be detected.

With respect to the TPR and TPO results, we could establish a correlation between the different influence of the reduction pretreatments on the activity of the Co_3O_4 and Fe_2O_3 supported Pd catalysts and the different redox properties. In the case of reduced Pd/CoO_x (red. 100 °C), the loss in activity seems to result from a change in the oxidation state of Co_3O_4 after the reduction pretreatment indicated by the H_2-TPR profile. This is consistent with the XRD results which proved the formation of CoO and metallic Co after a reduction at 100 °C. The inhibition of the activity by forming the phases CoO and metallic Co is assumed to result from a decreased mobility and availability of surface oxygen compared to Co_3O_4 which is known for its highly mobile oxygen [71]. However, it is not clear if CoO and metallic Co together leading to an inhibition or only the metallic Co as CoO was also reported to be an active phase in CO oxidation according to literature [13]. The reoxidation to the "active" Co_3O_4 phase seems to proceed not easily according to the TPO profile, and therefore the catalyst apparently required relatively high temperatures to reactivate and form Co_3O_4 again under reaction conditions indicated by a relatively high T_{50} value of ~ 135 °C.

In the case of the Pd/FeO_x catalyst (red. 100 °C), the Fe oxidation state might remained unchanged during the reduction pretreatment due to a relatively high stability of the Fe_2O_3 phase against reduction according to the H_2-TPR and therefore did not show any change in activity compared to the oxidized PdO/Fe_2O_3. In contrast, the Pd/FeO_x (red. 300 °C), which also showed the same activity as the oxidized PdO/Co_3O_4 catalyst, changed its oxidation state after the reduction pretreatment by forming the FeO and the metallic Fe phases indicated by the TPR profile and proven by XRD. However, due to an easy oxidation of the FeO and metallic Fe phases, as demonstrated by the TPO profiles, the catalyst can easily regain its activity under reaction conditions resulting in an unchanged activity compared to the oxidized PdO/Fe_2O_3. Another possibility could be that the availability and mobility of active oxygen is still very high in the presence of FeO and metallic Fe and thus, the catalytic activity is not limited by the presence of FeO and Fe.

3.4 *In situ* studies

In situ spectroscopy studies including *in situ* Fourier Transform Infrared (FTIR) and the *in situ* ambient pressure XPS (APXPS) were performed on PdO/Co_3O_4 and PdO/Fe_2O_3 under relevant catalytic working conditions to get a fundamental understanding of the dynamic interactions of the reactants CO, O_2 and the product CO_2 with the catalyst surface. The aim was to identify active states (e.g. SMSI state, oxidation states), reaction intermediates and inhibiting surface species which are the basis for clarifying the CO oxidation mechanism and deactivation mechanisms and for revealing active sites.

3.4.1 *In situ* FTIR

In situ FTIR spectroscopy was performed over the Pd supported catalysts to gain an insight into dynamic changes of the chemical and structural nature of the adsorbed surface species and of the catalyst itself (e.g. oxidation state and size of the Pd particles) on which the C-O stretching frequency strongly depends on. In addition, information about relative changes in the amount of the gaseous reactant CO and the product CO_2 could be obtained.

3.4.1.1 PdO/Co_3O_4

- **Time-On Stream reaction**

The time resolved *in situ* FTIR spectra of the PdO/Co_3O_4 catalyst recorded under CO oxidation conditions ($CO:O_2$ = 1:2) at RT are plotted in figure 3.9.

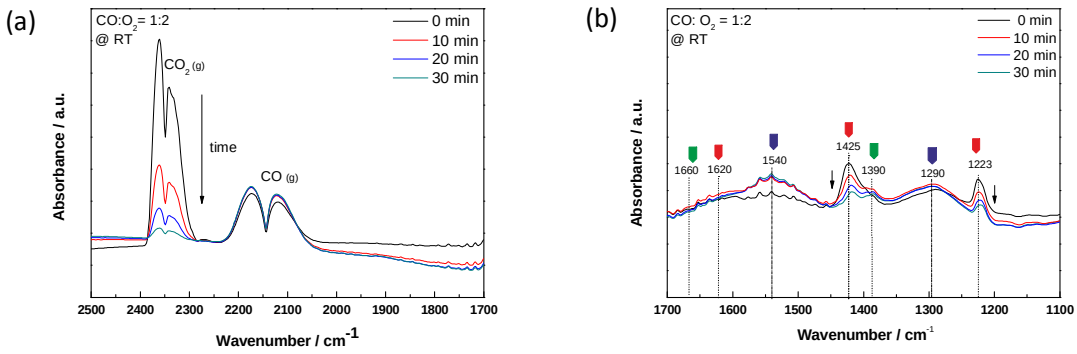

Figure 3.9: *In situ* FTIR spectra recorded of PdO/Co_3O_4 under reaction conditions ($CO:O_2$ = 1:2) at RT as a function of exposure time. The spectra were plotted in different spectral regions: (a) 2600-1700 cm^{-1} and (b) 1700-1100 cm^{-1}. The catalyst was pretreated in synthetic air (400 °C; ½ h).

The exposure of the PdO/Co_3O_4 catalyst to the reaction mixture resulted in an initial appearance of gaseous CO_2 associated to bands at 2360 and 2338 cm^{-1}, which indicated a CO conversion already at RT, shown in figure 3.9(a).With ongoing time of exposure the bands of CO_2 decreased gradually and finally disappeared after ~30 minutes indicating a deactivation of the catalyst. This is consistent with our time-on stream experiments in the fixed bed flow reactor, discussed in chapter 3.5, where a fast deactivation of the catalyst has also been observed at RT. Surprisingly, no clear bands corresponding to CO either adsorbed on ionic $Pd^{\delta+}$ or on Pd^{o} species were found suggesting that there are no accessible Pd adsorption sites for CO on the catalyst surface. However, when the CO gas flow was stopped and only O_2 in He was flushed over the catalyst, the presence of a small band at 2140 cm^{-1} was revealed which apparently corresponded to CO bonded on ionic $Pd^{\delta+}$ species as its stretching frequency is in the region reported for CO bonded to Pd^{1+} (2120-2110 cm^{-1}) and Pd^{2+} (2180-2160 cm^{-1}), shown in A20. Another possibility could be that the band corresponded to a carbonyl band bonded to Co^{2+} or Co^{3+} (2208-2120 cm^{-1}) however, this is unlikely as the band was not observed in the CO adsorption experiments.

In the spectral region between 1700-1100 cm^{-1}, shown in figure 3.9(b), the formation of carbonates/bicarbonates species was detected which were already observed in the CO adsorption experiments but with a greater intensity (see figure 3.5(a)). The carbonate bands remained more or less constant in intensity, in contrast to bicarbonates, which were declining with ongoing time or in other words with ongoing deactivation of the catalyst. No changes of bands corresponding to hydroxyl groups (3700-3600 cm^{-1}) or physisorbed water molecules (3800-2800 cm^{-1}) on the surface were observed.

The exact role of the observed carbonates and bicarbonates in CO oxidation cannot be clarified at the moment meaning that it is not possible to confirm whether carbonate/bicarbonates are participating in the reaction or they are just formed independently of the ongoing CO oxidation reaction. However, we can most likely exclude that the accumulation of carbonates and bicarbonates at the catalyst surface inhibits CO oxidation at ambient temperatures as the former were decreasing and the latter remained unchanged in intensity during deactivation of the catalyst. This is different to the study by Oh and Hoflund [72], who reported that the carbonate and bicarbonate species accumulation on the surface of a PdO/CeO_2 catalyst at 50 °C resulted in a fast decay of activity (Details about the possible deactivation mechanism are discussed later in chapter 3.5).

By comparison to the CO_2 adsorption experiments, (spectra shown in figure A13), we suggest that the carbonate and bicarbonate species were not evolving from the chemisorption of the produced CO_2 as the CO_2 adsorption experiments revealed no carbonate and almost no bicarbonate formation on the PdO/Co_3O_4 catalyst surface, respectively. However, the catalyst surface structure might be different in the presence of the reaction mixture (increased number of oxygen vacancies on the surface, different metal-support interactions) than in the presence of CO_2 atmosphere, and therefore we cannot exclude for sure that carbonates and bicarbonates arise from the readsorbed CO_2.

For the bicarbonate species, we can even assume that they participate (e.g. act as intermediates or promoters) in the CO oxidation reaction at RT, as they are simultaneously decreasing with the decreasing CO_2 production. Our suggestion on that bicarbonates acting as intermediates is supported by the results from the CO adsorption experiments, shown in figure 3.5(b), which showed that bicarbonates were weakly bonded and therefore can be easily converted and desorbed as CO_2. Furthermore, our suggestion would be consistent with the postulations by Daniells et al. [31] and Tang et al. [67]. Daniells proposed that bicarbonates act as CO oxidation intermediates based on FTIR studies over an Au/Fe_2O_3 catalyst, while Tang suggested that bicarbonates are responsible for the high catalytic activity in CO oxidation over CeO_2/Co_3O_4 at low temperatures.

In contrast, bidentate carbonates are presumably not participating in the CO oxidation reaction at RT as they are strongly bonded on the catalyst surface, according to the CO adsorption

experiments. On the one hand this would be in agreement with the study by Tang et al. [67], who proposed that temperatures of 100 °C and higher were required to convert bidentate carbonates to CO_2 over a CeO_2-Co_3O_4 catalyst, on the other hand this would be different to the studies by Luo et al. [23] in which they proposed that bidentate bicarbonates act as intermediates on a Co_3O_4-CeO_2 catalyst in the CO oxidation reaction already at RT.

Moreover, we can conclude that no CO bonded to metallic Pd was detected indicating the absence of metallic Pd on the surface at RT. In contrast, apparently small amounts of ionic Pd species were present on the surface which was indicated by the appearance of stable CO bands on $Pd^{\delta+}$. However, due to the high stability of the adsorbed CO-$Pd^{\delta+}$ species, it is unlikely that they are participating in CO oxidation at these low temperatures. These findings suggest that the Pd species are not directly involved in the CO reaction. It remarks an open question why there are much less Pd adsorption site for CO compared to the PdO/Fe_2O_3 containing the same amount of Pd (2 wt%), shown in the following figure 3.11(a).

According to previous studies, the following possible situations (1)-(4) could be responsible for the strongly decreased amount of Pd adsorption sites for CO of the PdO/Co_3O_4 catalyst.

(1) The formation of an CoO_x overlayer onto the Pd particles

The Pd particles could be partially “encapsulated” by the support in form of a reduced CoO_x overlayer resulted in a blocking of the Pd adsorption sites for CO. In literature the encapsulation effect was mostly reported after a reduction pretreatment or a high temperature annealing in vacuum for the noble metals Pd and Pt on different metal oxides (TiO_x, CeO_x, FeO_x) [7,17,18] although recently it had been stated that an oxidation pretreatment was sufficient to almost completely cover palladium particles supported on Al_2O_3 by a thin layer of an aluminate phase [20]. Details about the encapsulation effect are described in chapter 1.3.1.

(2) The presence of fully oxidized PdO particles

Another possibility could be that the majority of the Pd particles are present in their fully oxidized state under reaction conditions getting stabilized by the support. This would be in agreement with the observations by Zorn et al. [48], who reported about fully oxidized PdO particles supported on Al_2O_3 which were stable against reduction till temperatures of 250 °C (in 10 mbar CO) and exhibited no CO adsorption capacity at all. However, the fully oxidized Pd particles were obtained after strong oxidizing pretreatment conditions (1 bar O_2 at 800-1000 °C), in contrast to the relatively mild oxidizing conditions (10 mbar at 400 °C) that were applied in our case to the PdO/Co_3O_4 catalyst. Nevertheless, it is still reasonable to speculate about the presence of fully oxidized Pd particles due to the fact that in our case the Pd particles are in the size range from sub-nm to 2 nm and get therefore very easily oxidized compared to larger particles [73]. Furthermore, the support used in our study is a different one (Co_3O_4) which could also have a major effect on the stability of the Pd oxide particles.

(3) The formation of a solid solution $Co_{3-x}Pd_xO_{4-\delta}$.

Another possibility is the formation of a solid solution, where $Co^{2+}/^{3+}$ ions would have been partially substituted by $Pd^{\delta+}$ ions. The incorporation of ionic $Pd^{\delta+}$ species into the matrix of the support was mainly observed for catalysts prepared by a solution combustion method [38,74], though lately Hinokuma et al. [21] observed an incorporation of $Pd^{\delta+}$ into a CeO_2 matrix after a conventional wet impregnation method forming Pd-O-Ce bondings.

(4) The CO dissociation on Pd to C and CO_2.

A fourth possibility could be that the CO dissociates on the Pd particles resulting in the deposition of elemental carbon on the catalyst surface and thus, a blocking of Pd adsorption sites for CO [75]. However, it is still under debate if Pd can at all dissociates CO to CO_2 and C at RT [76]. On Pd single crystals no dissociation was observed [76], while some authors have reported

about CO dissociation on Pd nanoparticles [75,77]. In addition, it has been proposed that metal-support interactions could have an effect on the CO dissociation [78].

- **Temperature Programmed reaction**

Subsequently to the time resolved *in situ* FTIR studies at RT, a temperature programmed *in situ* FTIR experiment was carried out on the PdO/Co_3O_4 catalyst in which the temperature was increased to 200 °C. The FTIR spectra were recorded at different temperatures including 30, 70, 110, 150 and 200 °C and are plotted in figure 3.10.

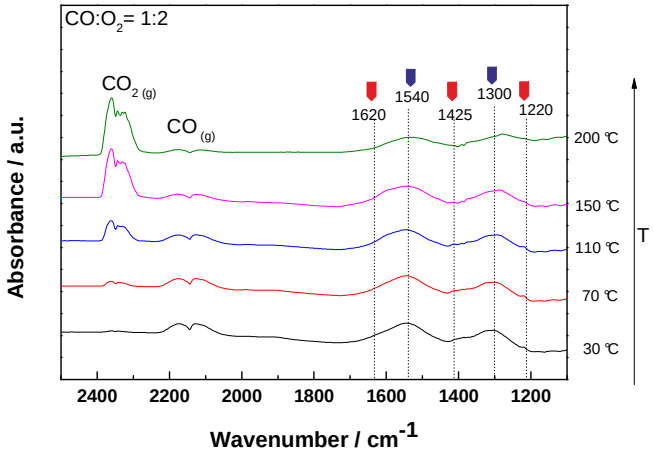

Figure 3.10: *In situ* FTIR spectra recorded of PdO/Co_3O_4 under reaction conditions ($CO:O_2$ = 1:2) as a function of temperature. The spectra were recorded after *in situ* time on stream FTIR experiments at RT.

Upon temperature increase, a gas phase CO_2 band at 2360 and 2320 cm^{-1} appeared at a temperature of ~110 °C and gradually increased up to a temperature of 150 °C, where a maximum CO_2 production was reached (T_{max}). The temperature of full CO conversion is not in agreement with the one from the experiment in the fixed bed flow reactor cell (T_{max} = 120 °C) due to a different sample amount (different amount of active sites for the reactants) and geometry of the reaction chamber (different contact time of the reactants with the catalyst surface). The additional bands between 2360–2320 cm^{-1} were due to physically adsorbed CO_2. Simultaneously with the increase of the CO_2 bands, a decrease of the carbonate bands located at 1540 and 1300 cm^{-1} (bidentate carbonates) and at 1620, 1425 and 1220 cm^{-1} (bicarbonates) [61,63] could be

noticed which is in agreement with the study by Tang et al. [67]. However, bidentate carbonates still remained partially on the catalyst surface till temperatures of 200 °C, while bicarbonates were disappearing already at temperatures of ~150 °C. This is consistent with the time on stream experiments which revealed also a lower stability of bicarbonates compared to bidentate carbonates. It is likely that the produced CO_2 at least partially originated from adsorbed carbonates/bicarbonates in the temperature range between 100 °C and 200 °C.

The CO adsorption bands on the $Pd^{\delta+}$ species seem to disappear upon heating up. Due to the disappearance of the CO-$Pd^{\delta+}$ bands, it is unclear in which oxidation states the Pd particles are present under these conditions. The *in situ* APXPS studies will give further insight into the nature of the present Pd species under reaction conditions.

From the *in situ* FTIR studies of the PdO/Co_3O_4 catalyst, we can conclude that CO oxidation is not limited by a self-poising of Pd by CO and therefore not following the competitive Langmuir-Hinshelwood mechanism on Pd as we already postulated in chapter 2.3 according to the calculated kinetic parameters (e.g. T_{50}, reaction rates, reaction orders). The results further indicate that CO oxidation most likely proceeds on the Co_3O_4 support via carbonate formation. The role of the apparently present ionic Pd species for the catalytic reaction remains unclear.

3.4.1.2 PdO/Fe_2O_3

- **Time on stream experiment**

The time resolved *in situ* IR spectra for the PdO/Fe_2O_3 catalyst, recorded under CO oxidation conditions ($CO:O_2$ = 1:2) at RT, are plotted in figure 3.11.

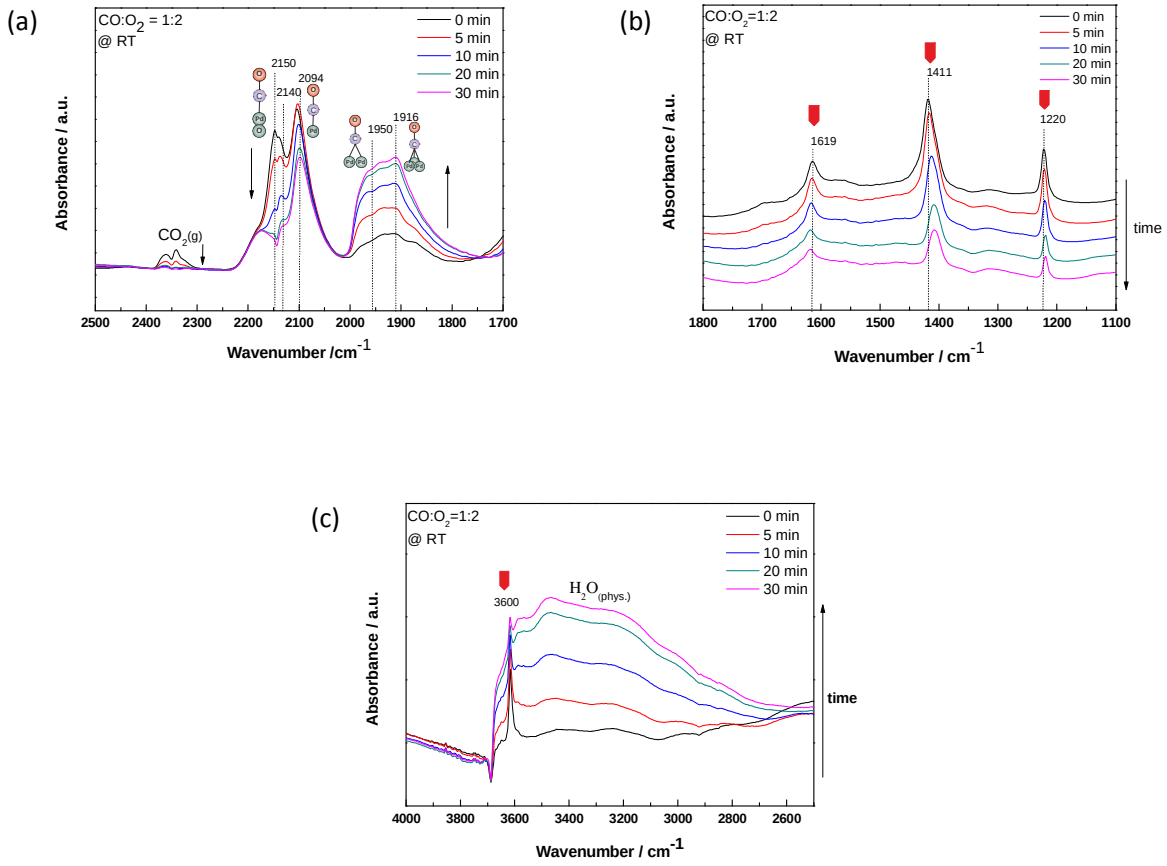

Figure 3.11: *In situ* FTIR spectra recorded of PdO/Fe_2O_3 under reaction conditions ($CO:O_2$ = 1:2) at RT as a function of exposure time. The spectra are plotted in different spectral regions: (a) 2500-1700 cm^{-1}, (b) 1800-1100 cm^{-1} and (c) 4000-2500 cm^{-1}. The catalyst was previously pretreated in synthetic air (400 °C; ½ h).

Upon the exposure of the reaction mixture to the PdO/Fe_2O_3 catalyst at RT, shown in figure 3.11(a), small gaseous CO_2 bands at 2360 and 2338 cm^{-1} appeared which declined already after 10 min. This is consistent with the fixed bed flow reactor experiments, discussed in chapter 3.5, where also a fast deactivation of the catalyst was observed at RT. Furthermore, linear bonded CO on Pd^{1+} and Pd^{2+} ions at 2150 and 2140 cm^{-1} and in addition linear CO bands on Pd^{o} at 2084 cm^{-1}

evolved when dosing the reaction mixture. Moreover, a rather broad feature at ~1930 cm^{-1} appeared which was assigned to CO species bonded on Pd^o in bridged (~1950 cm^{-1}) and 3-fold hollow (3-fh)-bond (~1920 cm^{-1}) configurations [64,65]. With prolonged exposure time, the band corresponding to CO bonded in bridged and 3-fh configuration on Pd^o species increased, while simultaneously the bands related to CO linear adsorbed on ionic Pd^{1+}, Pd^{2+} and metallic Pd^o species declined. This indicates that CO was able to reduce the supported PdO to metallic Pd already at RT consistent with observations stated in previous studies [35,79].

According to literature [65], it is known that a strong linear CO adsorption band on Pd^o in relation to the bridged and 3-fh bonded CO bands is characteristic for the presence of finely dispersed Pd particles. Therefore, the decrease of linear bonded CO on Pd^o during the reduction process originated apparently from the transformation into bridged bonded CO on Pd^o. This can be argued by an increasing extent of reduction and consequently increasing presence of metallic Pd particles on the catalyst surface resulting from the reduction of Pd oxide species. Whether the reduction process was accompanied by a sintering of the Pd particles we cannot confirm at this stage.

In addition in the low frequency range spectra, shown in figure 3.11(b), IR features at 1619, 1411 and 1220 cm^{-1}developed which were assigned to bicarbonate species and were already observed in the CO adsorption experiment, shown in figure 2.5(c). In the region of ~3700 cm^{-1}, see figure 3.11(c) a loss in intensity was noticed due to a loss in isolated hydroxyl groups bonded on the Fe_2O_3. Instead new bands appeared at ~3600 cm^{-1} corresponding to hydroxyl groups of bicarbonates [60,80]. This clearly indicates the reaction of CO, respectively CO_2 with surface hydroxyl groups to produce bicarbonates on the catalyst surface [81]. The broad band between 3700-3000 cm^{-1} which increased with prolonged exposure time could be assigned to hydrogen bonded water molecules bonded on the surface and interacting with other adsorbates [82].

To conclude, we observed that a small amount of CO_2 was produced as long as the reduction of PdO to metallic Pd proceeded suggesting that the CO_2 production resulted from the reduction of PdO. At the moment where only metallic Pd^o for the CO adsorption were available, the CO_2 evolution stopped due to the well-known Pd self-poisoning by CO. There may also be an influence of the increasing amount of hydrogen bonded water molecules on the deactivation of the catalyst which has to be investigated further.

Furthermore, it is evident that the bicarbonate species mainly arise from the readsorbed CO_2 based on the CO_2 adsorption experiments, shown in figure A14 (a), revealing very strong bicarbonate bands as it was proposed already by Szanyi et al. [79]. and Wang et al.[83].

Most likely there a dynamic equilibrium exists between bicarbonates and gaseous CO_2 [83] shown in equations (3.1-3.2).

$CO_2 + * \rightarrow$ *-bicarbonates (3.1)

*-bicarbonates $\rightarrow CO_2 + *$ (3.2)

- **Temperature-programmed experiment**

Subsequently to the time resolved *in situ* FTIR studies at RT, a temperature-programmed *in situ* FTIR experiment was performed over the PdO/Fe_2O_3 catalyst in which the temperature was increased to 200 °C, respectively. The FTIR spectra recorded at different temperatures including 30, 70, 110, 150 and 200 °C and are plotted in figure 3.12(a).

In addition, *in situ* FTIR spectra over the PdO/SiO_2 catalyst upon heating up to 250 °C were collected, and used as a reference and shown in figure 3.12(b).

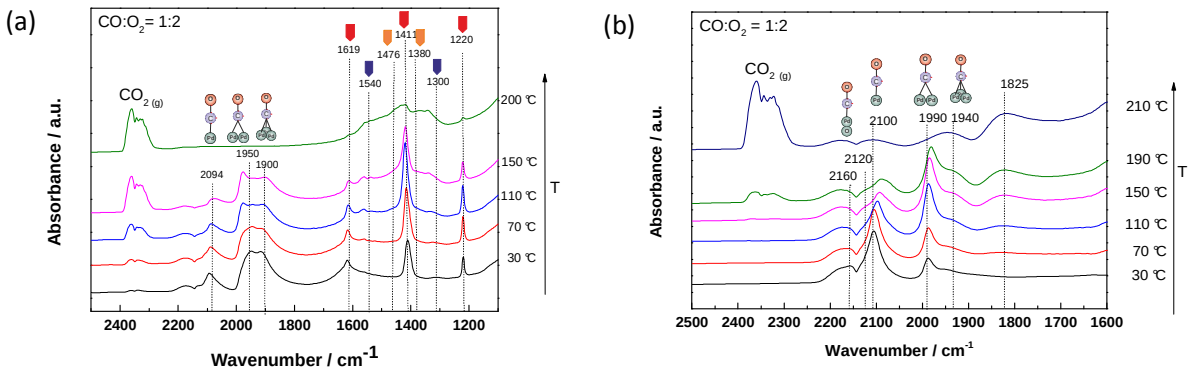

Figure 3.12: *In situ* IR spectra recorded of (a) PdO/Fe_2O_3 and (b) PdO/SiO_2 under reaction conditions ($CO:O_2$ = 1:2) as a function of temperature. The spectra were recorded after *in situ* time-on stream FTIR experiments at RT.

Upon heating the PdO/Fe_2O_3 catalyst in reaction mixture, CO_2 started to evolve at a temperature of ~ 110 °C and increased gradually up to a temperature of ~ 150 °C where a maximal CO conversion was reached (T_{max}) (see figure 3.12(a)). The linear, bridged and 3-fh bonded CO on Pd^o bands decreased up to a temperature of 70 °C, stayed more or less in the temperature range from 70 to 150 °C and finally disappeared at a temperature of ~ 190 °C.

Furthermore, in the carbonate region predominated IR features corresponding to bicarbonate species were observed which were constant in their intensity till a temperature of 110 °C was reached. At this temperature they started to decline and almost disappeared at 200 °C. Additional broad bands between 1700 and 1300 cm^{-1} started to appear at ~150 °C which were assigned to monodentate (1476 and 1383 cm^{-1}) and bidentate (1553 and 1316 cm^{-1}) carbonates [61,63,82]. As mentioned previously, bicarbonates presumably arise from the re-adsorbed CO_2 based on the CO_2 adsorption experiments, shown in figure A14. Readsorbed CO_2 was not strongly bonded as bicarbonates on the catalyst surface according to the CO_2 experiments and therefore it is unlikely that they are inhibiting the CO oxidation rate. In addition, it can be declared that the amount of mono- and bidentate carbonates was not correlating with the amount of produced CO_2 as a relatively high CO_2 production was already observed at temperatures between 110 and 150 °C where these carbonates were almost absent.

Furthermore, it is important to point out here that upon increasing the temperature from 110 to 150 °C, the CO_2 production is more than doubled, while the CO coverage on Pd kept nearly unchanged. Therefore, the CO_2 production rate is not limited by the CO coverage on Pd at these temperatures and therefore the reaction does not proceed according to the competitive Langmuir-Hinshelwood mechanism on Pd which we have already postulated in chapter 2.3 based on the calculated kinetic parameters.

This conclusion was also confirmed by the *in situ* FTIR results of the PdO/SiO_2, shown in figure 3.12(b). The spectra of PdO/SiO_2 revealed that the CO_2 production rate was limited by the CO coverage on Pd, specifically by a self-poisoning of Pd by the strongly adsorbed CO, as CO_2 started to appear at the same temperature (~210 °C) where the CO adsorption bands on Pd disappeared. This is characteristic for a CO oxidation reaction following the competitive Langmuir-Hinshelwood mechanism on Pd which is well known to occur on Pd on inert supports as SiO_2.

We attributed the different CO oxidation mechanism on PdO/Fe_2O_3 compared to PdO/SiO_2 either to a potential present SMSI state between Pd and Fe_2O_3 resulting in low temperature oxygen activation independent of the CO coverage of Pd or either to an oxygen activation occurring on the Fe_2O_3 surface (e.g. via an oxygen spillover effect) nearby the metal-support interface. CO oxidation on PdO/Fe_2O_3 is therefore assumed to proceed via a non-competitive Langmuir-Hinshelwood mechanism where CO and O_2 chemisorb on two different active sites. In this case, the adsorption of CO would occur on metallic Pd, while the adsorption of O_2 would occur on sites related to Fe_2O_3 which are not present on SiO_2 (e.g. oxygen vacancies of Fe_2O_3, at the metal-support interface, at the electronically modified Pd particles). Another possible reaction mechanism could be the Mars-Van Krevelen mechanism where the active oxygen reacting with CO adsorbed on Pd comes from the lattice of the Fe_2O_3.

As a main and unexpected result of the *in situ* FTIR experiments we can state that the interactions between the reactants and the surface of the PdO/Co_3O_4 and of the PdO/Fe_2O_3 catalysts are completely different. On PdO/Co_3O_4, no bands for CO adsorbed on metallic Pd were detected at RT, while on PdO/Fe_2O_3 strong bands corresponding to CO on Pd appeared. This let us conclude that apparently present PdO_x on Co_3O_4 did not get reduced by CO in the reaction mixture while on Fe_2O_3 PdO_x got easily reduced. This could result from different Pd particle sizes as the Pd particles were significant smaller on the Co_3O_4 (sub-2 nm range) than on the Fe_2O_3 support and thus, more stable in their oxidized state [73]. Another possibility could be the different nature of the supports resulting in different interactions with Pd (e.g. encapsulation, interdiffusion). Upon heating up in reaction mixture it seems that PdO_x on Co_3O_4 remains in its oxidized state under reaction mixture (absence of CO-Pd^o bands) while on PdO/Fe_2O_3, Pd stays in its metallic state at least till temperatures of 150 °C (indicated by strong CO-Pd^o absorption bands).

Thus, it is assumed that adsorbed CO on metallic Pd on Fe_2O_3 is involved in the CO oxidation reaction, while on PdO/Co_3O_4 there is most likely no CO bonded to Pd species involved. Instead, for PdO/Co_3O_4 it is assumed that adsorbed bicarbonates on the Co_3O_4 support participate in the CO oxidation reaction at RT (as intermediates or promoters) whereas bidentate carbonates apparently not. For PdO/Fe_2O_3, carbonates did not act as intermediates as the observed bicarbonates apparently resulted from a readsorption of CO_2. However, for both catalysts,

PdO/Co_3O_4 and PdO/Fe_2O_3, there are clear indications that the CO oxidation reaction does not follow the competitive Langmuir-Hinshelwood mechanism on Pd.

3.4.2 *In situ* Ambient-Pressure XPS (APXPS)

To study the changes of the oxidation states of Pd and Co_3O_4 and the surface composition of the PdO/Co_3O_4 catalyst in correlation with the CO oxidation activity, synchrotron based *in situ* APXPS at various degrees of surface sensitivity was performed under relevant catalytic reaction conditions. Furthermore, the technique should give information about the role of carbon containing species (e.g. carbonates, elemental carbon) as possible intermediates or deactivation factors.

The Pd 3d, Co 2p, O 1s and C 1s core levels were recorded under reaction conditions ($CO:O_2$ = 1:2) and at two different temperatures (RT and 100 °C). However, the O 1s core levels could not be reasonable evaluated as a dehydroxylation of the surface was noticed by to the photon beam. The Pd 3d spectra recorded after pre-oxidation (0.5 mbar O_2 at RT) and under reaction conditions (0.5 mbar CO + O_2 at RT and 100 °C) for the lowest kinetic photon energy (200 eV) i.e. in the most surface sensitive mode and are shown in figure 3.13.

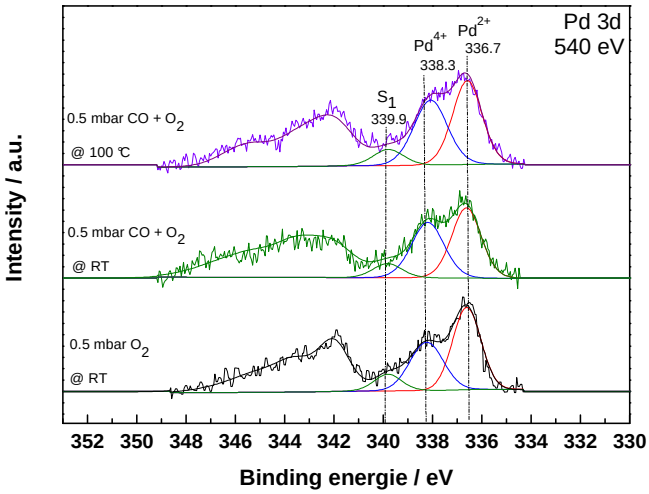

Figure 3.13: Pd 3d XPS spectra recorded before (0.5 mbar O_2 at RT) and under reaction conditions (0.5 mbar CO + O_2 at RT and 100 °C) with a photon excitation energy of 540 eV. The spectra were obtained after an oxygen pretreatment (0.5 mbar O_2 at 400 °C) of the sample. Herein only the fitted curves of the Pd $3d_{5/2}$ are shown.

The analysis of the Pd 3d doublet of the PdO/Co_3O_4 sample under oxygen atmosphere (0.5 mbar O_2) at RT, shown in figure 3.13, suggested the presence of two different Pd species including Pd^{2+} (PdO) and Pd^{4+} (PdO_2). The $3d_{5/2}$ peaks were located at binding energies of 336.7 eV (FWHM = 1.2) for Pd^{2+} and at 338.1 eV (FWHM = 1.5) for Pd^{4+} in agreement with the literature [84]. Furthermore, the small peak at 339.9 eV can attributed to a satellite peak S_1 of the PdO [84]. Additionally, a broad peak at an average value of 345-346 eV was observed which could not be identified as it is too intensive for a palladium oxide satellite peak [85]. Further investigations are required to identify this peak.

The Pd^{4+}/Pd^{2+} ratio was calculated from the areas of the fitted functions and turned out to be 0.70. The atomic ratio of Pd^{4+}/Pd^{2+} increased from 0.70 to 0.88 and stayed constant with prolonged exposure time of the reactants. The slight increase from 0.70 to 0.88 surprises as a decrease of the Pd^{4+}/Pd^{2+} was expected due to the presence of the reducing agent CO in the reaction mixture. However, it has to be kept in mind that large fitting errors can arise from a bad signal-to-noise ratio of the spectra and therefore it remains unclear whether the increase in the Pd^{4+}/Pd^{2+} ratio is in higher orders compared to the error range. Though, we can conclude that both ionic species Pd^{4+} and Pd^{2+} were stable when dosing the reaction mixture at RT and were not reduced to

metallic Pd by CO in the reaction mixture which is in excellent agreement with our *in situ* FTIR studies (chapter 3.4.1).

When increasing the reaction temperature from RT to 100 °C, the Pd^{4+}/Pd^{2+} ratio kept more or less constant (Pd^{4+}/Pd^{2+}= 0.89). Thus, we can declare that the temperature increase from RT to 100 °C under reaction conditions has no effect on the Pd^{4+}/Pd^{2+} ratio.

With respect to the activity of the PdO/Co_3O_4 catalyst, we observed a high activity of the catalyst at RT during the start of the reaction but a fast deactivation with ongoing reaction based on the data recorded by MS, shown in figure A24. In contrast, the activity at 100 °C was high and stable. This is in agreement with the results from kinetic measurements in the fixed bed flow reactor and the *in situ* FTIR studies, described in chapter 3.2.1 and 3.4.1.

We can conclude that the present Pd species under the high active and deactivated state of the catalyst at RT are Pd^{2+} and Pd^{4+}, and thus, are not correlating with the catalytic activity of the catalyst.

Surprisingly, the Pd^{4+} was even present during the pretreatment of the catalyst at 400 °C (Pd^{4+}/Pd^{2+} = 0.69), though it was reported in literature that the Pd^{4+} decompose at 200 °C [86]. However, lately other groups proposed that it can be stabilized by the interaction with oxides such as SnO_2, PdO and Al_2O_3 [84,85]. Therefore we suggested that the Pd^{4+} get stabilized by the Pd^{2+} species or by the Co_3O_4 support. Another possibility is that the peak located at 338.1 eV is actually not belonging to the highly oxidized Pd^{4+} but rather to highly dispersed Pd species strongly interacting with Co_3O_4 the by forming e.g. a Pd-O-Co moiety [87] resulting either from interdiffusion of $Pd^{\delta+}$ species into the Co_3O_4 lattice or the formation of an overlayer of CoO_x on Pd. The potential formation of a CoO_x overlayer would also explain the increased Pd^{4+}/Pd^{2+} ratio when dosing the reaction mixture.

Table 3.6: The calculated Pd^{4+}/Pd^{2+} ratios at different atmospheric conditions and temperatures.

Condition		Ratio of Pd^{4+}/Pd^{2+}
Atmosphere	T / °C	
0.5 mbar O_2	400	0.69
0.5 mbar O_2	RT	0.70
0.5 mbar CO + O_2	RT	0.88
0.5 mbar CO + O_2	100	0.89

In the Co 2p region under oxygen atmosphere (0.5 mbar O_2) , the Co $2p_{3/2}$ core level peak was centered at 779.6 eV and a weak and broad satellite peak appeared between 789-786 eV indicating the presence of Co_3O_4 [71], shown in figure 3.14(a). No modification of the peaks in the Co 2p region could be verified when dosing the reaction mixture, during the reaction with time or when heating up to 100 °C. This let us conclude that the reaction mixture has no influence on the surface chemical state of the Co species in the temperature range from RT to 100 °C, clarifying also that the surface oxidation state of Co does not correlate with the activity of the catalyst.

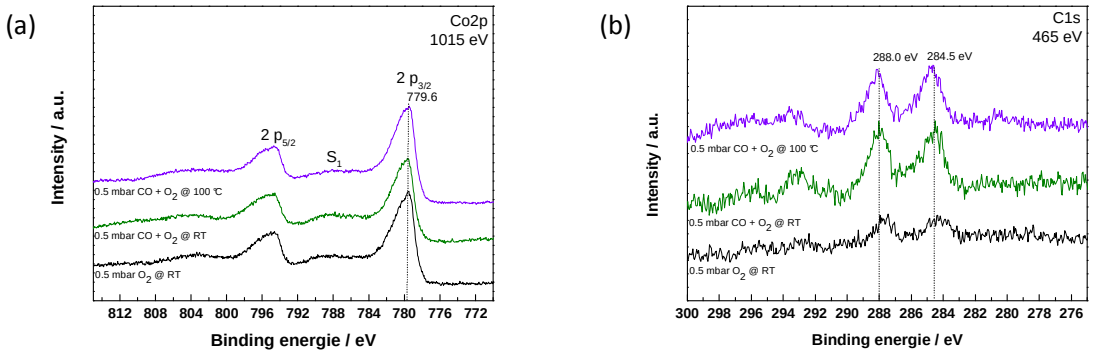

Figure 3.14: XPS spectra of (a) Co 2p (b) C 1s recorded before (0.5 mbar O_2 at RT) and during the reaction (0.5 mbar CO + O_2 at RT and 100 °C) with a photon excitation energy of 1015 eV for the Co 2p and 465 eV for the C 1s. The spectra were obtained after oxygen pretreatment (0.5 mbar O_2 at 400 °C).

The C 1s spectra of PdO/Co_3O_4 recorded under oxygen atmosphere (0.5 mbar O_2) are presented in figure 3.14(b) and exhibited two small peaks at 284.4 eV and 288 eV, where the former corresponds to carbon (amorphous, graphitic, etc.) [88] and the later to carbonates [89] indicating that the oxidation pretreatment could not completely remove the carbon containing species on the surface. Upon dosing the reaction mixture the total amount of the carbon and the carbonates species increased in relation to the total intensity of the Co 2p peak. The ratio of the peak intensities of carbonates:carbon amounts to 1:1 meaning that carbonates and carbon are present in the same amount on the catalyst surface. However, this is in disagreement to the assignments of

the peaks in the CO-TPD curve, discussed in chapter 3.2.3 which suggested a significant higher formation of carbonates compared to carbon. The increase of carbon upon dosing the reaction mixture apparently results from a dissociation of CO to C and CO_2 while the increase of carbonates arises from the adsorption of CO and is in agreement with the *in situ* FTIR studies. In contrast, a slight decrease in intensities of the core level peaks in the C 1s region was noticed with prolonged exposure time at RT, shown in figure 25A(a). The decrease of carbonates is consistent with the observations in the *in situ* time on stream FTIR experiments where bicarbonates partially declined. Thus, we can rather exclude that carbonates, respectively carbon formation causes the deactivation of the catalyst. Upon heating up to 100 °C, no change in the C 1s region could be noticed, plotted in figure 3.14(b).

It is assumed that the carbon had deposited on the Co_3O_4 support and not on the Pd oxide particles as the intensity of the Pd 3d core levels did not change when the total amount of carbon increased after dosing the reaction mixture. A potential carbon deposition covering the Pd particles would be detected in form of a decrease in intensity of the Pd core level peak due to the fact that the amount of deposited carbon is almost four times higher than the amount of Pd on the surface (The atomic ratio C:Pd amounts to 3.7).

To obtain the chemical compositional distribution of the Pd and the Co species from different information depths, a depth profile analysis was conducted. For the depth profile analysis of Co 2p only two different excitation energies, including 1050 and 1250 eV could be chosen as the energy range of the synchrotron based X-Ray radiation was limited towards higher energy values (~1500 eV). In the reaction mixture no significant change of the Pd^{4+}/Pd^{2+} ratio with increasing sample depth, shown in table A2, could be noticed neither at RT nor at 100 °C concluding that there was no enrichment of any of the ionic Pd species on the surface. Furthermore, it can be pointed out that the atomic ratio Pd:Co was different for two different information depths of the sample, shown in table 3.7. The atomic ratio of Pd:Co for the very surface sensitive conditions (E_{kin} = 200 eV) amounted to 0.02 while the less surface sensitive spectrum (E_{kin} = 400 eV) exhibited an atomic ratio of 0.03 (increase of 33 %) which suggests that the sample is enriched in Co at the topmost layers. However, based on the compositional information from only two information depths, it is difficult to draw any reliable conclusion with respect to a potential enrichment of the Co species at the outermost surface layers arising from an encapsulation effect.

Table 3.7: Excitation energies and kinetic energies of the Pd 3d and Co2p core levels with the corresponding inelastic mean free paths (IMFP) in elemental Pd [50] and the calculated atomic ratio Pd:Co. The spectra were recorded under reaction conditions (0.5 mbar $CO+O_2$) at 100 °C.

E_{kin} / eV	$E_{excitaction}$ / eV			IMFP (Pd) /Å*	Atomic ratio Pd:Co
	Pd 3d	Co 2p	C 1s		
200	540	1050	445	6	0.02
400	740	1250	645	9	0.03

In conclusion, the *in situ* XPS results confirmed the presence of two stable Pd oxide phases, namely PdO and PdO_2, on the PdO/Co_3O_4 catalyst surface. No evidence for the existence of metallic Pd was found which is in excellent agreement with the *in situ* FTIR results. Furthermore, no correlation between the activity of the catalyst and the amount of PdO, respectively PdO_2 could be established. Whether the stability of the PdO_2 species resulted from an encapsulation effect cannot be proved at this state. This motivates to further investigate the role of the highly oxidized Pd in CO oxidation. Moreover, the surface oxidation state of Co did not correlated with the catalytic activity as well.

3.5 Deactivation

The final chapter concerns the stabilities of the catalysts at RT.

The PdO/Co_3O_4, the PdO/Fe_2O_3 and the pure Co_3O_4 catalysts were deactivating at RT under reaction conditions ($CO:O_2$ = 1:2) according to the time-on stream studies in the fixed bed flow reactor, shown in figure 3.15, and in the *in situ* FTIR cell, shown in figure 3.9, 3.11 and A16. For PdO/Co_3O_4, deactivation at RT was also observed in the APXPS cell under reaction conditions (0.5 mbar $CO + O_2$) according to the conducted MS analysis of the gas phase composition at the exit of the flow cell, shown in figure A24. The pure Fe_2O_3 catalyst exhibited no activity at RT at all and is therefore not discussed here.

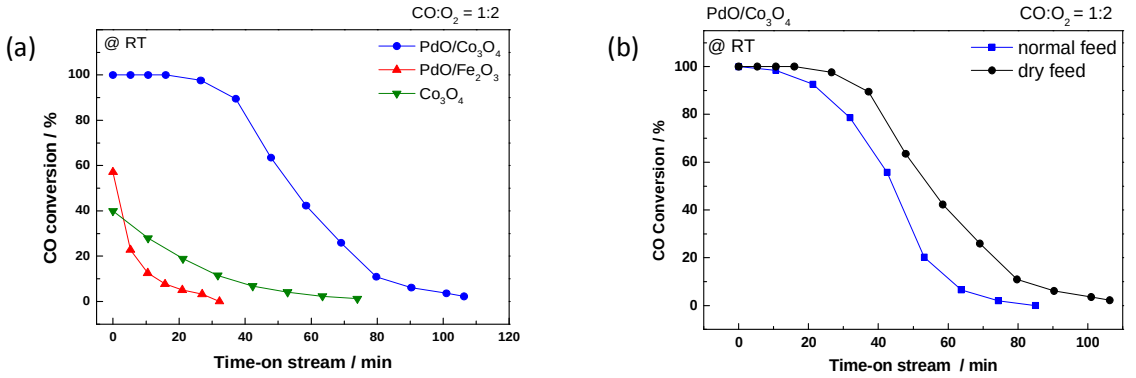

Figure 3.15: (a) CO conversion over the PdO/Co_3O_4 (blue curve) and the PdO/Fe_2O_3 (red curve) catalysts at RT as a function of reaction time. (b) CO conversion over the PdO/Co_3O_4 catalyst at RT in normal feed (blue curve) and dry feed (black curve)The catalysts were previously subjected to an oxidation pretreatment at $_4$00 °C for ½ h.

When comparing the stabilities of the PdO/Co_3O_4, PdO/Fe_2O_3 and Co_3O_4 catalysts under reaction conditions after a reaction time of 30 min at RT, see figure 3.15(a), we can note that PdO/Co_3O_4 was the most stable catalyst (loss of only 5 % in CO conversion) followed by Co_3O_4 (loss of 70 % in CO conversion) and PdO/Fe_2O_3 with the lowest stability (complete loss of its activity). However, after a reaction time of 70, respectively 110 min also Co_3O_4 and PdO/Co_3O_4 lost their activities completely and therefore none of the catalysts exhibit long-term stability at RT which is consistent with the time resolved *in situ* FTIR experiments.

For the PdO/Fe_2O_3 catalyst, the *in situ* FTIR study indicated that the fast deactivation of the catalyst at RT resulted from the ongoing reduction process of PdO to metallic Pd as it is known that metallic Pd gets self-poisoned by CO resulting in an inhibition of the CO oxidation reaction. Whether the reduction process is accompanied by a sintering of the Pd particles cannot be answered at this state.

In contrast, for the PdO/Co_3O_4 we can exclude a deactivation at RT resulting from a reduction process of the PdO particles and a resulting self-poisoning of Pd by CO as the presence of only oxidized Pd species, namely PdO and PdO_2, was evident based on *in situ* APXPS and *in situ* FTIR. Moreover, the decrease in CO conversion at RT did not originate from a relative change of the oxidation state of the oxidized Pd species as the Pd^{4+}/Pd^{2+} ratio kept constant during the deactivation of the catalyst. Furthermore, the accumulation of carbonate species or the deposition of carbon as a reason for deactivation could also be excluded based on the C 1s core level spectra

derived from the *in situ* APXPS, and *in situ* FTIR studies. Also a reduction of Co_3O_4 could not be verified as a deactivation mechanism with respect to the Co 2p core level spectra. However, it is questionable if a slight reduction of Co_3O_4 e.g. at the metal-support interface could already be detected via a change in the Co 3p spectra as the XPS analysis might not be sensitive enough. Our observations are consistent with the observations by Jansson et al. [39] on pure Co_3O_4 in CO oxidation, who did not observe a deactivation due to carbonates, carbonyls, C_{surf} or an irreversible reduction of Co_3O_4 and instead suggested a reconstruction of the Co_3O_4 surface as the reason for deactivation.

The reason for the difference in the stabilities of the PdO/Co_3O_4 and the Co_3O_4 catalysts with prolonging reaction time cannot be clarified at this point as the time resolved *in situ* FTIR spectra at RT, shown in figure A16, showed besides the faster decrease of the CO_2 band over the Co_3O_4 compared to the PdO/Co_3O_4 no significant difference neither in the hydroxyl, carbonyl nor in the carbonate region.

The fixed bed flow experiments were also carried out in the reaction mixture applying an additional drying step with a cold trap (“dry feed”) over the PdO/Co_3O_4 catalyst at RT, shown in figure 3.15(b), to estimate the influence of moisture on the catalytic activity. In our study the catalyst had deactivated in the normal feed after 90 min while in the dry feed it lost its activity completely after 110 min. Therefore, we proved that the moisture is a deactivation factor at RT which was also revealed by the *in situ* FTIR studies, shown in A18(a), and is in agreement with the study by Skoglundh et al. [42]. However, the results also indicate that moisture is not the only reason for deactivation of the catalyst and further unknown deactivation processes apparently occur in parallel. The *in situ* FTIR, shown in figure A18, further revealed that the exclusion of moisture increased the stability of bicarbonates during time-on stream experiments. However, the formation of bicarbonates need the presence of hydroxyl groups on the catalyst surface and thus, it is believed that the dry feed contains some residues of moisture. Further investigations are required to find the fundamentals of the increased stability of bicarbonates and the underlying deactivation mechanism of moisture.

Chapter 4

4 Summary and Outlook

In this work Co_3O_4 and Fe_2O_3 supported Pd catalysts were successfully synthesized, characterized and studied in their catalytic performance in CO oxidation ($CO:O_2$ = 1:2) after different pretreatments (oxidative or reductive). Via ex situ methods, namely N_2-sorption, XRD and TEM, structural information (texture and morphology) of the catalysts could be gained while chemical information (redox and adsorption/desorption chemistry) was obtained through FTIR spectroscopy, CO- and O_2-TPD, H_2-TPR and TPO measurements. In addition, *in situ* methods, namely *in situ* FTIR spectroscopy and *in situ* APXPS, provided deeper insight into the chemical nature of Pd states, surface species and adsorption sites under relevant reaction conditions and thus, CO oxidation and deactivation pathways.

The two catalysts with similar surface areas were synthesized by wet impregnation method yielding highly dispersed Pd particles with a mean size of sub-nm to 2 nm on the Co_3O_4 and of 5 to 10 nm on the γFe_2O_3 support according to TEM images.

The kinetic CO oxidation studies revealed that after loading Pd on Co_3O_4, respectively Fe_2O_3 an enhancement of the activity for both catalysts was achieved with respect to decreased T_{50} and increased reaction rates. The greatest enhancement in activity was achieved for the PdO/Fe_2O_3 catalyst (decrease of T_{50} by 120 °C) compared to pure Fe_2O_3 with a low intrinsic activity (T_{50}= 230 °C). The activity of the PdO/Co_3O_4 was only slightly increased (decrease of T_{50} by 30 °C), though the catalyst revealed a higher activity than PdO/Fe_2O_3 due to a high intrinsic activity of pure Co_3O_4 (T_{50}= 105 °C).

The following findings derived from CO- and O_2-TPD and CO adsorption experiments followed by FTIR were in good agreement with the different intrinsic activities of the pure oxides and the enhanced activities after loading Pd.

Co_3O_4 vs Fe_2O_3:

- CO adsorption as carbonates on pure Co_3O_4 (weakly bonded bicarbonates and strongly bonded bidentate carbonates)

- No CO adsorption on pure Fe_2O_3

After loading Pd on Co_3O_4:

(1) Very small CO adsorption on metallic Pd sites
(2) Increase of the amount of weakly bonded bicarbonates
(3) Decrease of the total amount of carbonates
(4) Lower desorption temperature of CO as CO_2
(5) Higher availability of easily removable oxygen

After loading Pd on Fe_2O_3:

(1) Large CO adsorption on metallic Pd sites (weakly bonded CO on Pd)
(2) Formation of weakly bonded bicarbonates

Interestingly, these findings clearly show some differences in the CO adsorption and desorption behavior on the two supported Pd catalysts. Via *in situ* studies under relevant catalytic working conditions it was shown that the Pd catalysts also exhibited different Pd oxidation states, surface species and adsorptions sites under reaction conditions and thus, different CO oxidation pathways and intermediates. *In situ* FTIR studies revealed that CO did not bond to metallic Pd and solely very small CO-$Pd^{\delta+}$ bands were present under reaction conditions suggesting the presence of PdO_x species. In contrast, for PdO/Fe_2O_3 strong CO bands on metallic Pd were detected already at RT indicating the reduction of PdO by CO. The CO-Pd^o bands on PdO/Fe_2O_3 were also present at higher temperatures (~150 °C), where a full CO conversion was observed. *In situ* APXPS proved the absence of metallic Pd on Co_3O_4 and revealed the presence of two oxidized Pd states, namely Pd^{2+} (PdO) and Pd^{4+} (PdO_2). During the course of the reaction i.e. when the catalyst was altered from an active to an inactive state, the ratio of Pd^{4+}/Pd^{2+} kept constant. Thus, a correlation between the oxidation state of Pd on Co_3O_4 and the activity could not be established. The stability of the highly oxidized Pd^{4+} species was suggested to result from an interdiffusion of the Pd^{4+} ions into the Co_3O_4 lattice or coverage by a CoO_x layer forming Pd-O-Co bonds.

Besides the small CO adsorption on ionic $Pd^{\delta+}$ species on PdO/Co_3O_4, *in situ* FTIR further revealed that CO had mainly adsorbed as two different kinds of carbonates, namely weakly bonded bicarbonates and strongly bonded bidentate carbonates, where bicabonates were

decreasing and bidentate carbonates kept constant with decreasing CO_2 production. In contrast, on PdO/Fe_2O_3 only bicarbonates were evident under reaction conditions which were found to result from readsorbed CO_2 according to CO_2 adsorption experiments.

Based on these results, CO oxidation pathways including involved intermediates can be postulated. For PdO/Co_3O_4 it is assumed that the reaction proceeds via bicarbonates serving as intermediates on Co_3O_4 with PdO and PdO_2 acting as promoters. Over PdO/Fe_2O_3, the reaction apparently proceeds via CO adsorption on metallic Pd sites while carbonates are not involved as intermediates. As an explanation for Pd present in different oxidation states on the Co_3O_4 and the Fe_2O_3, the different Pd particle sizes, observed in HRTEM or/and the different chemical nature of the supports resulting in different metal-support interactions (e.g. charge transfer, encapsulation, interdiffusion) are assumed. Furthermore, the results indicate that the CO oxidation rate is not affected by a CO poisoning of Pd for both catalysts, and the supports Co_3O_4, respectively Fe_2O_3 provide active oxygen (lattice or chemisorbed oxygen) at or close to the metal-support interface. Thus, the reaction does not follow the competitive Langmuir-Hinshelwood mechanism on Pd (CO and O_2 compete for the same active sites) which is well-known for Pd supported on inert oxides e.g. SiO_2.

Moreover, the influence of the pretreatment was assessed by subjecting the catalysts to either an oxidation (synthetic air flow) or a reduction (5 % H_2 in He flow) prior to the kinetic CO oxidation measurements. After the reduction pretreatment the catalytic activity of the Pd/CoO_x (red. 100 °C) catalyst decreased while the activity of Pd/FeO_x (red. 100 or 300 °C) was unaffected. The different influence of the reduction pretreatment on the catalytic behavior of the catalysts was attributed to the different redox chemistry. For Pd/CoO_x the decrease of the catalytic activity was ascribed to the phase transformation from Co_3O_4 to CoO and metallic Co resulting in an insufficient availability of active oxygen. The unaffected activity of Pd/FeO_x after the reduction pretreatment can be explained by a higher stability against reduction of the Fe_2O_3 phase and thus, higher availability of active oxygen species.

Finally, deactivation of the catalysts during the course of reaction at RT was investigated. The time on stream *in situ* FTIR studies revealed that the deactivation of the PdO/Fe_2O_3 catalyst at RT occurred due to a reduction of PdO_x to metallic Pd by CO in reaction mixture.

For PdO/Co_3O_4, it was found out that a low content of moisture (~3 ppm) decreased the stability of the catalyst at RT. Though, carbon and carbonate species were observed under reaction conditions, they could be excluded as reasons for deactivation as they were not increasing during the course of deactivation. Furthermore, a reduction of the surface of the support Co_3O_4 or the oxidized Pd phases were not evident during the decrease of activity according to *in situ* FTIR and *in situ* APXPS. Nevertheless, according to our results moisture is not the only deactivation factor at RT and other unknown deactivation processes apparently occur in parallel.

In near future, for PdO/Fe_2O_3, *in situ* APXPS studies would be useful to get more insight into the active phases of Pd and Fe_2O_3, CO oxidation pathways. In addition, a comparison of the Pd core level intensities with those of PdO/Co_3O_4 would help to reveal a potential present encapsulation of Pd by CoO_x.

In addition, low-energy ion scattering (LEIS) [90] can be a useful surface analyzing method to reveal the potentially present encapsulation of Pd by a CoO_x layer by determining the quantitative chemical composition in the outermost layer but also in the second or third layer [91].

To clarify whether Pd in the unusually high oxidation state is stabilized by a dispersion within the Co_3O_4 lattice via forming e.g. Pd-O-Co moieties, extended X-Ray absorption fine structure (EXAFS) studies shall be performed to get an insight into the local chemical and structural environment of the ionic Pd species by determining the bond length, the coordination number and most important the nature of neighboring atoms in surrounding coordination shells (e.g. Pd-O-Pd, Pd-O-Co) [38]. To obtain surface sensitive spectra the total electron yield or the elastic Auger-electron yield [92] is usually detected.

Appendix A

BET

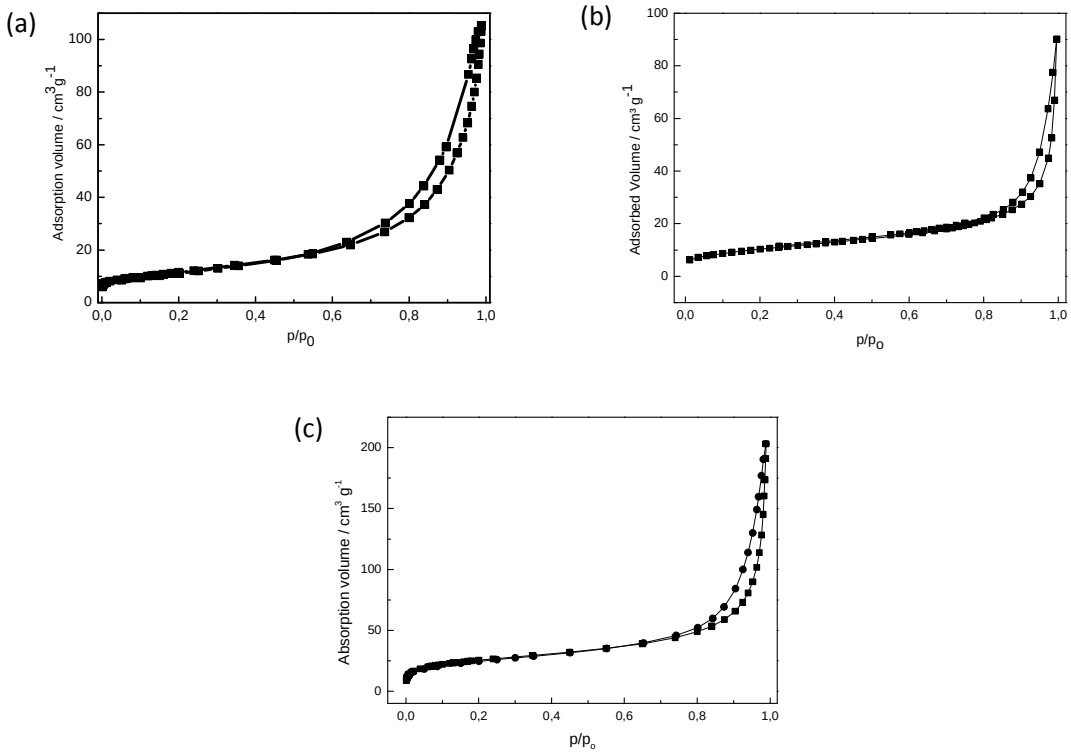

Figure A1: N_2-adsorption-desorption isotherm for the (a) Fe_2O_3, the (b) Co_3O_4 and the (c) SiO_2 support.

TEM

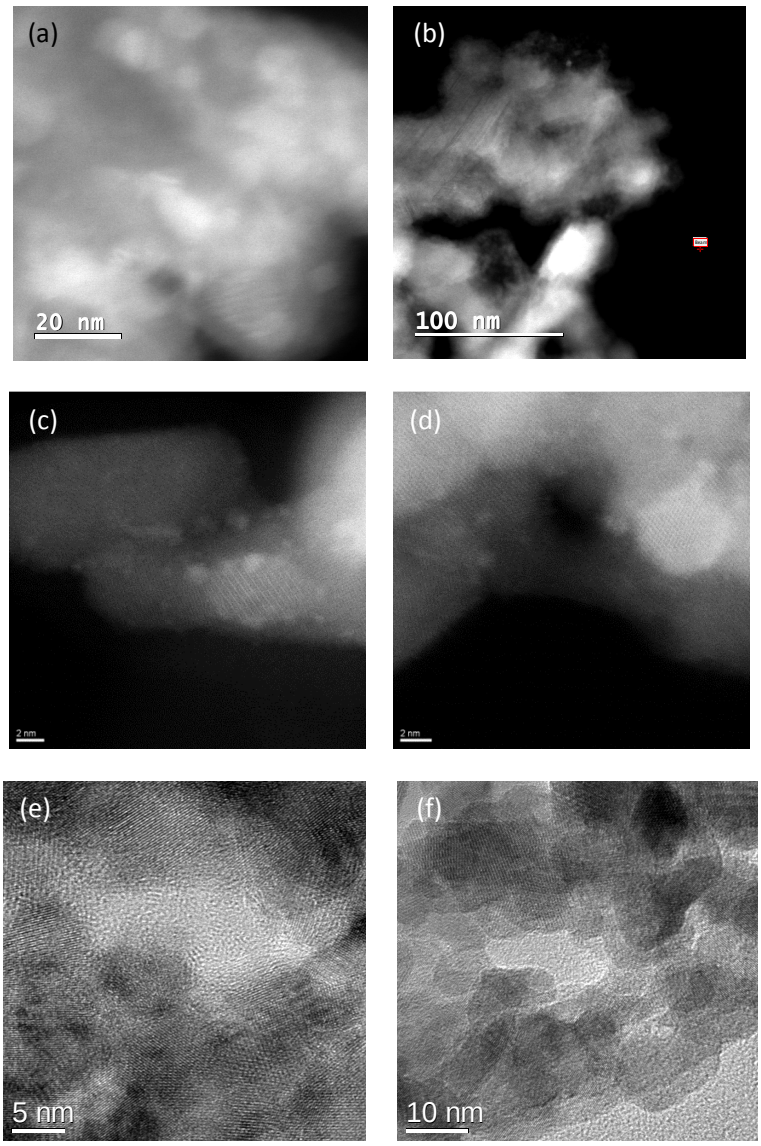

Figure A2: The (a-d) HAADF images and (e,f) HRTEM of the PdO/Co_3O_4. (c,d) were obtained from the STEM Hitachi at Zurich where the bright spots representing the Pd particles.

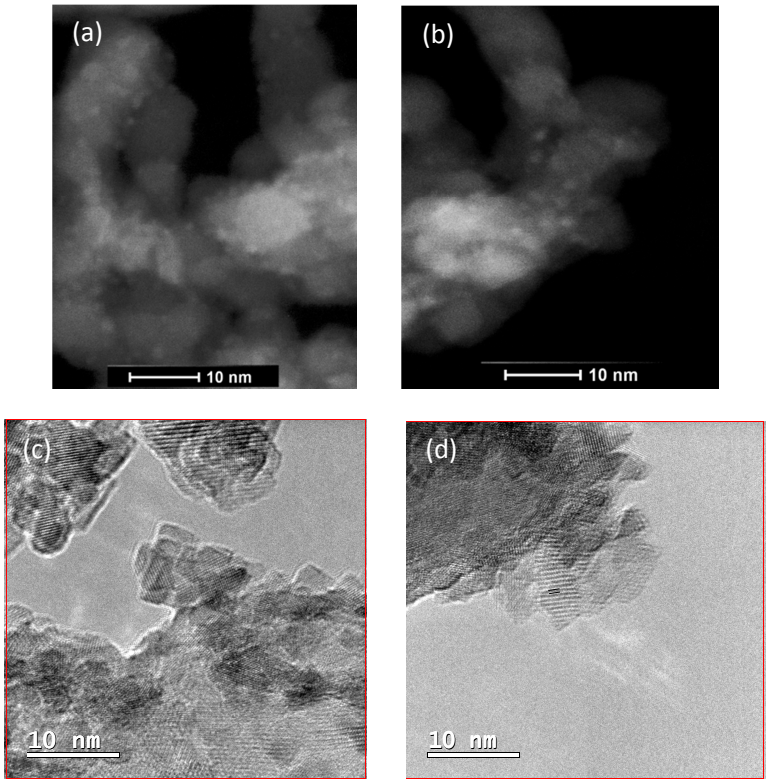

Figure A3: (a,b) HAADF and (c,d) HRTEM images of the Pd/CoO_x (red. 100 °C) in HRTEM images of the PdO/Co_3

O_4.

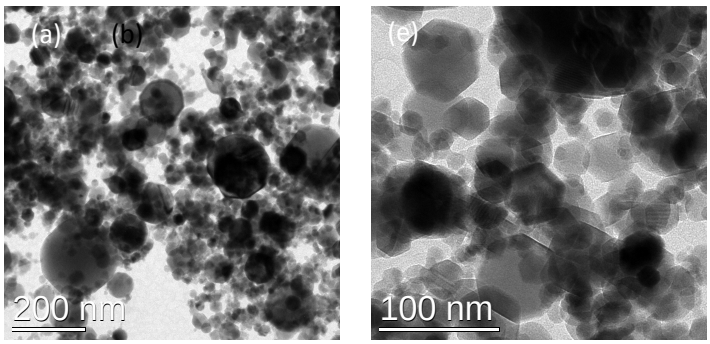

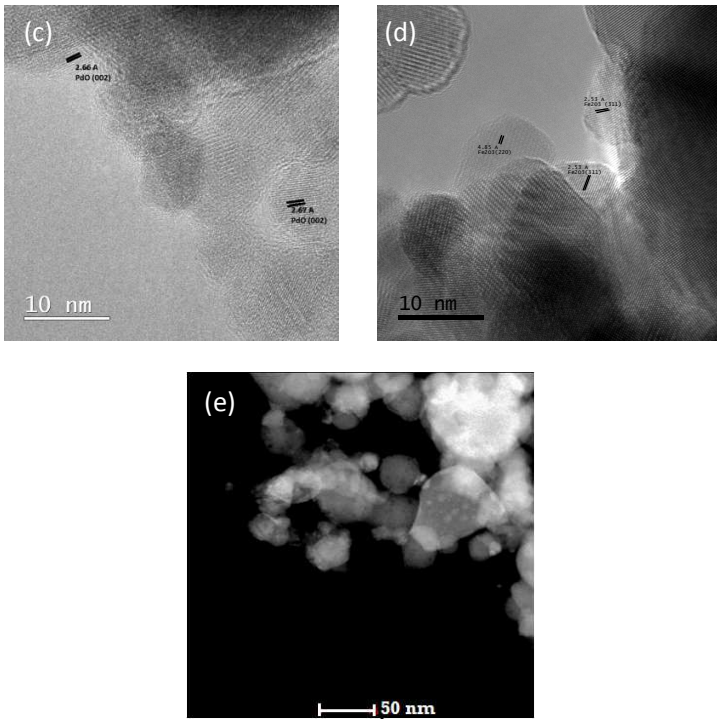

Figure A4: (a,b) Bright field TEM and (c,d) HRTEM images of the PdO/Fe_2O_3 catalyst and (e) HAADF image of the Pd/FeO_x (red. 300 °C) catalyst.

EDX

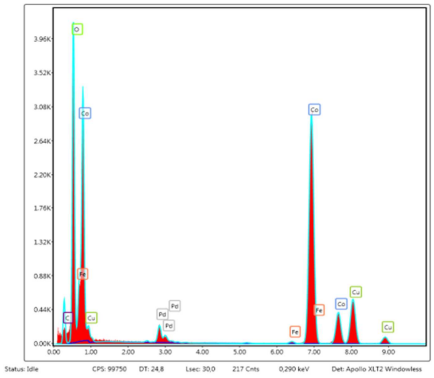

Figure A5: EDX spectrum of the bulk phase of PdO/Co3O4 corresponding to figure A2 (a).

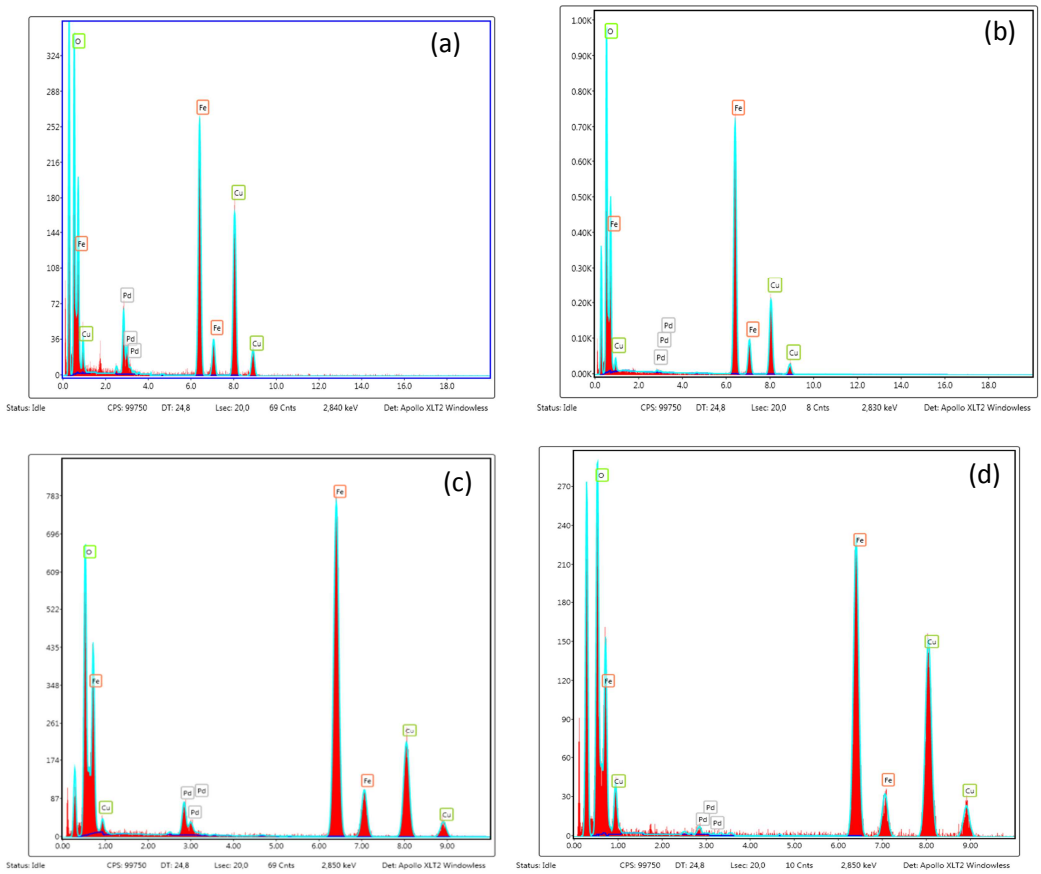

Figure A6: EDX spectra of the PdO/Fe_2O_3 sample at the position (a) 1, (b) 2 from figure 3.3(c) and at the position (c) 3 and (d) 4 in the figure 3.3(d).

Kinetic measurements

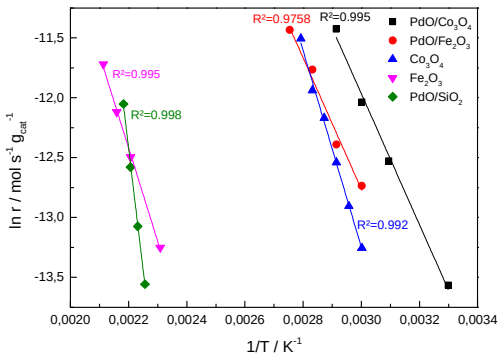

Figure A7: Arrhenius plots of the reaction rates over the different catalysts.

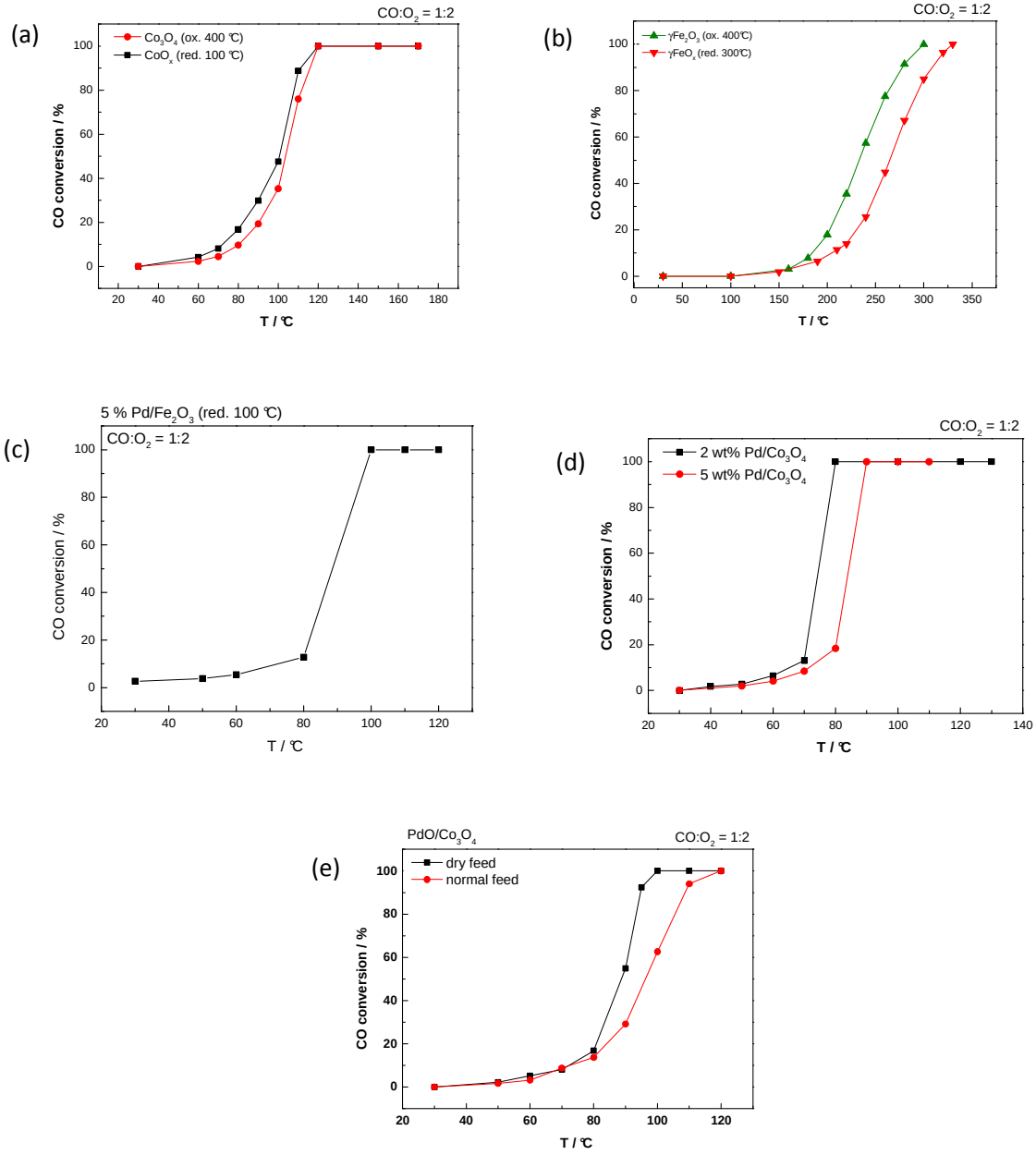

Figure A8: Light-off curves for CO oxidation over (a) Co_3O_4 and CoO_x (red. 100 °C), (b) Fe_2O_3 and FeO_x (red. 300 °C), (c) 5 % Pd/Fe_2O_3, (d) 2 and 5 wt% PdO/Co_3O_4 and (e) PdO/Co_3O_4 in dry and normal feed.

TPD

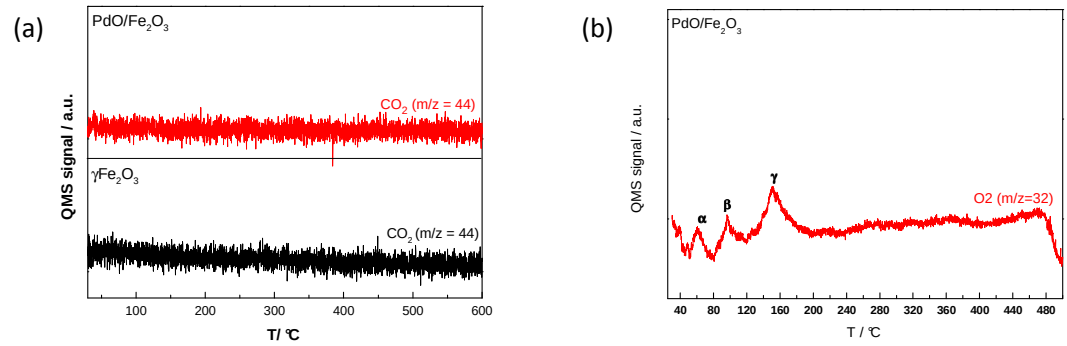

Figure A9: (a) CO_2 desorption profiles during CO-TPD of the PdO/Fe_2O_3 (red curve) and the Fe_2O_3 (black curve) and (b) O_2 desorption profiles during TPO of the PdO/Fe_2O_3 catalyst.

H_2-TPR

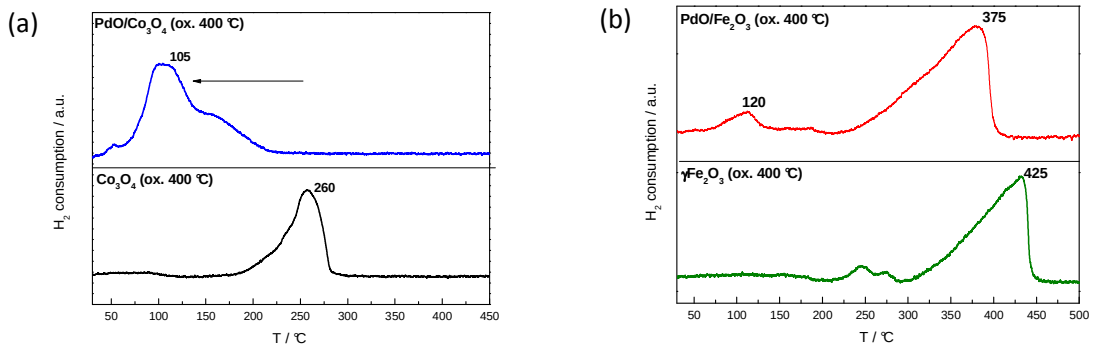

Figure A10: H_2-TPR profiles of the (a) PdO/Co_3O_4 (blue) and the Co_3O_4 (black) and (b) PdO/Fe_2O_3 (red) and Fe_2O_3 (green).

CO-TPR

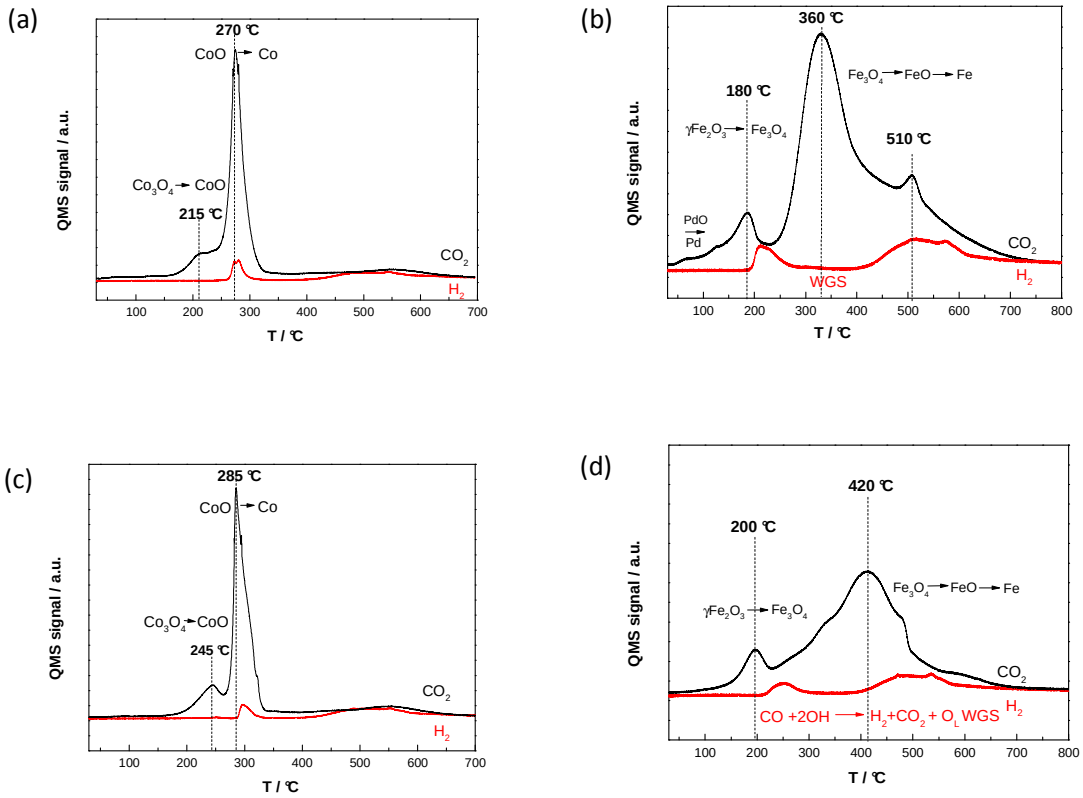

Figure A11: H_2 and CO_2 desorption profiles during the CO-TPR of the (a) PdO/Co_3O_4, (b) PdO/Fe_2O_3, (c) Co_3O_4 (black), and (d) Fe_2O_3.

FTIR

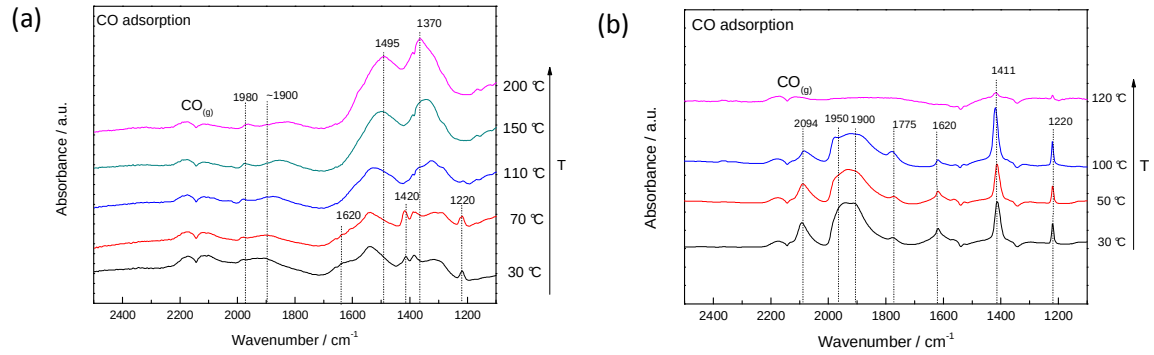

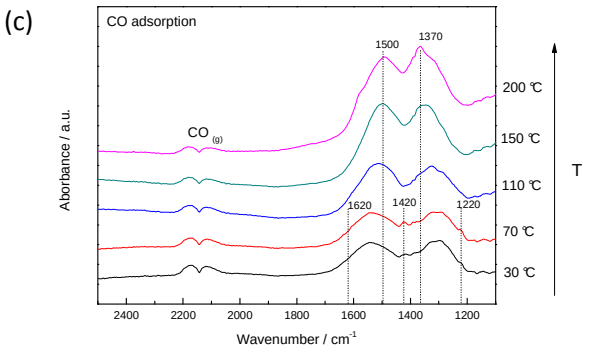

Figure A12: FTIR spectra of the (a) PdO/Co_3O_4 and (b) PdO/Fe_2O_3 and (c) Co_3O_4 catalysts in 5 % CO (50 mbar) in He flow. The catalyst was previously pretreated in synthetic air (400 °C; ½ h).

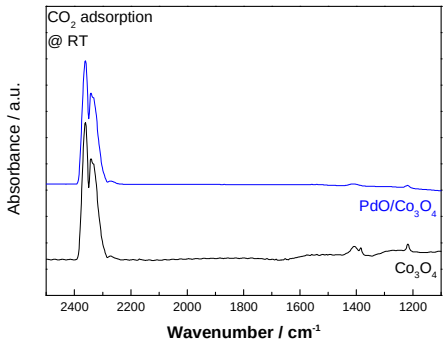

Figure A13: FTIR spectra of PdO/Co_3O_4 (blue) and Co_3O_4 (black) in 5 % CO_2 in He flow at RT. The samples were previously subjected to an oxidation pretreatment at 400 °C.

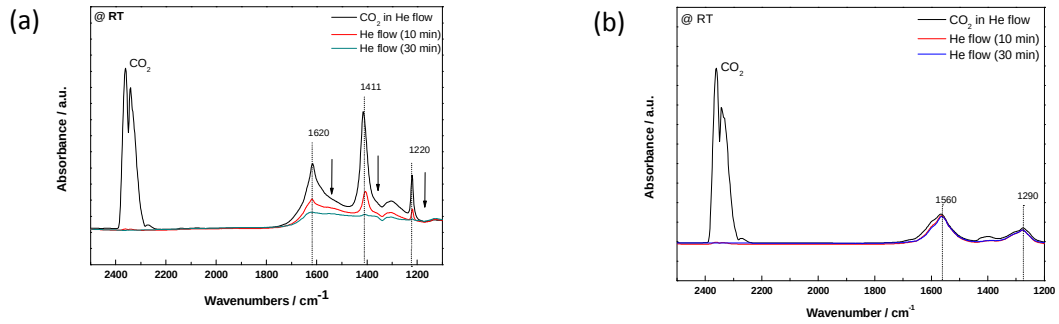

Figure A14: FTIR spectra of (a) PdO/Fe_2O_3 and (b) Fe_2O_3 recorded in 5 % CO_2 (50 mbar) in He flow and in pure He flow after 10 and 30 min. All spectra were recorded at RT and after an oxidation pretreatment at 400 °C.

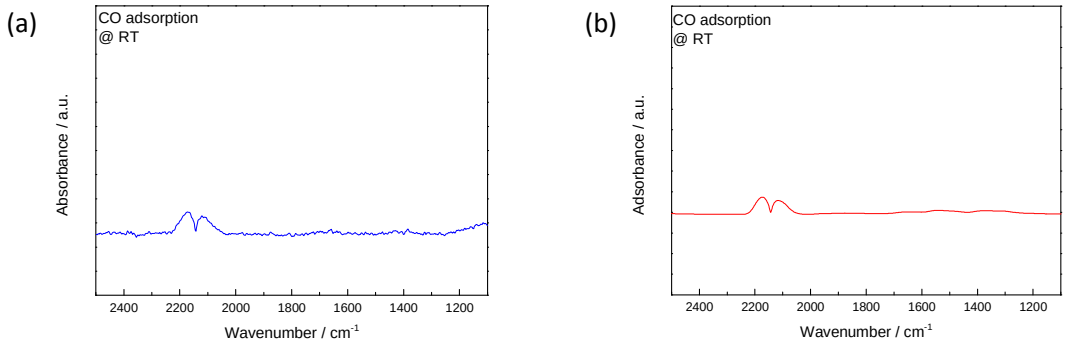

Figure A15: FTIR spectra of the (a) PdO/CoO_x (red. 100 °C) and (b) PdO/FeO_x (red. 100 °C) catalysts in 5 % CO (50 mbar) in He flow.

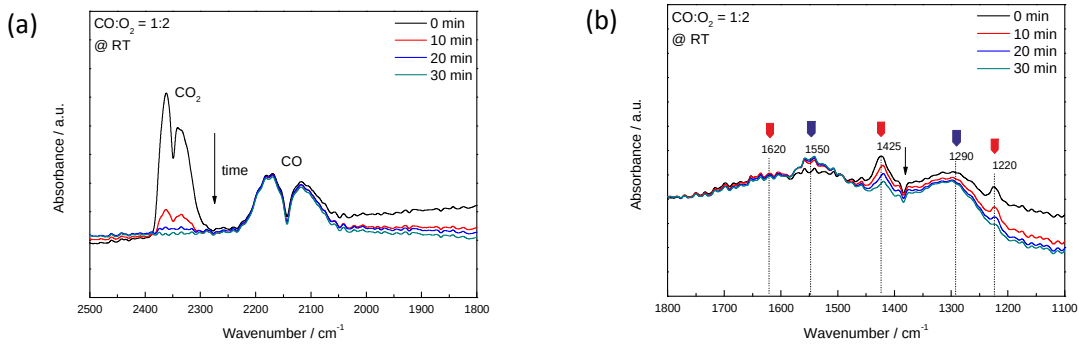

Figure A16: *In situ* FTIR spectra recorded of Co_3O_4 under reaction conditions ($CO:O_2$ = 1:2) at RT as a function of exposure time and plotted in the spectral range of (a) 2500-1800 cm^{-1} and (b) 1800-1100 cm^{-1}. The catalyst was previously pretreated in synthetic air (400 °C; ½ h).

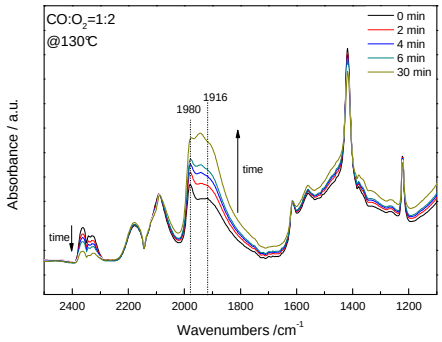

Figure A17: *In situ* FTIR spectra recorded of PdO/Fe_2O_3 under reaction conditions ($CO:O_2$ = 1:2) at 130 °C as a function of exposure time. The catalyst was previously pretreated in synthetic air (400 °C; ½ h).

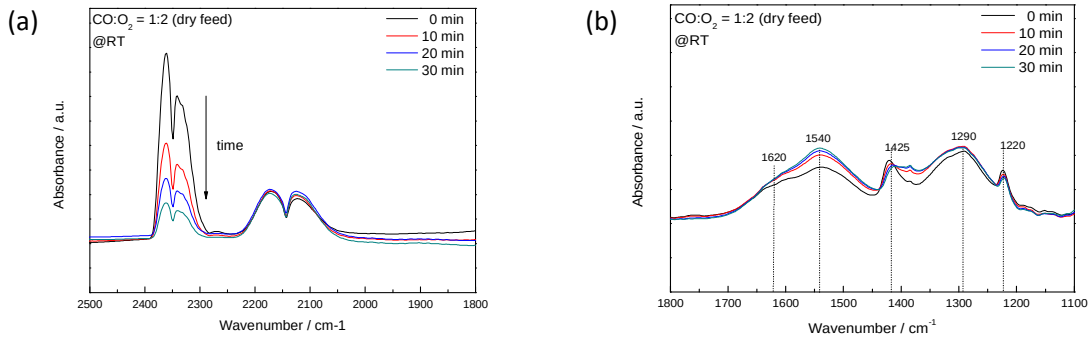

Figure A18: *In situ* FTIR spectra recorded of PdO/Co_3O_4 in dry feed under reaction conditions ($CO:O_2$ = 1:2) at RT as a function of exposure time and plotted in the spectral range of (a) 2500-1800 cm^{-1} and (b) 1800-1100 cm^{-1}. The catalyst was previously pretreated in synthetic air (400 °C; ½ h).

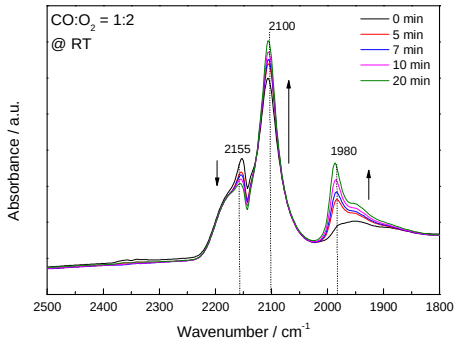

Figure A19: *In situ* FTIR spectra recorded of PdO/SiO_2 under reaction conditions ($CO:O_2$ = 1:2) at RT as a function of exposure time. The catalyst was previously pretreated in synthetic air (400 °C; ½ h).

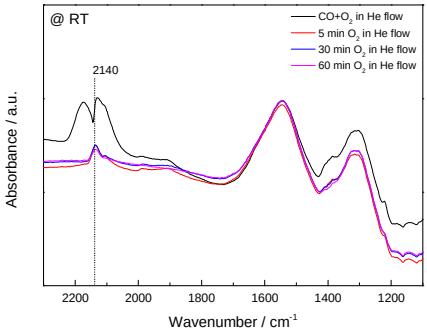

Figure A20: *In situ* IR spectra recorded of PdO/Co_3O_4 under reaction conditions ($CO:O_2$ = 1:2) and in He flow (10 and 30 min).

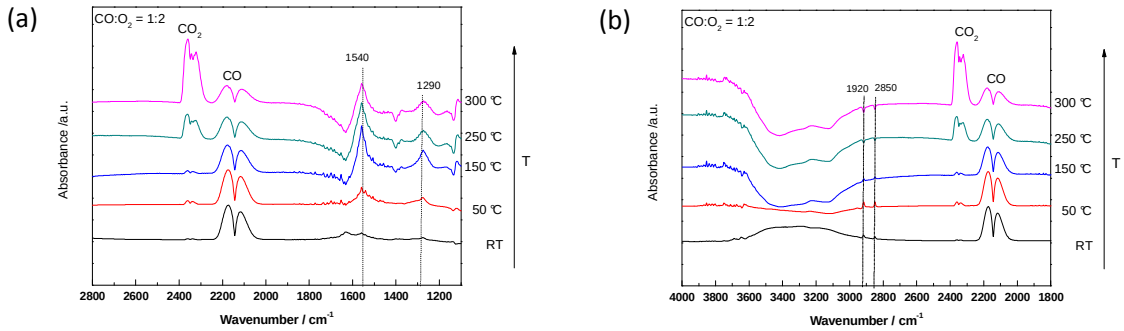

Figure A21: *In situ* IR spectra recorded of Fe_2O_3 under reaction conditions ($CO:O_2$ = 1:2) as a function of temperature plotted in the spectral range of (a) 4000-1800 cm^{-1} and (b) 2800-1100 cm^{-1}. The spectra were recorded after *in situ* time-on stream FTIR experiments at RT.

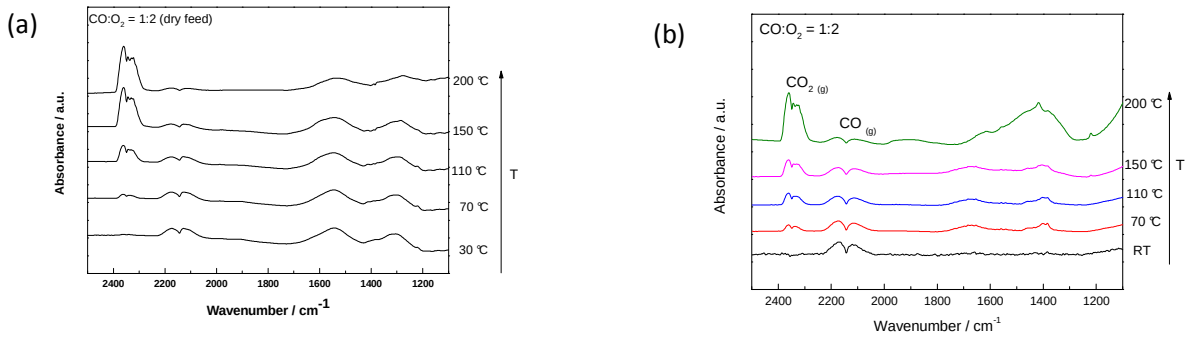

Figure A22: *In situ* IR spectra recorded of (a) PdO/Co3O4 in dry feed and (b) Pd/FeOx (red. 100 °C) under reaction conditions ($CO:O_2$ = 1:2) as a function of temperature. The catalyst was previously pretreated in synthetic air (400 °C; ½ h).

In situ APXPS

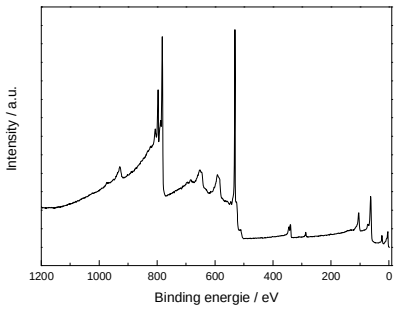

Figure A23: XPS spectrum (survey scan) of the freshly PdO/Co_3O_4 catalyst.

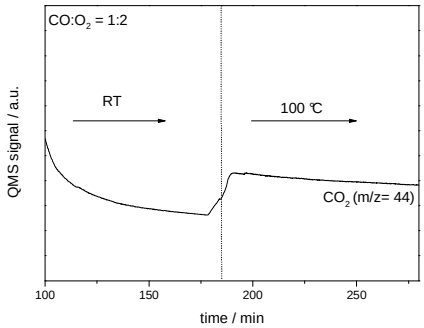

Figure A24: QMS signal of CO_2 (m/z = 44) as a function of time under CO oxidation conditions ($CO:O_2$ = 1:2) at RT and at 100 °C.

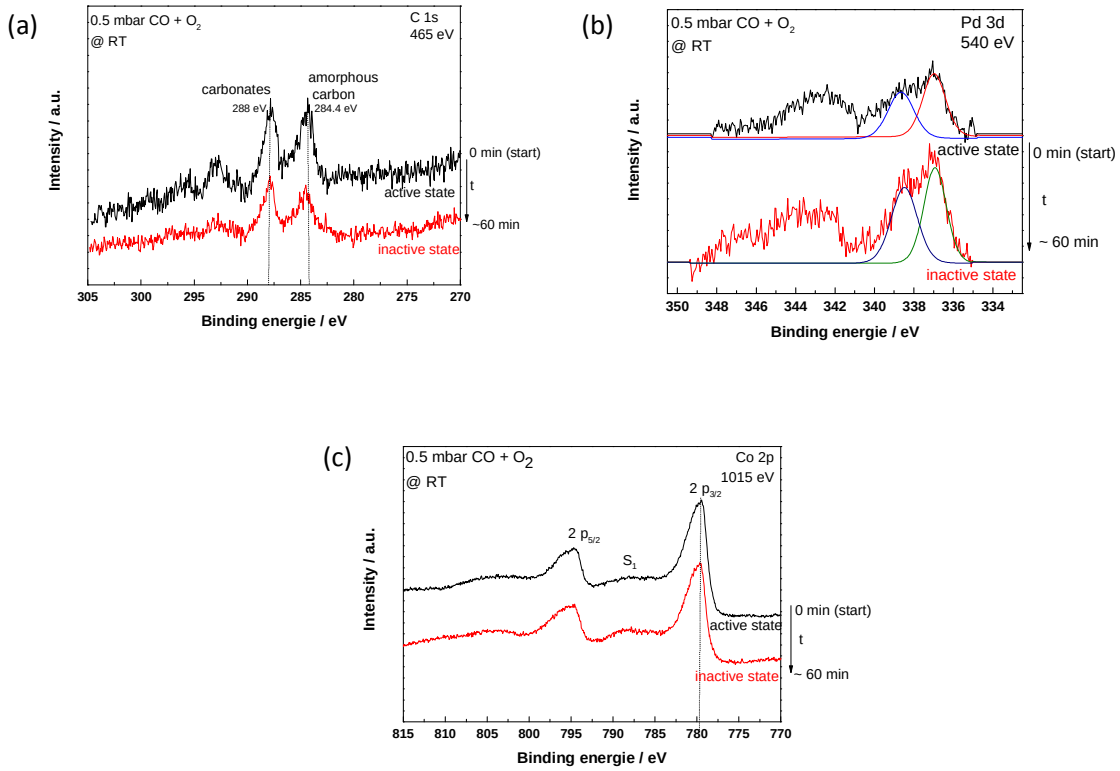

Figure A25: XPS spectra of (a) C 1s, (b) Pd 3d and (c) Co 2p recorded during the reaction (0.5 mbar CO + O_2 at RT) at the start of the reaction (t = 0min) and after a reaction time of t ~ 60 min with a photon excitation energy of 465 eV. The spectra were obtained after oxygen pretreatment (0.5 mbar O_2 at 400 °C).

Table A1: Atomic cross sections for photo ionization of the electrons from the core levels Pd 3d, Co 2p and C 1s.

E_{kin} /eV	Atomic cross sections		
	Pd 3d	Co 2p	C 1s
200	2.84	0.643	0.323
400	1.456	0.4121	0.131

Table A2: Kinetic and excitation energies of the Pd 3d core levels with the corresponding inelastic mean free paths (IMFP) in elemental Pd [50] and the calculated atomic ratio Pd^4/Pd^{2+}. The spectra were recorded under reaction (0.5 mbar CO + O_2) at RT and at 100 °C.

E_{kin}/ eV	$E_{excitation}$/ eV	IMFP (Pd) /Å	Atomic Ratio Pd^{4+}/Pd^{2+} at RT	Atomic Ratio Pd^{4+}/Pd^{2+} at 100 °C
200	540	6	0.91	0.88
400	740	9	0.83	0.89
600	940	12	0.91	0.80
800	1140	15	0.90	0.89

Table A3: Calculated atomic ratio Pd^{4+}/Pd^{2+} recording during an active and inactive catalytic state of the catalyst under reaction (0.5 mbar CO + O_2) at RT.

Catalytic state	Atomic Ratio Pd^{4+}/Pd^{2+} at RT
active	0.87
inactive	0.83

Appendix B

Abbreviations

APXPS Ambient Pressure X-ray Photoelectron Spectroscopy

BET Brunauer, Emmett and Teller

DFT Density functional theory

EDX Energy dispersive X-ray spectroscopy

EXAFS Extended X-ray absorption fine structure

FTIR Fourier-Transform infrared

FID Flame ionization detector

GC Gas chromatograph

HAADF High angle annular dark field

HRTEM High resolution TEM

IMFP Inelastic mean free paths

MS Mass spectrometer

RT Room temperature

SMSI Strong metal-support interaction

STM Scanning tunneling micrograph

TEM Transmission electron microscopy

TPD Temperature programmed desorption

TPO Temperature programmed oxidation

TPR Temperature programmed reduction

UPS Ultraviolet photoelectron spectroscopy

XANES X-ray absorption near edge structure

XRD X-Ray diffraction

Bibliography

[1] U.Ozkan, “Designe of heterogeneous catalysis”, Wiley-VCH, 2009.

[2] R. Westerholm and A. Christensen, “Regulated and unregulated exhaust emissions from two-three wy catalyst equpped gasoline fuelled vehicles,” vol. 30, no. 20, pp. 3529–3536, 1996.

[3] M. Skoglundh and E. Fridell, “Strategies for enhancing low-temperature activity,” *Topics in catalysis*, vol. 28, no. 1-4, pp. 79–87, 2004.

[4] http://anbuvelavan.blogspot.co.at/2012/11/catalytic-converter.html, Dec. 2014.

[5] Q. Fu, T. Wagner, S. Olliges, and H.-D. Carstanjen, “Metal-oxide interfacial reactions: encapsulation of Pd on TiO_2 (110).,” *J. Phys. Chem. B*, vol. 109, no. 2, pp. 944–51, Jan. 2005.

[6] K. Hayek, M. Fuchs, and B. Klötzl, W. Reicher and G. Rupprechter, “Studies of metal – support interactions with ‘ real ’ and ‘ inverted ’ model systems : reactions of CO and small hydrocarbons with hydrogen on noble metals in contact with oxides,” *Topics in catalysis*, vol. 13, pp. 55–66, 2000.

[7] R. Naumann d’Alnoncourt, M. Friedrich, E. Kunkes, D. Rosenthal, F. Girgsdies, B. Zhang, L. Shao, M. Schuster, M. Behrens, and R. Schlögl, “Strong metal–support interactions between palladium and iron oxide and their effect on CO oxidation,” *J. Catal.*, vol. 317, pp. 220–228, Aug. 2014.

[8] H. Zhu, Z. Qin, W. Shan, W. Shen, and J. Wang, “Low-temperature oxidation of CO over Pd/CeO_2–TiO_2 catalysts with different pretreatments,” *J. Catal.*, vol. 233, no. 1, pp. 41–50, Jul. 2005.

[9] L. Meng, A. Jia, J. Lu, L. Luo, W. Huang, and M. Luo, “Synergetic Effects of PdO Species on CO Oxidation over PdO-CeO_2 Catalysts,” *J. Catal.* , vol 115, pp. 19789–19796, 2011.

[10] L. S. F. Feio, C. E. Hori, S. Damyanova, F. B. Noronha, W. H. Cassinelli, C. M. P. Marques, and J. M. C. Bueno, “The effect of ceria content on the properties of $Pd/CeO_2/Al_2O_3$ catalysts for steam reforming of methane,” *Appl. Catal. A Gen.*, vol. 316, no. 1, pp. 107–116, Jan. 2007.

[11] E. B. Fox, A. F. Lee, K. Wilson, and C. Song, “In-situ XPS Study on the Reducibility of Pd-Promoted Cu/CeO_2 Catalysts for the Oxygen-assisted Water-gas-shift Reaction,” *Top. Catal.*, vol. 49, no. 1–2, pp. 89–96, Apr. 2008.

[12] K. Sun, “Characterization and catalytic performances of La doped Pd/CeO_2 catalysts for methanol decomposition,” *Appl. Catal. A Gen.*, vol. 268, no. 1–2, pp. 107–113, Aug. 2004.

[13] K. An, S. Alayoglu, N. Musselwhite, S. Plamthottam, G. Melaet, A. E. Lindeman, and G. a Somorjai, “Enhanced CO oxidation rates at the interface of mesoporous oxides and Pt nanoparticles.,” *J. Am. Chem. Soc.*, vol. 135, no. 44, pp. 16689–96, Nov. 2013.

[14] Y. Yu, T. Takei, H. Ohashi, H. He, X. Zhang, and M. Haruta, “Pretreatments of Co3O4 at moderate temperature for CO oxidation at −80°C,” *J. Catal.*, vol. 267, no. 2, pp. 121–128, Oct. 2009.

[15] S. J. Tauster, S. C. Fung, and R. L. Garten, “Strong Metal-Support Interactions . Group 8 Noble Metals Supported on $Ti0_2$,” *J. Am. Chem. Soc.*, pp. 170–175, 1978.

[16] J.-Y. Luo, M. Meng, J.-S. Yao, X.-G. Li, Y.-Q. Zha, X. Wang, and T.-Y. Zhang, “One-step synthesis of nanostructured Pd-doped mixed oxides MO_x-CeO_2 (M=Mn, Fe, Co, Ni, Cu) for efficient CO and C_3H_8 total oxidation,” *Appl. Catal. B Environ.*, vol. 87, no. 1–2, pp. 92–103, Mar. 2009.

[17] Z. Qin, M. Lewandowski, Y. Sun, S. Shaikhutdinov, and H. Freund, “Encapsulation of Pt Nanoparticles as a Result of Strong Metal - Support Interaction with Fe_3O_4 (111),” *J. Phys. Chem.*, vol. 4, no. 111, pp. 10209–10213, 2008.

[18] S. Bonanni, K. Aït-mansour, H. Brune, and W. Harbich, “Overcoming the Strong Metal - Support Interaction State : CO,” *ACS Cat.*, vol. 2, no. 110, pp. 385–389, 2011.

[19] C. Ertel, H. Knözinger, J. Weitkamp,“Handbook of heterogeneus catalysis”, Wiley-VCH, Weinheim, 2008

[20] S. Ivanova, E. M. Slavinskaya, R. V. Gulyaev, V. I. Zaikovskii, O. A. Stonkus, I. G. Danilova, L. M. Plyasova, I. a. Polukhina, and a. I. Boronin, “Metal–support interactions in Pt/Al_2O_3 and Pd/Al_2O_3 catalysts for CO oxidation,” *Appl. Catal. B Environ.*, vol. 97, no. 1–2, pp. 57–71, Jun. 2010.

[21] S. Hinokuma, H. Fujii, M. Okamoto, K. Ikeue, and M. Machida, “Metallic Pd Nanoparticles Formed by Pd−O−Ce Interaction: A Reason for Sintering-Induced Activation for CO Oxidation,” *Chem. Mater.*, vol. 22, no. 22, pp. 6183–6190, Nov. 2010.

[22] M. Jin, J.-N. Park, J. K. Shon, J. H. Kim, Z. Li, Y.-K. Park, and J. M. Kim, “Low temperature CO oxidation over Pd catalysts supported on highly ordered mesoporous metal oxides,” *Catal. Today*, vol. 185, no. 1, pp. 183–190, May 2012.

[23] J. Luo, M. Meng, X. Li, Y. Zha, T. Hu, Y. Xie, and J. Zhang, “Mesoporous Co_3O_4–CeO_2 and Pd/Co_3O_4–CeO_2 catalysts: Synthesis, characterization and mechanistic study of their catalytic properties for low-temperature CO oxidation,” *J. Catal.*, vol. 254, no. 2, pp. 310–324, Mar. 2008.

[24] M. Skoglundh, “Low temperature catalytic activity of cobalt oxide and ceria promoted Pt and Pd : - influence of pretreatment and gas composition,” *Appl. Catal. B Environ.*, vol. 14, pp. 131–145, 1997.

[25] Y. J. Mergler, a. van Aalst, J. van Delft, and B. E. Nieuwenhuys, “CO oxidation over promoted Pt catalysts,” *Appl. Catal. B Environ.*, vol. 10, no. 4, pp. 245–261, Dec. 1996.

[26] J.-Y. Luo, M. Meng, H. Xian, Y.-B. Tu, X.-G. Li, and T. Ding, “The Nanomorphology-Controlled Palladium-Support Interaction and the Catalytic Performance of Pd/CeO_2 Catalysts,” *Catal. Letters*, vol. 133, no. 3–4, pp. 328–333, Oct. 2009.

[27] I. Ulrych, K. C. Prince, S. Trieste, A. Science, and V. Baso, "Encapsulation of Rh Nanoparticles Supported on TiO_2 (110) - (1×1) Surface : XPS and STM Studies," *J. Phys. Chem.*, vol. 2, no. 110, pp. 3379–3386, 1998.

[28] O. Dulub, W. Hebenstreit, and U. Diebold, "Imaging cluster surfaces with atomic resolution: the strong metal-support interaction state of Pt supported on TiO_2 (110)," *Phys. Rev. Lett.*, vol. 84, no. 16, pp. 3646–9, May 2000.

[29] H.-J. Freund, G. Meijer, M. Scheffler, R. Schlögl, and M. Wolf, "CO oxidation as a prototypical reaction for heterogeneous processes.," *Angew. Chem..*, vol. 50, no. 43, pp. 10064–94, Oct. 2011.

[30] T. Schalow, B. Brandt, M. Laurin, S. Schauermann, S. Guimond, H. Kuhlenbeck, J. Libuda, and H.-J. Freund, "Formation of interface and surface oxides on supported Pd nanoparticles," *Surf. Sci.*, vol. 600, no. 12, pp. 2528–2542, Jun. 2006.

[31] S. T. Daniells, A. R. Overweg, M. Makkee, and J. A. Moulijn, "The mechanism of low-temperature CO oxidation with Au/Fe_2O_3 catalysts : a combined Mössbauer , FT-IR , and TAP reactor study," *J. Catal.*, vol. 230, pp. 52–65, 2005.

[32] M. Harute, S. Tsubota, T. Kobayashi, H. Kageyama, M. Genet, "Low temperature oxidation of CO over Gold supported over TiO_2, α-Fe_2O_3 and Co_3O_4", *J. Catal*., vol. 144, pp.175-192, 1993.

[33] M. M. Schubert, S. Hackenberg, A. C. van Veen, M. Muhler, V. Plzak, and R. J. Behm, "CO Oxidation over Supported Gold Catalysts—'Inert' and 'Active' Support Materials and Their Role for the Oxygen Supply during Reaction," *J. Catal.*, vol. 197, no. 1, pp. 113–122, Jan. 2001.

[34] Z. Zou, M. Meng, and Y. Zha, "Surfactant-Assisted Synthesis , Characterizations , and Catalytic Oxidation Mechanisms of the Mesoporous MnO_x-CeO_2 and Pd/MnO_x-CeO_2 Catalysts Used for CO and C_3H_8 Oxidation," *J. Phys. Chem.*, vol. 114, no. 1, pp. 468–477, 2010.

[35] T. Schalow, B. Brandt, M. Laurin, S. Schauermann, J. Libuda, and H. Freund, "CO oxidation on partially oxidized Pd nanoparticles," *J. Catal.*, vol. 242, no. 1, pp. 58–70, Aug. 2006.

[36] A. Satsuma, K. Osaki, M. Yanagihara, J. Ohyama, and K. Shimizu, "Activity controlling factors for low-temperature oxidation of CO over supported Pd catalysts," *Appl. Catal. B Environ.*, vol. 132–133, pp. 511–518, Mar. 2013.

[37] M. Luo and X. Zheng, "Redox behaviour and catalytic properties of $Ce_{0.5}Zr_{0.5}O_2$ -supported palladium catalysts," *Appl. Catal.*, vol. 189, pp. 15–21, 1999.

[38] K. R. Priolkar, P. Bera, P. R. Sarode, M. S. Hegde, S. Emura, R. Kumashiro, and N. P. Lalla, "Formation of $Ce_{1-x}Pd_xO_{2-\delta}$ Solid Solution in Combustion-Synthesized Pd/CeO_2 Catalyst : XRD , XPS , and EXAFS Investigation," *Chem. Matter*, no. 14, pp. 2120–2128, 2002.

[39] J. Jansson, A. E. C. Palmqvist, E. Fridell, M. Skoglundh, L. Österlund, P. Thormählen, and V. Langer, "On the Catalytic Activity of Co_3O_4 in Low-Temperature CO Oxidation," *J. Catal.*, vol. 211, no. 2, pp. 387–397, Oct. 2002.

[40] J. Jansson, "Low-Temperature CO Oxidation over Co_3O_4/Al_2O_3," *J. Catal.*, vol. 194, no. 1, pp. 55–60, Aug. 2000.

[41] F. Grillo, “Low temperature oxidation of carbon monoxide: the influence of water and oxygen on the reactivity of a Co_3O_4 powder surface,” *Appl. Catal. B Environ.*, vol. 48, no. 4, pp. 267–274, Apr. 2004.

[42] P. Thormählen, M. Skoglundh, E. Fridell and B. Andersson, “Low-Temperature CO Oxidation over Platinum and Cobalt Oxide Catalysts,” vol. 310, pp. 300–310, 1999.

[43] X. Xie, Y. Li, Z.-Q. Liu, M. Haruta, and W. Shen, “Low-temperature oxidation of CO catalysed by Co(3)O(4) nanorods.,” *Nature*, vol. 458, no. 7239, pp. 746–9, Apr. 2009.

[44] M. Pollard, B. Weinstock, T. Bitterwolf, P. Griffiths, a Piersnewbery, and J. Paineiii, “A mechanistic study of the low-temperature conversion of carbon monoxide to carbon dioxide over a cobalt oxide catalyst,” *J. Catal.*, vol. 254, no. 2, pp. 218–225, Mar. 2008.

[45] R. Grau-Crespo, A. Y. Al-Baitai, I. Saadoune, and N. H. De Leeuw, “Vacancy ordering and electronic structure of γ-Fe_2O_3 (maghemite): a theoretical investigation.,” *J. Phys. Condens. Matter*, vol. 22, no. 25, p. 255401, Jun. 2010.

[46] S. M. El-Sheikh, F. a. Harraz, and K. S. Abdel-Halim, “Catalytic performance of nanostructured iron oxides synthesized by thermal decomposition technique,” *J. Alloys Compd.*, vol. 487, no. 1–2, pp. 716–723, Nov. 2009.

[47] R. Tiefenthaller, “Adsorption and reactivity studies on oxide (V_2O_5, Bi_2O_3) -Carbon nanotube hybrid materials, 2012.

[48] K. Zorn, S. Giorgio, E. Halwax, C. R. Henry, and H. Gro, “CO Oxidation on Technological Pd - Al_2O_3 Catalysts : Oxidation State and Activity,” *J. Phy. Chem.*, vol. 114, no.1, pp. 1103–1111, 2011.

[49] H. Bluhm, M. Hävecker, A. Knop-Gericke, E. Kleimenov, R. Schlögl, D. Teschner, V. I. Bukhtiyarov, D. F. Ogletree, and M. Salmeron, “Methanol Oxidation on a Copper Catalyst Investigated Using in Situ X-ray Photoelectron Spectroscopy,” *J. Phys. Chem. B*, vol. 108, no. 38, pp. 14340–14347, Sep. 2004.

[50] S. Tanuma and D. R. Penn, “Calculations of Electron Inelastic Mean Free Paths,” *Surface and Interface anal.,*. vol. 17, pp. 911–926, 2000.

[51] J. Kugai, V. Subramani, C. Song, M. Engelhard, and Y. Chin, “Effects of nanocrystalline CeO_2 supports on the properties and performance of Ni–Rh bimetallic catalyst for oxidative steam reforming of ethanol,” *J. Catal.*, vol. 238, no. 2, pp. 430–440, Mar. 2006.

[52] J. Liu, B. Sun, J. Hu, Y. Pei, H. Li, and M. Qiao, “Aqueous-phase reforming of ethylene glycol to hydrogen on Pd/Fe_3O_4 catalyst prepared by co-precipitation: Metal–support interaction and excellent intrinsic activity,” *J. Catal.*, vol. 274, no. 2, pp. 287–295, Sep. 2010.

[53] P. Panagiotopoulou, “Effect of morphological characteristics of TiO_2-supported noble metal catalysts on their activity for the water-gas shift reaction,” *J. Catal.*, vol. 225, no. 2, pp. 327–336, Jul. 2004.

[54] S. Wang, J. He, J. Xie, Y. Zhu, Y. Xie, and J. G. Chen, "Synthesis of bimetallic systems using replacement reactions," *Appl. Surf. Sci.*, vol. 254, no. 7, pp. 2102–2109, Jan. 2008.

[55] S. Bertarione, "Surface reactivity of Pd nanoparticles supported on polycrystalline substrates as compared to thin film model catalysts: infrared study of CH_3OH adsorption," *J. Catal.*, vol. 223, no. 1, pp. 64–73, Apr. 2004.

[56] L. Liu, F. Zhou, L. Wang, X. Qi, F. Shi, and Y. Deng, "Low-temperature CO oxidation over supported Pt, Pd catalysts: Particular role of FeO_x support for oxygen supply during reactions," *J. Catal.*, vol. 274, no. 1, pp. 1–10, Aug. 2010.

[57] Y. Teng, Y. Kusano, M. Azuma, M. Haruta, and Y. Shimakawa, "Morphology effects of Co_3O_4 nanocrystals catalyzing CO oxidation in a dry reactant gas stream," *Catal. Sci. Technol.*, vol. 1, no. 6, p. 920, 2011.

[58] S. Royer and D. Duprez, "Catalytic oxidation of carbon monoxide over transition metal oxides," *ChemCatChem*, vol. 3, no. 1, pp. 24–65, Jan. 2011.

[59] M. Rothensteiner, "Selective oxidation of ethanol on supported AuAg bimetallic catalysts," Vienna 2012.

[60] K. Föttinger, R. Schlögl, and G. Rupprechter, "The mechanism of carbonate formation on Pd–Al_2O_3 catalysts," *Chem. Commun.*, vol. 3, no. 3, pp. 320-322, 2008.

[61] K. Hadjiiavanov, G. Vayssilov, "Characterization of oxide surfaces and zeolites by carbon monoxide as an IR probe molecule," *Adv. Catal.*, vol. 47, pp. 307-511, 2002.

[62] Y. Zro, E. Ko, M. Kogler, T. Bielz, B. Klo, and S. Penner, "In situ FT-IR spectroscopic study of CO_2 and CO adsorption on Y_2O_3 ,"*J. Phys. Chem*, vol. 117, pp. 17666-17673, 2013.

[63] A. Davydov, "Infrared spectroscopy of adsorbed species on the surface of transition metal oxides," John Wiley & Sons., England, 1990.

[64] W. Daniell, H. Landes, N. E. Fouad, and H. Knözinger, "Influence of pretreatment atmosphere on the nature of silica-supported Pd generated via decomposition of Pd $(acac)_2$: an FTIR spectroscopic study of adsorbed CO," *J. Molec. Catal.*, vol. 178, pp. 211–218, 2002.

[65] T. Lear, R. Marshall, J. A. Lopez-Sanchez, S. D. Jackson, T. M. Klapötke, M. Bäumer, G. Rupprechter, H.-J. Freund, and D. Lennon, "The application of infrared spectroscopy to probe the surface morphology of alumina-supported palladium catalysts.," *J. Chem. Phys.*, vol. 123, no. 17, p. 174706, Nov. 2005.

[66] G. Šmit, S. Zrnčević, and K. Lázár, "Adsorption and low-temperature oxidation of CO over iron oxides," *J. Mol. Catal. A Chem.*, vol. 252, no. 1–2, pp. 103–106, Jun. 2006.

[67] C.-W. Tang, L.-C. Hsu, S.-W. Yu, C.-B. Wang, and S.-H. Chien, "In situ FT-IR and TPD-MS study of carbon monoxide oxidation over a CeO_2/Co_3O_4 catalyst," *Vib. Spectrosc.*, vol. 65, pp. 110–115, Mar. 2013.

[68] J. Li, G. Lu, G. Wu, D. Mao, Y. Wang, and Y. Guo, “Promotional role of ceria on cobaltosic oxide catalyst for low-temperature CO oxidation,” *Catal. Sci. Technol.*, vol. 2, no. 9, pp. 1865-1871, 2012.

[69] Y. M. Choi, H. Abernathy, H.-T. Chen, M. C. Lin, and M. Liu, “Characterization of O_2-CeO_2 interactions using in situ Raman spectroscopy and first-principle calculations.,” *Chemphyschem*, vol. 7, no. 9, pp. 1957–1963, Sep. 2006.

[70] N. Osakoo, R. Henkel, S. Loiha, F. Roessner, and J. Wittayakun, “Palladium-promoted cobalt catalysts supported on silica prepared by impregnation and reverse micelle for Fischer–Tropsch synthesis,” *Appl. Catal. A Gen.*, vol. 464–465, pp. 269–280, Aug. 2013.

[71] S. Zafeiratos, T. Dintzer, D. Teschner, R. Blume, M. Hävecker, a. Knop-Gericke, and R. Schlögl, “Methanol oxidation over model cobalt catalysts: Influence of the cobalt oxidation state on the reactivity,” *J. Catal.*, vol. 269, no. 2, pp. 309–317, Feb. 2010.

[72] S.-H. Oh and G. B. Hoflund, “Chemical state study of palladium powder and ceria-supported palladium during low-temperature CO oxidation.,” *J. Phys. Chem. A*, vol. 110, no. 24, pp. 7609–7613, Jun. 2006.

[73] T. Schalow, B. Brandt, D. E. Starr, M. Laurin, S. K. Shaikhutdinov, S. Schauermann, J. Libuda, and H.-J. Freund, “Size-Dependent oxidation mechanism of supported Pd nanoparticles,” *Angew. Chemie Int. Ed.*, vol. 45, no. 22, pp. 3693–3697, May 2006.

[74] L. Meng, A. Jia, J. Lu, L. Luo, W. Huang, and M. Luo, “Synergetic effects of PdO species on CO oxidation over PdO A CeO_2 catalysts,” *J. Phys. Chem.*, vol. 115, pp. 19789–19796, 2011.

[75] H. Dropsch and M. Baerns, “CO adsorbtion on supported Pd catalysts studied by adsorption microcalorimetry and temperature programmed desorption,” *Appl. Catal.*, vol. 158, pp. 163–183, 1997.

[76] V. V. Kaichev, M. Morkel, H. Unterhalt, I. P. Prosvirin, V. I. Bukhtiyarov, G. Rupprechter, and H.-J. Freund, “C–O bond scission on ‘defect-rich and perfect’ Pd(111)?,” *Surf. Sci.*, vol. 566–568, pp. 1024–1029, Sep. 2004.

[77] F. Prinetto, M. Manzoli, G. Ghiotti, M. D. J. Martinez Ortiz, D. Tichit, and B. Coq, “Pd/Mg(Al)O catalysts obtained from hydrotalcites: investigation of acid–base properties and nature of Pd phases,” *J. Catal.*, vol. 222, no. 1, pp. 238–249, Feb. 2004.

[78] I. Stara, K. Veltruska, V. Matolı, N. Tsud, and V. Joha, “CO adsorption on palladium model catalysts : XPS Pd–Al_2O_3 interaction study,” *Surface Science*, vol. 467, pp. 169–176, 2000.

[79] J. Szanyi and J. H. Kwak, “Dissecting the steps of CO_2 reduction: The interaction of CO and CO_2 with Pd/γ-Al_2O_3: an in situ FTIR study.,” *Phys. Chem. Chem. Phys.*, vol. 16, no. 29, pp. 15126–38, Jul. 2014.

[80] J. Baltrusaitis, J. Schuttlefield, E. Zeitler, and V. H. Grassian, “Carbon dioxide adsorption on oxide nanoparticle surfaces,” *Chem. Eng. J.*, vol. 170, no. 2–3, pp. 471–481, Jun. 2011.

[81] C. Weilach, C. Spiel, K. Föttinger, and G. Rupprechter, "Carbonate formation on Al_2O_3 thin film model catalyst supports," *Surf. Sci.*, vol. 605, no. 15–16, pp. 1503–1509, Aug. 2011.

[82] J. Baltrusaitis, J. H. Jensen, and V. H. Grassian, "FTIR spectroscopy combined with isotope labeling and quantum chemical calculations to investigate adsorbed bicarbonate formation following reaction of carbon dioxide with surface hydroxyl groups on Fe_2O_3 and Al_2O_3," *J. Phys. Chem. B*, vol. 110, no. 24, pp. 12005–16, Jun. 2006.

[83] C.-B. Wang, C.-W. Tang, H.-C. Tsai, M.-C. Kuo, and S.-H. Chien, "In situ FT-IR spectroscopic studies on the mechanism of the catalytic oxidation of carbon monoxide over supported cobalt Catalysts," *Catal. Letters*, vol. 107, no. 1–2, pp. 31–37, Feb. 2006.

[84] L. S. Kibis, A. I. Stadnichenko, S. V Koscheev, V. I. Zaikovskii, and A. I. Boronin, "Highly oxidized palladium nanoparticles comprising Pd^{4+} Species: spectroscopic and structural aspects, thermal stability, and reactivity," *J. Phys. Chem.*, vol.116, pp. 19342–19348, 2012.

[85] L. S. Kibis, a. I. Titkov, a. I. Stadnichenko, S. V. Koscheev, and a. I. Boronin, "X-ray photoelectron spectroscopy study of Pd oxidation by RF discharge in oxygen," *Appl. Surf. Sci.*, vol. 255, no. 22, pp. 9248–9254, Aug. 2009.

[86] Q. Liu, J. Kim, T. Fukaya, and J. Tominaga, "Thermal-induced optical properties of a PdO_x mask layer in an optical data storage system with a superresolution near-field structure," vol. 11, no. 21, pp. 955–957, 2003.

[87] A. Sarkany, z. Zsoldos, G. Stefler, J. Hightower, L. Guzci, "Promoter effect of Pd in Hydrogenation of 1,3-Butadiene over Co-Pd Catalysts", *J. Catal.*, vol. 157, pp. 179-189, 1995.

[88] R. Blume, D. Teschner, S. Zafeiratos, R. Schlögl, and V. I. Bukhtiyarov, "X-Ray photoelectron spectroscopy for Investigation of heterogeneous catalytic processes", *Advances in Catal.*, vol. 52, pp. 213–272, 2009.

[89] J. a Rodriguez, S. Ma, P. Liu, J. Hrbek, J. Evans, and M. Pérez, "Activity of CeO_x and TiO_x nanoparticles grown on Au (111) in the water-gas shift reaction.," *Science*, vol. 318, no. 5857, pp. 1757–1760, Dec. 2007.

[90] S. Labich, E. Taglauer, and H. Knözinger, "Metal–support interactions on rhodium model catalysts," *Appl. Catal.*, vol. 14, no. 1, pp. 153–161, 2001.

[91] H. R. J. ter Veen, T. Kim, I. E. Wachs, and H. H. Brongersma, "Applications of high sensitivity-low energy ion scattering (HS-LEIS) in heterogeneous catalysis," *Catal. Today*, vol. 140, no. 3–4, pp. 197–201, Feb. 2009.

[92] T. Kendelewicz, "Auger and photoelectron contributions to the electron-yield x-ray-absorption fine-structure," *Physical Review*, vol. 30, no. 10, pp. 5571–5579, 1984.